

Microwave Electronics

**INVESTIGATIONS ON THE SCATTERING
PROPERTIES OF METALLIC OBJECTS
LOADED WITH DIELECTRIC BACKED
FRACTAL STRUCTURES**

Thesis submitted by

CYRIAC M ODACKAL

*in partial fulfilment of the requirements
or the award of the degree of*

DOCTOR OF PHILOSOPHY

Under the guidance of

Prof. C.K. AANANDAN



**DEPARTMENT OF ELECTRONICS
FACULTY OF TECHNOLOGY
Cochin University of Science and Technology**

**INVESTIGATIONS ON THE SCATTERING PROPERTIES OF METALLIC
OBJECTS LOADED WITH DIELECTRIC BACKED FRACTAL STRUCTURES**

Ph.D thesis under the Faculty of Technology

Author:

CYRIAC M ODACKAL

Microwave Material Research Lab

Department of Electronics

Cochin University of Science and Technology

Cochin-682022, Kerala, India

E-mail: cyriacpala@yahoo.co.uk

Supervisor:

Dr. C.K. AANANDAN

Professor and Head

Department of Electronics

Cochin University of Science and Technology

Cochin-682022, Kerala, India

E-mail: aanandan@gmail.com

March 2019

Declaration

I hereby declare that the work presented in this thesis entitled “**Investigations on the Scattering Properties of Metallic Objects Loaded with Dielectric Backed Fractal Structures**” is based on the original research work carried out by me under the supervision and guidance of Prof. C.K. Aanandan, Professor and Head, Department of Electronics, Cochin University of Science and Technology, Cochin-682022 and has not been included in any other thesis submitted previously for the award of any degree

Cochin-22
March 2019

CYRIAC M ODACKAL
Research Scholar
Dept. of Electronics
Cochin University of Science and Technology

Certificate

This is to certify that this thesis entitled “**Investigations on the Scattering Properties of Metallic Objects Loaded with Dielectric Backed Fractal Structures**” is a bonafide record of work done by Mr. Cyriac M Odackal under my guidance in the Microwave Material Research Laboratory, Department of Electronics, Cochin University of Science and Technology. The results embodied in the thesis or part of it has not been included anywhere previously for the award of any degree or title.

Certify that all the relevant corrections and modifications suggested by the audience during the pre-synopsis seminar and recommended by the Doctoral Committee of the candidate have been incorporated in the thesis

Cochin-22
October 2018

Dr. C.K. Aanandan
Professor
Department of Electronics
Cochin University of Science and Technology

*DEDICATED TO
MY PARENTS*

ACKNOWLEDGEMENT

I express my sincere gratitude to Dr. C K Aanandan my guide and Professor and Head of the Department for the invaluable help and guidance given to me, spending his precious time, by discussing ideas, excellent suggestions and constant encouragement with an innovative mind and boundless knowledge.

My words of sincere gratitude to Dr. Thomaskutty Mathew, Reader, School of Technology and Applied Sciences, M G University, Edappally, for the wholehearted infinite help given to me throughout my research by sharing invaluable knowledge, excellent suggestions, fruitful discussions and encouragement.

I am duty bound to record my words of sincere thanks to Dr. K T Mathew, Professor Emeritus, Dept. of Electronics. CUSAT for the invaluable help and constant encouragements given to me throughout my research which enabled me to complete this work successfully.

I express my sincere thanks to Prof PRS Pillai, Prof K Vasudevan and Prof Supriya M H, former heads of Departments, Dept. of Electronics for the help rendered to me in pursuing the research. My words of sincere thanks to Prof James Kurian, Prof P Mohanan and Prof. Tessamma Thomas for their valuable help during my research. My wholehearted thanks to Dr. Beena C, Librarian of CUSAT central Library and Mr. Padamakumar Department Librarian for the very valuable help.

I thank all faculty members Mr. Arun A Balakrishnan, Mr. Midhun Haridas, Dr. Binoy A Jose, Dr. Deepthi Das Krishna, Dr. Nalesh, Dr. Tripti S Warriar and Mrs. Kumari vidhu for their moral support during research.

I owe my sincere thanks to, Dr. Joseph Kunjupaul Principal, Viswajyothi College of Engineering & Technology for the boundless help given to me for completing the research.

I express my sincere thanks to the Manager and Rev Dr. George Thanathuparambil, Director of Viswajyothi College of Engineering and Technology, Muvattupuzha for giving me all support to successfully complete the research work.

I thank Prof Jose P Varghese the former Head of the Department. Dept. of ECE, VJCET for all the valuable help and guidance rendered to me. I also thank Mrs. Smitha Cyriac HoD ECE for her valuable help. My sincere thanks to Somy P Mathew, Vice Principal VJCET. My words of sincere thanks to Pro T S Chacko former director VJCET and Fr Thomas Malekkudy for their very valuable help.

I thank my colleagues in the department Tony D, Nelson K J, Lindo A O, Neeraj K Pushkaran, Abhilash A P, Paulbert Thomas, Sruthi Dinesh, Ullas G Kalappura, Prasanth M N, Libimol VA, Sreekala P S, Dibin Mary George and Anju P Mathews.

My sincere thanks to all research scholars of the department especially, Suraj Kamal, Kurian Thomas, Manoj M, Satheesh Chandran, Aji George, Midhun M S, Athul Thomas, Prasanth P P, Navya Mohan, Ann Varghese, Remsha M, Vivek R, Vinisha C V, Prakash K C, DrShameena V A, DrSarin, Anitha P V, Sangeetha, Deepthi, Suja, Bindhya, Jisha, Akhil and Titu Samson, Aju John and Fijo.

My words of sincere thanks to Dr. Joe Jacob, Dr. Narayanan KK, Dr. Bijukumar S, Dr U Raveendranath and Dr. Binoy G S.

My words of sincere thanks to Mr. Ibrahimkutty P M, Mr. Anil PY, , Mr. Russel E P , Mr. Pradeep Kumar S and Mrs. Anitha who helped me a lot to complete the research.

I mention the valuable help from my friends and colleagues in VJCET, Anilkumar R, Anish M Jose, Melvin C Jose, Manu Jose, Krishnendu K, Jiby P Dcruz, Dr Rajesh Cherian Roy, Naveen Jacob. My special thanks to Jekson George, Shiju Jose, Renji Issac, Thankachan P J, Jinu Jose, Thomas Mathew, Denny Joseph, Anish George, James Alex, Shaji and Ullas.

Last but not least I thank my nephew Elbin Thomas who helped me a lot to design the front cover and prepare this manuscript in this shape.

Above all I thank lord almighty for helping me in each of my steps in my research time.

CYRIAC

Abstract

Complex targets like aircrafts, missiles, ships etc. can be modelled as a combination of simple shapes such as flat plates, corner reflectors, cones and wedges. Backscattering from these objects is a measure of the monostatic radar cross section of the target. Control of radar cross section (RCS) is very important in reducing or improving the visibility of targets, which can be achieved in different ways. Corrugated surfaces were effectively used for this purpose but were bulky and difficult to fabricate. It is already established that dielectric backed planar strip gratings simulate corrugated structures. Various structures based on Euclidian geometry are reported in the literature for controlling the scattering from metallic surfaces.

Fractal structures have an additional advantage in the control of radar cross section of targets. The self-similar structure of fractal geometry makes it different from the conventional Euclidian geometry. Sierpinski carpet fractals are simple in design and can be utilized for backscattering reduction applications. Arrays of fractal structures are even though popular in antenna design are not investigated for backscattering reduction studies. A detailed study the scattering properties of fractal arrays loaded metallic objects such as flat metal plates and Dihedral Corner Reflectors, wedges etc. is presented in this thesis. The study revealed that by properly choosing the parameters of the arrays we can achieve backscattering reduction, backscattering enhancement, elimination of specular reflection and perfect blazing at desired frequency or angular range. Simulation studies are validated by experiment.

LIST OF FIGURES

Chapter	Title	Page No
1		
1.1	Electromagnetic spectrum.....	3
1.2	Plot of the radar cross section as a function of the electrical size of the target.....	9
1.3	RCS pattern of a flat metal plate.....	10
1.4	Schematic diagram of a corrugated surface.....	15
1.5	Schematic diagram of a strip grating.....	15
1.6	Simple fractal geometries.....	17
1.7	Initiator and different stages of Sierpinski gasket...	17
1.8	4 × 4 Sierpinski carpet fractal arrays of first second and third iteration.....	18
3		
3.1	Pyramidal absorbers in the wall of an anechoic chamber.....	49
3.2	Schematic diagram of the Arch Method.....	50
3.3	Photograph of Arch method.....	51
3.4	Working of a VNA.....	52
3.5	Rhode & Schwartz ZVB 20 used in measurement..	52
3.6	Second iterated stage of (a) Sierpinski Carpet (b) Sierpinski Carpet Array.....	55
3.7	First and third iterated stages of (a) Sierpinski Carpet (b) Sierpinski Carpet Array.....	55
3.8	Flat metallic plate loaded with dielectric backed second stage of SCF Array.....	56
3.9	Stacked SCF arrays over flat plate.....	57
3.10	Fully interleaved structure.....	57

3.11	Plane dihedral corner reflector.....	58
3.12	Plane metallic wedge.....	59

4

4.1	Different sizes of SCF arrays investigated.....	63
4.2	Variation of relative backscattered power with frequency for second iterated stage SCF array for different combinations	63
4.3	Different iterated stages of the SCF 4×4 array.....	64
4.4	Schematic diagram of Flat metal plate loaded with SCF array backed with dielectric of thickness(h).....	65
4.5	Variations of relative backscattered power for metallic plate loaded with 2 nd iterated stage of SCF array with different dielectric thickness.....	65
4.6	Variation of relative backscattered power with frequency for various iterated stage of dielectric backed Sierpinski carpet array with thickness $h=3.2\text{mm}$	66
4.7	Variation of backscattered power with frequency response for the second iterated stage of dielectric backed 4×4 SCF array.....	67
4.8	Variations of relative backscattered power with angle of incidence at $f = 11.08$ GHz for second iterated stage of SCF array and thickness $h=3.2\text{mm}$	68
4.9	Variations of relative backscattered power with angle of incidence for frequency $f = 9.5$ GHz for second iterated stage of SCF array	

(h=3.2mm.).....	69
4.10 Variation of scattered power with scattering angle at 11.08 GHz and 9.5 GHz for the second iterated stage of the SCF array with thickness h=3.2mm at normal incidence.....	70
4.11 Variation of relative backscattered power with dielectric thickness for second iterated stage of the SCF array for frequency of 11.08.....	71
4.12 Schematic diagram of the dielectric backed 4×4 SCF array.....	72
4.13 Variation of relative reflected power with angle of incidence for the SCF array at 9.8 GHz. (h ₁ =0.8mm & h ₂ =4.5mm).....	73
4.14 Variation of relative backscattered power with angle of incidence for the SCF array at 9.8 GHz. (h ₁ =0.8mm& h ₂ =4.5mm).....	74
4.15 Variation of relative reflected power with frequency for the second iterated stages of the SCF arrays for $\theta_i = 26^0$ and $\theta_i = 39^0$. (h ₁ =0.8mm & h ₂ =4.5mm).....	74
4.16 Relative backscattered power with frequency at angle of incidence $\theta_i=39^0$ and $\theta_i = 26^0$ for the second iterated stage of SCF array. (h ₁ =0.8mm & h ₂ =4.5mm).....	75
4.17 Variation of relative reflected power with dielectric thickness (h ₂) for the second iterated stage of the SCF array with h ₁ =0.8mm.....	76

4.18	Stacking of two different iterated stages of SCF array.....	77
4.19	Variation of backscattered power with frequency for different dielectric thickness.....	77
4.20	Variation of backscattered power with dielectric thickness at $f=11.08$ GHz.....	78
4.21	Variation of relative backscattered power with angle of incidence at $f=11.08$ GHz for stacked SCF array.....	79
4.22	Variation of received power with scattering angle at normal incidence for $f= 11.08$ GHz.....	80
4.23	Interleaved structure.....	80
4.24	Variation of relative backscattered power with frequency for the fully interleaved structure.....	81
4.25	Variation of relative backscattered power with frequency when loaded with vertical interleaved structure.....	82
4.26	Variation of relative backscattered power with frequency when loaded with horizontal interleaved structure.....	83
4.27	Variation of relative backscattered power with angle of incidence of the horizontally interleaved SCF array loaded over the flat plate.....	84

5

5.1	Schematic diagram of the dihedral corner reflector loaded with second iterated stage of the SCF array.....	88
5.2	Variation of backscattered power with frequency	

	for the 80 ⁰ dihedral corner loaded with dielectric backed first iterated SCF array of different dielectric thickness (h).....	89
5.3	Variation of backscattered power with frequency for the 80 ⁰ dihedral corner loaded with dielectric backed second iterated SCF array of different dielectric thickness (h).....	90
5.4	Variation of backscattered power with frequency for the 80 ⁰ dihedral corner loaded with dielectric backed third iterated SCF array of different dielectric thickness (h).....	91
5.5	Variation of backscattered power with frequency for the 90 ⁰ dihedral corner loaded with dielectric backed first iterated SCF array of different dielectric thickness (h).....	92
5.6	Variation of backscattered power with frequency for the 90 ⁰ dihedral corner loaded with dielectric backed second iterated SCF array of different dielectric thickness (h).....	93
5.7	Variation of backscattered power with frequency for the 90 ⁰ dihedral corner loaded with dielectric backed third iterated SCF array of different dielectric thickness (h).....	94
5.8	Scattering pattern for the 90 ⁰ metallic corner and the dielectric backed SCF array loaded corner for frequency 11.64 GHz.....	95
5.9	Variation of backscattered power with frequency for the 100 ⁰ dihedral corner loaded with dielectric backed first iterated SCF array of different dielectric thickness(h).....	96
5.10	Variation of backscattered power with frequency	

	for the 100^0 dihedral corner loaded with dielectric backed second iterated SCF array of different dielectric thickness (h).....	97
5.11	Variation of backscattered power with frequency for the 100^0 dihedral corner loaded with dielectric backed third iterated SCF array of different dielectric thickness (h).....	98
5.12	Variation of backscattered power with frequency for the 110^0 dihedral corner loaded with dielectric backed first iterated SCF array of different dielectric thickness (h).....	99
5.13	Variation of backscattered power with frequency for the 110^0 dihedral corner loaded with dielectric backed second iterated SCF array of different dielectric thickness (h).....	100
5.14	Variation of backscattered power with frequency for the 110^0 dihedral corner loaded with dielectric backed third iterated SCF array of different dielectric thickness (h).....	101
5.15	Variation of backscattered power with frequency for the 120^0 dihedral corner loaded with dielectric backed first iterated SCF array of different dielectric thickness (h).....	102
5.16	Variation of backscattered power with frequency for the second iterated stage of 120^0 dielectric backed SCF array.....	103
5.17	Variation of backscattered power with frequency for the third iterated stage of 120^0 dielectric backed SCF array.....	104

6.1	Schematic diagram of (a) plain wedge (b) wedge loaded with second iterated stage of SCF array with dielectric thickness (h) with wedge angle α ...	107
6.2	Measured variation of relative backscattered power with frequency for 80^0 wedge loaded with first iterated SCF array.....	108
6.3	Measured variation of relative backscattered power with frequency for 80^0 wedge loaded with second iterated SCF array	109
6.4	Measured variation of relative backscattered power with frequency for 80^0 wedge loaded with third iterated SCF array	110
6.5	Measured variation of relative backscattered power with frequency for 90^0 wedge loaded with first iterated SCF array.....	111
6.6	Measured variation of relative backscattered power with frequency for 90^0 wedge loaded with second iterated SCF array.....	112
6.7	Measured variation of relative backscattered power with frequency for 90^0 wedge loaded with third iterated SCF array.....	113
6.8	Measured variation of relative backscattered power with frequency for 100^0 wedge loaded with first iterated SCF array.....	114
6.9	Measured variation of relative backscattered power with frequency for 100^0 wedge loaded with second iterated SCF array.....	115
6.10	Measured variation of relative backscattered power with frequency for 100^0 wedge loaded with third iterated SCF array.....	116
6.11	Measured variation of relative backscattered	

	power with frequency for 110^0 wedge loaded with first iterated SCF array.....	117
6.12	Measured variation of relative backscattered power with frequency for 110^0 wedge loaded with second iterated SCF array	118
6.13	Measured variation of relative backscattered power with frequency for 110^0 wedge loaded with third iterated SCF array.....	119
6.14	Measured variation of relative backscattered power with frequency for 120^0 wedge loaded with first iterated SCF array.....	120
6.15	Measured variation of relative backscattered power with frequency for 120^0 wedge loaded with second iterated SCF array.....	121
6.16	Measured variation of relative backscattered power with frequency for 120^0 wedge loaded with third iterated SCF array.....	122

LIST OF ABBREVIATIONS

CST	Computer Simulation Technology
RADAR	Radio Detection And Ranging
RAM	Radar Absorbent Material
RCS	Radar Cross Section
RF	Radio Frequency
SCF	Sierpinski Carpet Fractal
SCS	Simulated Corrugated Surface
TE	Transverse Electric
TM	Transverse Magnetic
VNA	Vector Network Analyzer

TABLE OF CONTENTS

Chapter	Title	Page No
1	Introduction.....	1
1.1	Electromagnetic Spectrum & Microwave bands.....	3
1.2	History of Radar.....	5
1.3	Backscattering from objects.....	6
1.3.1	Radar cross section.....	6
1.3.2	Radar cross section of simple shape.....	9
1.3.2.1	Sphere.....	9
1.3.2.2	Flat plate.....	10
1.3.2.3	Corner reflector.....	10
1.4	RCS reduction methods.....	12
1.4.1	Shaping of objects.....	12
1.4.2	Passive cancellation.....	12
1.4.3	Active cancellation.....	12
1.4.4	Radar Absorbers.....	12
1.5	RCS Enhancement.....	13
1.6	Scattering properties of dihedral backed strip graings.....	13
1.7	Fractals.....	16
1.8	Fractal Electrodynamics.....	18
1.9	Motivation of the present work.....	19
1.10	Organisation of the Thesis.....	19

REFERENCES	20
2	Litreture Review.....	23
2.1	Electromagnetic Scattering.....	23
2.1.1	Scattering from Dihedral Corner.....	26
2.1.2	Scattering from a Wedge.....	27
2.2	Scattering properties of Corrugated Surfaces.....	27
2.3	Backscattering reduction using stip gratings.....	29
2.4	Fractals.....	32
2.5	Fractal Electrodynamics.....	33
2.5.1	Sierpinski Carpet Fractals.....	34
2.6	Fractal Arrays.....	36
2.6.1	Sierpinski Carpet Fractal Arrays.....	37
REFERENCES	38
3	Methodology.....	48
3.1	Overview of Instrumentation for Scattering Measurements.....	48
3.2	Subsystems used in Scattering Measurements.....	49
3.2.1	Anechoic Chamber.....	49
3.2.2	Arch Method.....	50
3.2.3	Vector Network Analyzer.....	51

3.3	Measurement Procedure.....	53
3.4	Design and fabrication of fractal arrays.....	54
3.4.1	Sierpinski Carpet and Sierpinski Carpet Array.....	54
3.5	Flat Metallic Plate Loaded with Dielectric Backed SCF Arrays.....	55
3.5.1	Various iterated stages of the SCF arrays.....	56
3.5.2	Stacking of SCF Arrays for Backscattering Reduction.....	56
3.5.3	Interleaving of second and third iterated stages of SCF Arrays for Backscattering reduction....	57
3.6	Non planar structures.....	58
3.6.1	Dihedral Corner Reflector.....	58
3.6.2	Wedge.....	58
	REFERENCES	59
4	Backscattering reduction of a flat metal plate using dielectric backed fractal arrays..	61
4.1	Introduction	61
4.2	Simulated Results of Backscattering Reduction of Flat Metal Plate Loaded with Dielectric Backed SCF Array.....	62
4.3	Measured results.....	64
4.4	Wide Angle Elimination of Specular Reflection with Dielectric backed SCF array...	71

4.5	Stacked SCF Arrays for Backscattering Reduction.....	76
4.6	Interleaved SCF array for Backscattering Reduction.....	80
4.7	Conclusion.....	84
REFERENCES	86
5	Scattering behaviour of dihedral corner reflector loaded with dielectric backed fractal arrays.....	87
5.1	Introduction	87
5.2	80 ⁰ Dihedral Corner Reflector Loaded With Dielectric Backed SCF Array.....	89
5.3	90 ⁰ Dihedral Corner Reflector Loaded With Dielectric Backed SCF Array.....	92
5.4	100 ⁰ Dihedral Corner Reflector Loaded With Dielectric Backed SCF Array.....	95
5.5	110 ⁰ Dihedral Corner Reflector Loaded With Dielectric Backed SCFArray.....	98
5.6	120 ⁰ Dihedral Corner Reflector Loaded With Dielectric Backed SCFArray.....	102
5.7	Conclusions.....	104

6	Enhancement of backscattering from a metallic wedge using dielectric backed fractal arrays.....	106
6.1	Introduction.....	106
6.2	80 ⁰ Metallic wedge loaded with dielectric backed SCF array.....	108
6.3	90 ⁰ Metallic wedge loaded with dielectric backed SCF array.....	110
6.4	100 ⁰ Metallic wedge loaded with dielectric backed SCF array.....	113
6.5	110 ⁰ Metallic wedge loaded with dielectric backed SCF array.....	117
6.6	120 ⁰ Metallic wedge loaded with dielectric backed SCF array.....	119
6.7	Conclusion	122
7	Conclusions.....	123
7.1	Flat Plates.....	123
7.2	Dihedral Corner Reflectors.....	125
7.3	Metallic Wedge.....	125
7.4	Scope for future Work.....	126

1 INTRODUCTION

This chapter begins with a brief description of Electromagnetic scattering, Electromagnetic spectrum, Microwave bands and history of RADAR. The chapter also provides an overview of backscattering from Objects, Radar Cross Section of simple shapes and RCS reduction methods. It further discusses the scattering properties of dielectric backed strip gratings. Description of fractals and fractal electrodynamics are also presented. Finally the motivation for the present work and the organization of the thesis are also presented.

TABLE OF CONTENTS

- 1.1 Electromagnetic spectrum and Microwave bands**
- 1.2 History of Radar**
- 1.3 Backscattering from Objects**
- 1.4 RCS Reduction Methods**
- 1.5 RCS Enhancement**
- 1.6 Scattering Properties of Dielectric Backed Strip Gratings**
- 1.7 Fractals**
- 1.8 Fractal Electrodynamics**
- 1.9 Motivation of the present work**
- 1.10 Organization of the Thesis**

When an electromagnetic wave is incident on an object, the energy is dispersed in all directions. The spatial distribution of the dispersed energy depends on the shape, size and composition of the object, and on the nature and frequency of the incident

electromagnetic wave [1- 4]. This spatial distribution of energy is termed as scattering. Bistatic scattering occurs when the scattering direction is not back towards the source of radiation. Forward scattering occurs when the angle between incident direction and scattering direction is 180° . When the source and receiver are located at the same point, it is called monostatic scattering or backscattering. The scattering from various objects is a subject of immense interest in electromagnetics and was studied by many researchers in various frequency ranges of the electromagnetic spectrum for wide variety of applications from radio frequency to optical range.

RADAR which is an acronym for “Radio Detection And Ranging,” works on received scattered energy from objects [5]. Many types of radars were built for different applications. The early stages use radars in military applications for detection of enemy targets and later in civilian applications like navigation and traffic control. However, as radar became more widespread, and as technology improved, automobile speed detection, weather detection and tracking, collision avoidance and buried object detection also became important as civilian applications. Military radars are also used for surveillance, weapons control and early warning. Military has been a strong driver in the development of radar technology. A radar operates by analyzing the scattered field towards some specific direction to locate the target. The design of efficient radars require an understanding of the scattering mechanism of the object. The development of radar technology triggered tremendous proliferation of investigations on the scattering and diffraction phenomena, with specific emphasis on the determination of radar response of objects.

In most of the radars, the source and receiver are located at the same point, which detects the objects based on monostatic scattering. In some measurement situations separate transmitting and receiving antennas are used, which represent a bistatic condition. However, when the angle subtended by the transmitting and receiving antennas is small it can also be considered as a monostatic case.

With the development of antenna research and design, scattered energy or scattered power is characterized by a cross section or a fictitious area property of the target. An antenna is regarded as having an aperture of effective area which extracts

energy from the passing radio frequency wave. The available power at the terminals of a receiving antenna can be expressed as the product of an incident power density and an effective area exposed to the power density. The power reflected or scattered by a target can be expressed as the product of an effective area and an incident power density. That area is called scattering cross section. For directions other than back towards the radar, it can also be called bistatic cross section and when the direction is back towards the radar, it is called backscattering cross section or the radar cross section.

1.1 ELECTROMAGNETIC SPECTRUM AND MICROWAVE BANDS

Electromagnetic wave is a non-mechanical wave in which electric and magnetic fields are varying in mutually perpendicular directions with respect to space and time. The propagation of electromagnetic waves are governed by Maxwell's equations. Poynting's Theorem is used for explaining the flow of power through a medium. The cross product of electric and magnetic fields at a point gives the intensity of power flowing out. Depending on the frequency of electromagnetic waves the electromagnetic spectrum is defined in several bands. Electromagnetic wave is transverse in nature. They can be polarised, can exhibit interference and diffraction properties and finally the existence of a medium is not at all required for the propagation.

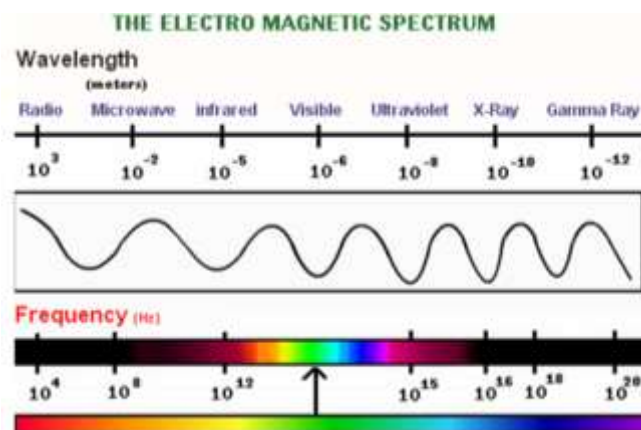


Fig 1.1 Electromagnetic spectrum

The electromagnetic spectrum list the electromagnetic waves in ascending order of frequency. Fig 1.1 depicts the electromagnetic spectrum with wavelength and frequency for different regions. Electromagnetic spectrum consist of Radio waves, microwaves, infrared, visible light, ultraviolet, X rays and Gamma rays.

The term microwave has first appeared in the Italian Journal *Alta Frequenza* in a writing by Nello Carrarra and microwaves gain more attention during World War II. The term microwave was used to describe wavelengths less than about 30 cm (1- 300 GHz). Microwaves occupy a position in the electromagnetic spectrum which covers a wide range of all possible electromagnetic radiations. The spectrum is characterized by the wavelength which is inversely proportional to the frequency of the wave.

Since 1976 the Institute of Electrical and Electronics Engineers (IEEE) has been maintaining the standard letter designations for representing radar frequency band and recently and revised in 2002. The letter designations are assigned to frequency range which are spaced at intervals of about an octave from the frequency range 1 GHz to 300 GHz. The IEEE 521-2002 standard microwave frequency band designations and is given in table 1.1.

The microwave frequency bands are listed as follows.

Microwave Bands		
Designation	frequency	Wavelength
L Band	1 – 2GHz	30cm - 15cm
S Band	2 – 4GHz	15cm - 7.5cm
C Band	4 – 8GHz	7.5cm - 3.75cm
X Band	8 – 12GHz	3.75cm – 2.50cm
Ku Band	12-18GHz	2.50cm – 1.67cm
K Band	18 – 27GHz	1.67cm – 1.11cm
Ka Band	27 – 40GHz	1.11cm – 0.75cm
V Band	40 -75GHz	7.5mm – 4.0mm
W Band	75 -110GHz	4.0mm - 2.7mm
mm Band	110 – 300GHz	2.7mm – 1.0mm

Table 1.1 Microwave frequency bands

1.2 HISTORY OF RADAR

The history of radar extends to the time of modern electromagnetic theory. In 1886 Heinrich Hertz demonstrated reflection of radio waves and in 1900 Nicola Tesla explained the concept of electromagnetic detection and velocity measurement. Hulsmeyer, a German scientist performed ship detection by radio wave reflection in 1904.

In 1922 Taylor and Young of US National Research lab demonstrated ship detection by radar. In 1930 Hyland (NRL) first detected aircraft by radar and was patented by United States. This was a continuous wave radar. In 1936 the first pulsed radar was demonstrated. Only High frequency (HF) and Very high frequency (VHF) were used during that time. But by the invention of Magnetron by Massachusetts Institute of Technology, radar development began at microwave frequencies. By the end of World War II the value of radar and the advantages of microwave frequencies and pulsed radars were widely recognized. Military is still the dominant user of radar. Military applications include surveillance, navigation and weapons guidance.

Radars can be classified in many ways:

Pulsed Radar and Continuous wave radar: Pulsed radars use modulated pulses for transmission while continuous wave radars use modulated or unmodulated continuous waves. Transmitting power is comparatively high for pulsed radar. Continuous wave radars are usually used for speed measurements while pulsed radars are used in air traffic control.

Monostatic and Bistatic Radars: In monostatic radars the transmitter and receiver are placed nearby while or use the same antenna in bistatic radars they are placed at different locations. Bistatic radars are used in satellite fences where there is only one transmitter and several widely spaced receivers.

Another classification of radars is based on their frequency of operation. L band radars are generally ground based and ship based systems. These radars are used in long range military and air traffic control applications. S band radars are medium

range radars. These radars are also ground based and ship based. C band radars are primarily used for weather detection. Other applications of these radars include medium range search and fire control and metric instrumentation radars. X band is used for radar systems where the size of the antenna is a concern. Most multimode airborne radar comes under this category. Radar systems that require fine target detection capability and which cannot tolerate atmospheric weather attenuation also use X band. The K band radars are prone to atmospheric attenuation and is mainly used in police speed control radars. Millimeter wave radars are used for only short distance applications.

1.3 BACKSCATTERING FROM OBJECTS

1.3.1 Radar Cross Section

The term Radar Cross Section (RCS) is a measure the amount of scattered power from the target towards the radar when the target is illuminated by an electromagnetic wave. Radar cross section is the area which would intercept sufficient power out of the transmitted field to produce the given echo. The radar range equation is the basis for the design and operation of a Radar. The radar equation for free space propagation is given by

$$P_r = \frac{P_t G_t G_r \lambda^2 \sigma}{(4\pi)^3 R^4}$$

Where

P_t is the transmitted power

P_r is the received power

G_t is the transmitting antenna gain

G_r is the receiving antenna gains

λ is the operating wavelength

R is the range from the radar to target

σ is the RCS of the target

The reflected or scattered power by a target is the product of the effective area and incident power density. In general this area is called the scattering cross section of the target. RCS is an angle dependent target property. Physical area of the object is not related to RCS.

Electromagnetic waves with any specific polarization are scattered in all directions when incident on a target. The scattered waves have either the same polarization or a different polarization as that of the receiving antenna. If the polarization is different, the receiving antenna will not respond to the scattered back wave. The intensity of the backscattered energy that has the same polarization as that of the receiving antenna is used for defining the target RCS. Since the target is in the far field of the antenna the backscattered waves are plane waves.

If the target is located at a range R from the radar and let the power density of the electromagnetic wave incident on the target be P_i then the amount of reflected power back from the target

$P = \sigma P_i$ where σ is the target cross section.

The power density of the scattered waves at the receiving antenna is $P_r = P/4\pi R^2$

We get $\sigma = 4\pi R^2 \frac{P_r}{P_i}$. Since the target is located at a far distance the distance R can be approximated to infinity.

Therefore $\sigma = 4\pi R^2 \lim_{R \rightarrow \infty} \frac{P_r}{P_i}$ is defined as the backscattered RCS or Radar Cross Section. The physical area of the target is not related with RCS even though RCS is having the dimensions of an area.

But RCS is an angle dependent property of the target.

RCS can be expressed in terms of Electric and Magnetic field strengths also.

$$\sigma = 4\pi \lim_{R \rightarrow \infty} R^2 \frac{|E_s|^2}{|E_i|^2} = 4\pi \lim_{R \rightarrow \infty} R^2 \frac{|H_s|^2}{|H_i|^2}$$

Where E_s and H_s are the scattered electric and magnetic fields while E_i and H_i are the incident electric and magnetic fields.

The definition of radar cross section implies that the cross section is to be determined by taking the ratio of the magnitude of the scattered electric field to the incident electric field. Based on this definition σ will be a scalar quantity. To remove the dependence of the radar cross section on the radar polarization it is necessary to define σ as a tensor operator which relates the incident field to the scattered field. This tensor is called the scattering matrix.

RCS varies with frequency also. This variation can be classified into three regions by comparing the dimensions of the target to the wave length. If the target dimensions are small compared to wavelength it is called Rayleigh region. In the second region called resonance region target dimensions are approximately equal to the wavelength. In the third region the object dimensions are much greater than the wavelength. This region is called high frequency region. Radar cross section is usually expressed in square meters. In most cases it is expressed in logarithmic scale as dBsm. (Decibels over a square meter).

The understanding of the RCS of various objects is fundamental to the design of targets and the use of a radar. The predictions of RCS of objects with simple and complex structures is a difficult electromagnetic problem that has challenged scientists and engineers. The prediction of RCS using the basic principles of electromagnetic theory often leads to extensive computations. There is always the need to test theory and verify predictions. This can be accomplished only by means of measurements on test ranges.

The knowledge of the RCS characteristics of some simple targets are very important in RCS measurement and analysis. Complex targets such as missiles, ships, aircrafts etc. can be described as collections of relatively simple shapes like wedges, spheres, flat plates, cylinders, and corner reflectors, which approximate the overall target profile. Moreover if we are interested in measuring the RCS of complicated objects, the measurements are often calibrated by comparing the echo levels of test

objects with those of calibration target. As the echo strength of the calibration target must be known with high degree of accuracy, the calibration target is always a simple on

1.3.2 Radar Cross Section of Simple Shapes

Sphere, Flat plates, Dihedral Corner reflectors etc. are simple shapes which are used to model the RCS of complex targets like aircrafts and missiles [1].

1.3.2.1 Sphere

The sphere is the simplest three dimensional body. It is rotationally symmetric about the origin. For a sphere the radar cross section is independent of the angle of incidence and polarization of the radar signal [6].

It was one of the first shapes for which the exact solution for the wave equation was found.

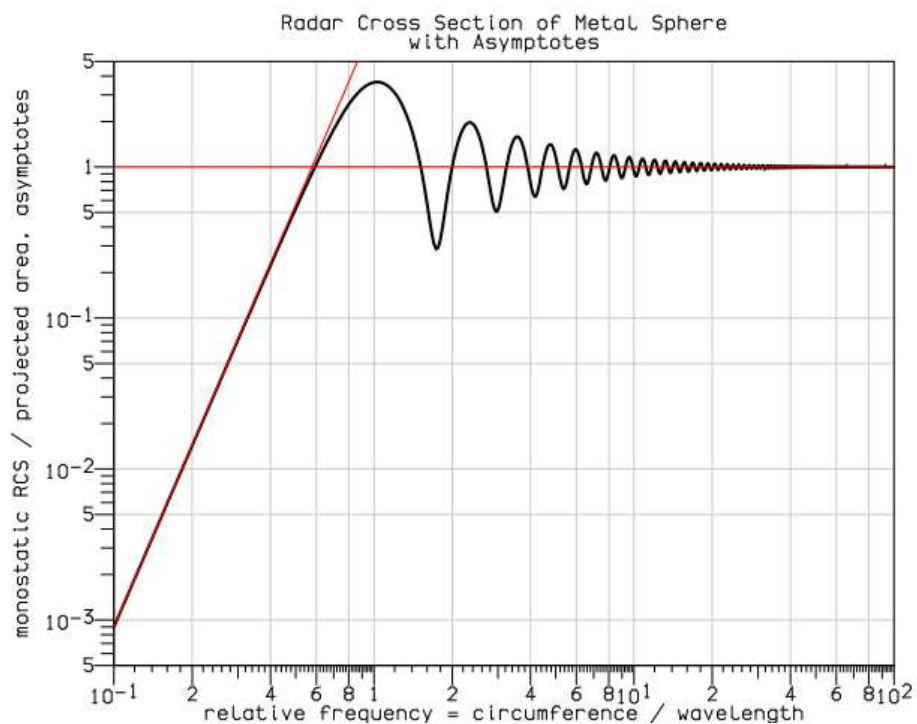


Fig 1.2 Plot of the radar cross section as a function of the electrical size of the target

A plot of radar cross section as a function of the electrical size of the sphere is shown in figure 1.2.

1.3.2.2 Flat plate

In flat plate multiple diffraction occurs due to the edges of the plate. For normal incidence the scattered wave within 30° to normal can be predicted accurately by physical optics [1], [7], [8], [9]. The RCS pattern of a flat plate is shown in Figure 1.3.

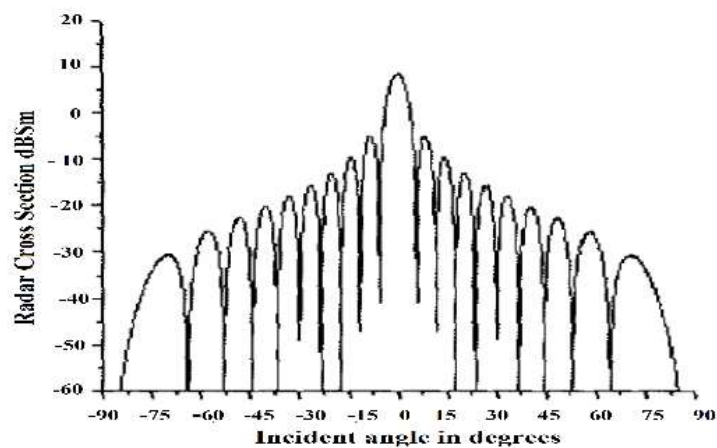


Fig 1.3 RCS pattern of a flat metal plate

1.3.2.3 Corner reflector

The intersection of two or three mutually perpendicular flat surfaces forms a corner reflector. The trihedral corner reflector has three faces. Due to triple internal bounce mechanism its scattering pattern is broad. Since the dihedral corner reflector is formed by the intersection of two flat surfaces, its pattern is in the plane perpendicular to the dihedral axis [10]. In this case also the pattern is broad due to a double bounce mechanism [11], [12].

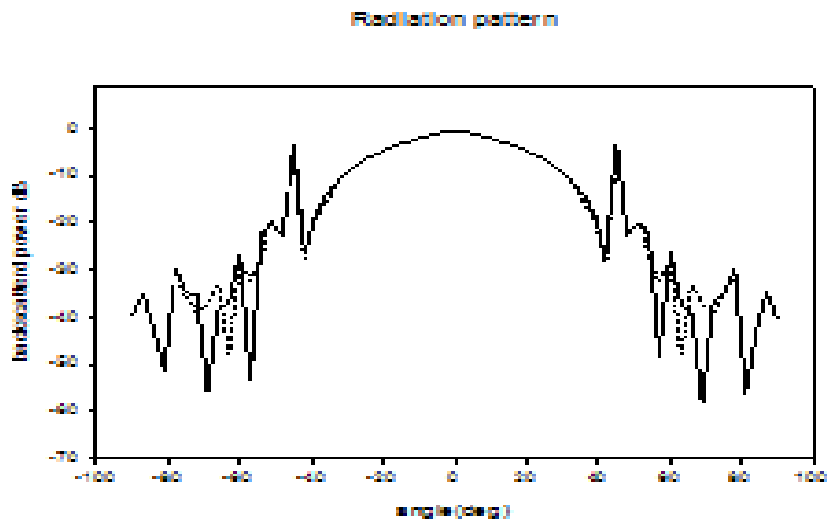


Fig 1.3 RCS pattern of dihedral corner reflector

Typical RCS pattern of a 90° dihedral corner reflector is shown in the figure 1.3. The broad central part of the pattern is due to the interaction between the two faces with the incident wave being reflected twice one from each face. The direct return from the individual faces forms the peaks at either side of the pattern. The ripples are due to the side lobes of the individual face patterns. If the dihedral corner angle is other than 90° the broad double bounce contribution can be reduced considerably.

The reduction in RCS from a dihedral corner reflector by varying intersection angle is given by

$$R = (k b \sin r \cos \gamma)^2$$

$\gamma = \arctan (b/a)$ where a is the width of the larger face and b is the width of the smaller face of the corner. The angle by which the faces of a dihedral corner varies is given by r . Since $k = 2\pi/\lambda$, the reduction in RCS also depends on frequency.

1.4 RCS REDUCTION METHODS

Electromagnetic scattering problems by reflectors, dielectrics and magnetic objects are very important in the study of reducing RCS of aircraft, missiles, rockets etc.

For defense applications visibility of the target is to be reduced to a maximum to the radar. So in this context radar cross section reduction is needed.

There are three basic techniques for reducing radar cross section.

They are Shaping, Radar Absorbing Materials, Passive cancellation and Active cancellation

1.4.1 Shaping of objects

Shaping of objects is an effective way for reducing target radar cross section. Target surfaces and edges which reflect back energy are reshaped such that energy is scattered away from the direction of the radar [5]. A reduction at one viewing angle may enhance RCS in another viewing angle. Dihedral and trihedral corners are major scattering centers of complex targets. For targets other than aircrafts RCS can be reduced by avoiding dihedral and trihedral corners such that surfaces are designed to intersect at obtuse or acute angles.

1.4.2 Passive cancellation

The amplitude and phase of echo produced by one source is cancelled by the echo produced by another source is the technique behind passive cancellation [5]. But this depends on frequency and so now this technique is obsolete.

1.4.3 Active cancellation

Active cancellation is a complex technique. The reflected waves from the target is cancelled by waves of proper amplitude and phase generated by the target [5]. This technique involves a lot of complexity and is only rarely used.

1.4.4 Radar Absorbers

Electromagnetic energy is converted to heat energy by Radar Absorbing Materials (RAM). Carbon was used in early absorbers. But these absorbers are fragile and bulky. These absorbers were replaced by magnetic absorbers due to their compactness. But magnetic absorbers are also very heavy. Iron ball paint absorber,

foam absorber, Jaumanns absorber, split ring resonator absorber, carbon nanotube and silicon carbide are some examples of radar absorbing materials.

1.5 RCS ENHANCEMENT

Whenever flat surfaces meet at an angle, corners and wedges are formed. The backscattering from these corners and wedges are an important standard in radar cross section studies [5]. The large echoes from corners arise from multiple reflections between the two mutually orthogonal flat surfaces dominating the backscattered pattern in the forward region. The large RCS of the 90° dihedral corner over a wide angular range makes it a suitable reference target in remote sensing and synthetic aperture radar applications. The RCS of dihedral corner reflectors with acute and obtuse corner angles is very small. A slight variation from the 90° corner angle reduces the RCS drastically. This is a major drawback in designing corner reflectors for the aforementioned applications.

For commercial aircrafts and ship navigation increasing visibility to the radar is needed. In this case enhancement of RCS is required.

1.6 SCATTERING PROPERTIES OF DIELECTRIC BACKED STRIP GRATINGS

Corrugated surface reflection gratings with rectangular grooves on a conducting surface have been studied by many researchers during the past few decades [13-22]. Perfect blazing, the complete conversion of the power of an incident electromagnetic wave to the diffracted wave can be achieved with these surfaces.

Schematic diagram of a corrugated surface is shown in figure 1.4.

According to Bragg's law of diffraction

$$\sin \theta_n = \sin \theta_i + n\lambda/d$$

where θ_i is the angle of incidence

θ_n is the angle of diffraction

$n = 0, \pm 1, \dots$ and λ is the wavelength and d is the period of the grating.

$n=0$ corresponds to specular reflection i.e. $\theta_n = \theta_i$

while $n = -1$ corresponds to blazing.

Perfect blazing to $n = -1$ spectral order for both TE and TM polarizations has been demonstrated. This shows that the strip gratings are simulating the effects of rectangular corrugated surfaces. Simultaneous elimination of specular reflection and backscattered power from a plane metallic surface by simulated corrugated surfaces of constant period and variable strip width for TM polarization was also reported. SCS with trapezoidal strip grating surface can eliminate specular reflection almost over the entire X band of frequencies for TM polarization. Metasurface gratings can reflect most of the incident power back in the path of incidence and with reduced power reflected in the specular direction. All these gratings used Euclidean geometries of metallization over a dielectric substrate.

When $d < \lambda/2$, the surface behaves as a plane conductor. Specular reflection can be reduced by increasing the period. Reflection gratings with rectangular and triangular grooves were used for eliminating specular reflections of both TE and TM polarizations.

Corrugated surfaces are difficult to fabricate and due to its weight loading it on a target for backscattering reduction is also inconvenient.

Low profile strip gratings, as shown in figure 1.5 is fabricated by etching metallic strips on a low loss dielectric substrate. These surfaces can perform similar scattering behaviors as a corrugated surfaces and are also called simulated corrugated surfaces (SCS). Metallic strip grating on a dielectric slab backed by a conductor are found to simulate the properties of corrugated surfaces. These surfaces have the advantages of ease of fabrication and light weight which finds wide applications in RCS control, frequency selective surfaces and antenna design. Gratings have been used in different applications such as frequency scanned reflector antennas, radar cross section, Littrow mounts and external cavity lasers.

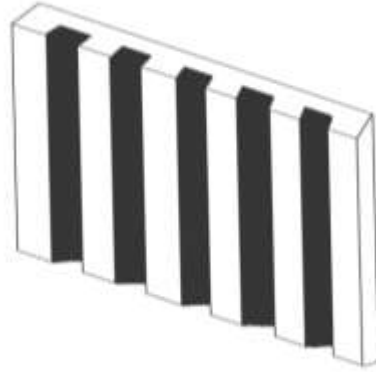


Fig 1.4 Schematic diagram of a corrugated surface

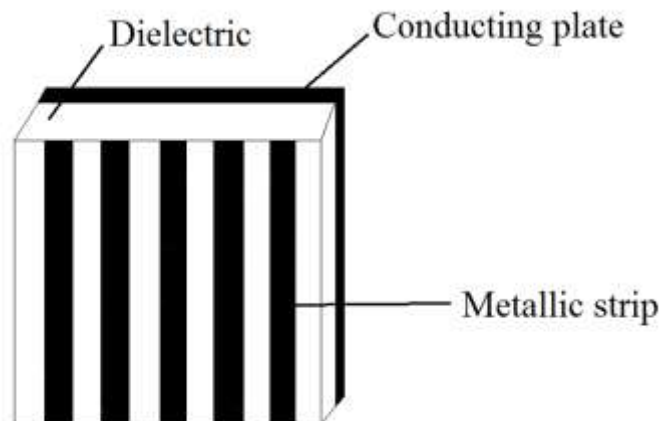


Fig 1.5 Schematic diagram of a strip grating

Perfect blazing to $n = -1$ spectral order for both TE and TM polarizations has been demonstrated [15], [20], [23]. This shows that the strip gratings are simulating the effects of rectangular corrugated surfaces. Simultaneous elimination of specular reflection and backscattered power from a plane metallic surface by simulated corrugated surfaces of constant period and variable strip width for TM polarization was also reported. SCS with trapezoidal strip grating surface can eliminate specular reflection almost over the entire X band of frequencies for TM polarization. Metasurface gratings can reflect most of the incident power back in the path of

incidence and with reduced power reflected in the specular direction. All these gratings used Euclidean geometries of metallizations over a dielectric substrate.

1.7 FRACTALS

The word fractal is derived from the word Greek “fractus,” meaning “fractured.” The self-similar structure of fractal geometry makes it different from the conventional Euclidian geometry. Its dimension is also non integer. In 1975 Mandelbrot introduced the concept of fractal geometry [24]. A fractal is a never ending pattern that repeats itself at different scales. This property is called self-similarity. If a fractal is magnified many times and after every step it will maintain the same shape, which is characteristic of that particular fractal. Although fractals are very complex they are made by repeating a simple process. Natural fractals include branching patterns like trees, river networks, lightning bolts, blood vessels etc. and spiral patterns like sea shells, hurricanes and galaxies. Mathematical fractals like the Mandelbrot set are formed by calculating a simple equation thousands of times feeding the equation back to the start in a loop. Fractals can be zoomed in forever making it infinitely complex. A tree grows by repetitive branching. A fractal triangle is formed by a simple repetition. The infinite Mandelbrot set is formed by repeating a simple calculation.

When a fractal is zoomed up the structure repeats. Fundamental building blocks cannot be found in fractals. Euclidean geometry has whole number dimensions while fractals have fractional dimensions. The length of coastlines, density of clouds, branching of trees were difficult to be measured by Euclidean geometry, but fractals made it possible. There was in need of a geometry which can handle problems which cannot be done by Euclidean geometry and fractals solved such complex situations.

Some examples of fractals are shown in figure 1.6

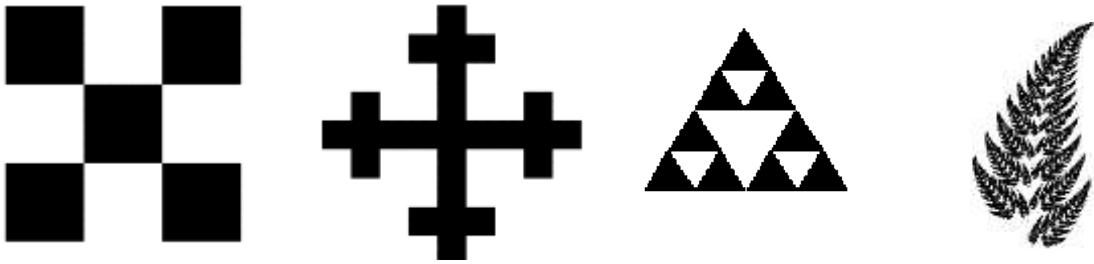


Fig 1.6 Simple fractal geometries

Some of the deterministic fractal structures are Sierpinski gasket, Sierpinski carpet, cantor bar etc. For example, a Sierpinski gasket fractal is constructed by taking a filled equilateral triangle as the 'initiator' and an operation which excises an inverted equilateral triangle as the 'generator' which is the initiator inverted and scaled by one half. Each stage of fractal growth is found by applying the generator, or its scaled replica, to the initiator. The initiator governs the gross shape of the fractal structure while the generator provides the detailed structure and ensures self-similarity and long range correlation. Repeated scaling and application of the generator yields a structure as shown in figure 1.7. The Sierpinski triangle is formed by repeatedly removing the middle triangle from the prior generation. The number of triangles increases by a factor 3 in each step 1, 3, 9, 27, 81 etc.

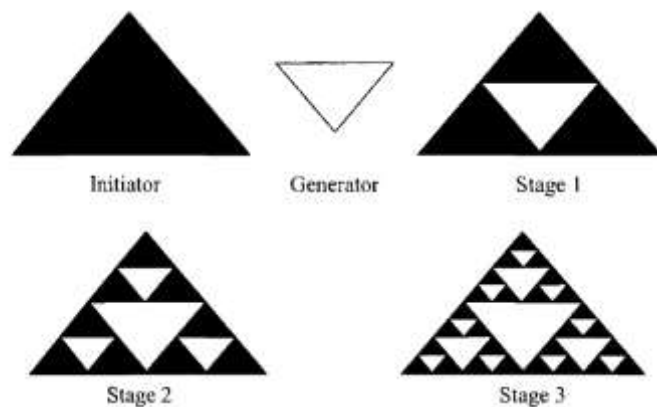


Fig 1.7 Initiator and different stages of sierpinski gasket

Sierpinski Carpet is different from Sierpinski Gasket in which the initiator is a square and generator is small filled square of $1/3$ of the initiator as shown in figure 1.8

Different iterated stages of the Sierpinski Carpet can be repeated in two dimensions to create a Sierpinski Carpet Fractal (SCF) array. Figure 1.8 shows a 4×4 array of first, second and third iterated stages of the SCF array.

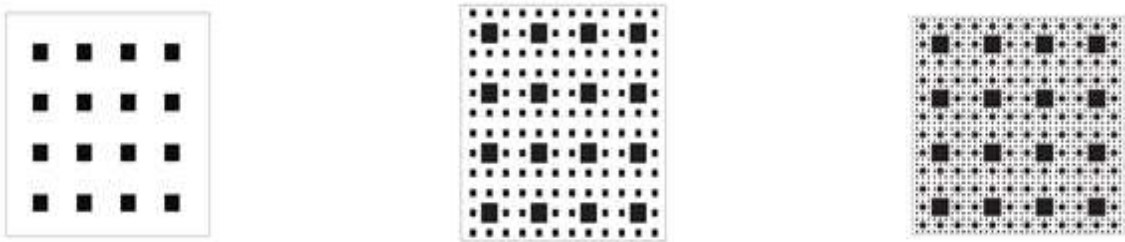


Fig 1.8 4×4 Sierpinski carpet fractal arrays of first second and third iteration

1.8 FRACTAL ELECTRODYNAMICS

Ever since fractals were mathematically re-invented by Mandelbrot, fractals have found wide spread applications in several branches of Science and Engineering. Disciplines such as Science, geology, remote sensing, material science, image processing etc. has have benefitted significantly by fractal modelling.

Another important area is fractal Electrodynamics, [25] in which fractal geometry is combined with electromagnetic theory for the purpose of investigating a new class of radiation, propagation and scattering problems. One of the important areas of fractal electrodynamics is in its application to antenna engineering, with the invention of a variety of antennas for multiband operation and miniaturization.

Scattering and diffraction from fractal screens have been studied extensively. Diffraction fields from self-similar Sierpinski gasket in the Fraunhofer zone have been shown to be self-similar. Some of these studies indicate that scattering patterns fractal geometries have features of those geometries imprinted on them. The use of

fractal geometries in the design of Frequency selective surfaces have been investigated by many researchers and very useful results have been obtained.

1.9 MOTIVATION OF THE PRESENT WORK

Complex targets like aircrafts, ships, etc. can be modeled by a combination of objects like plane plates, dihedral corner reflectors, wedges etc.

Several researchers have explored the concept of backscattering reduction using strip gratings and fractal structures. Instead of conventional Euclidean based strip gratings and simple fractal geometry structures a Sierpinski Carpet Fractal (SCF) array is utilized in scattering applications for reduction in backscattering from plane metallic plates and 90^0 dihedral corner reflectors which produce considerable backscattered power. In defense applications the target detectability is reduced only if backscattering is considerably reduced. The feasibility of using a simple SCF array for backscattering reduction by loading dielectric backed SCF array of various iterated stages is considered in the proposed work. The possibility of using the same SCF array in areas of non-defense applications like commercial aircrafts and ships. Wedge like surfaces form part of these complex targets and an enhancement in backscattering is desirable.

From literature, it can be seen that some structures which produce a reduction in backscattering from plane plates and 90^0 dihedral corners produce an enhancement when loaded over corner reflectors with angles other than 90^0 .

Exploring the possibility of using the proposed SCF array of various iterations for enhancement in backscattering is also a motivation behind the work.

1.10 ORGANISATION OF THE THESIS

The Thesis entitled “Investigations on the Backscattering Properties of Metallic Objects loaded with Dielectric Backed Fractal Structures” is organized in 7 Chapters.

A brief review of the work done in the field of scattering, back scattering reduction and RCS reduction using corrugated surfaces, strip gratings and fractals are presented in chapter 2.

In chapter 3 description of the methodology adopted for measuring Radar cross section of Flat plate, Corner reflector and Wedge is presented.

Chapter 4 discusses the scattering behavior of flat metal plates by loading Sierpinski Carpet Arrays of various iterations. Experimental results showing elimination of specular reflection and there by RCS reduction is discussed in detail.

In Chapter 5 scattering behavior of dihedral corner reflectors loaded with dielectric backed fractal array is investigated.

Ships and commercial aircrafts need more detectability by a radar. Here wedge shaped metallic surfaces contribute to the external structure. Scattering properties of metallic wedge can be enhanced by loading dielectric backed SCF array. This study is investigated in Chapter 6.

Conclusions based on experimental results are illustrated in Chapter 7. The scope for future work based on SCF Array based fractal gratings are also discussed in this chapter.

REFERENCES

- [1] E F Knott "Radar Cross Section" Its Prediction, Measurement and Reduction, Artech House 1985.
- [2] H. Kobayashi and K. Hongo, "Scattering of electromagnetic plane waves by conducting plates," *Electromagnetics*, vol. 17, no. 6, pp. 573-587,1997.
- [3] William B. Gordon "Far-field approximations to the Kirchhoff-Helmholtz representations of scattered fields," *IEEE Trans. Antennas Propagation*, vol. AP-23, 1975.

-
- [4] R. J. Wagner and P. J. Lynch, "Theorem on electromagnetic backscatter," *Phys. Rev.*, vol. 131, pp. 21-23, 1963.
- [5] M. I. Skolnik, *Introduction to Radar Systems*, 3rd Edition, McGraw-Hill, New York, 2001.
- [6] V. V. Liepa and T. B. A. Senior, "Modification of the scattering behavior of a sphere by loading", *Proc. of IEEE*, Vol. 53, pp. 1004-1011, Aug 1965.
- [7] Gökhan Apaydin, Feray Hacivelioglu, Levent Sevgi, William B. Gordon, Pyotr Ya Ufimtsev, "Diffraction at a Rectangular Plate: First-Order PTD Approximation" *IEEE Transactions on Antennas and Propagation*, Volume: 64, Issue: 5, May 2016.
- [8] R. A. Ross, "Backscattering from square plates illuminated with vertical polarization," *IEEE Trans. Antennas Propag.*, vol. 54, no. 1, pp. 272-275, Jan. 2006.
- [9] Gökhan Apaydin, Feray Hacivelioglu, Levent Sevgi, William B. Gordon, Pyotr Ya Ufimtsev, "Diffraction at a Rectangular Plate: First-Order PTD Approximation" *IEEE Transactions on Antennas and Propagation*, Volume: 64, Issue: 5, May 2016.
- [10] P. Corona, G. Ferrara and C. Gennarelli "Backscattering by loaded and unloaded dihedral corners" *IEEE Transactions on Antennas and Propagation*, Vol 35 , No 10, October 1987.
- [11] T. Griesser and C. Balanis "Backscatter analysis of dihedral corner reflectors using physical optics and the physical theory of diffraction", *IEEE Transactions on Antennas and Propagation* Vol 35, Issue: 10, October 1987.
- [12] T. Griesser and C. Balanis "Dihedral corner reflector backscatter using higher order reflections and diffractions" *IEEE Transactions on Antennas and Propagation* Volume: 35, Issue: 11, November 1987.

- [13] K.A. Jose, P. Mohanan, K.G. Nair and N. Sridhar “Effect of periodic strip structure on reduction of radar cross section of planar surfaces” Digest on Antennas and Propagation Society International Symposium June 1989.
- [14] V. Ajaikumar, K. A. Jose, C. K. Aanandan, P. Mohanan, and K. G. Nair “Backscattering reduction of corner reflectors using SCS techniques”, Microwave and Optical Technology Letters Vol 5, No 11, October 1992.
- [15]. K.A. Jose and K.G. Nair, “Reflector-backed perfectly blazed strip gratings simulate corrugated reflector effects,” Electronics Letters, Vol 23, No 2, January 16, 1987.
- [16] K.A. Jose, C.K. Aanandan and K.G. Nair “Low backscattered TM-polarised strip gratings, Electronics Letters, Vol 23 , No 17 , August 1987.
- [17] D. Saji Stephen, Thomaskutty Mathew, P. Mohanan, and K. G. Nair “A modified strip grating for dual periodicity for RCS reduction, “Microwave and Optical Technology Letters, Vol7, No 7, May 1994.
- [18] D. S. Stephen, T. Mathew, K. A. Jose, C. K. Aanandan, P. Mohanan and K. G. Nair, “New Simulated corrugated Scattering Surface giving wideband characteristics,” Electronic Letters, Voi.29, No 4, February 1993.
- [19] Thomaskutty Mathew, D. Saji Stephen, K. A. Jose, C. K. Aanandan, P. Mohanan and K. G. Nair “The performance of a novel simulated corrugated surface for the reduction of radar cross section” Microwave and Optical Technology Letters, Vol. 6, No. 10, August 1993.
- [20] T. Mathew, D.S. Stephen, C.K. Aanandan, P. Mohanan and K.G. Nair “Wideband trapezoidal strip grating for elimination of specular reflection” Electronics Letters, Volume: 30, Issue: 13, 23 Jun 1994.
- [21] T. Mathew, S.D. Saji, C.K. Aanandan, P. Mohanan and K.G. Nair “Development of a blazed reflection grating with enhanced bandwidth and angular range giving circularly polarised backscattering” IEEE Antennas and Propagation Society International Symposium. June 1995.

-
- [22] K A Jose, C K Aanandan, P Mohanan and K G Nair “Moment method solution for the RCS of a strip grating backed with reflector” Antennas and Propagation Society Symposium June 1991.
- [23] Xiaqiang Li, Mohammad Memarian, Kirti Dhvaj and Tatsuo Itoh “Blazed Metasurface Grating: The Planar Equivalent of a Sawtooth Grating” IEEE MTT-S International Microwave Symposium (IMS) May 2016.
- [24] Mandelbrot, B. “The Fractal Geometry of Nature” W. H. Freeman and Co.: New York, 1982.
- [25] Werner D. H and Ganguly S “An Overview of Fractal Antenna Engineering Research” IEEE Antennas Propagation. Magazine, Vol 45,

2 LITERATURE REVIEW

This chapter gives a review of the past works in the related field. The research works in the field of Backscattering and scattering properties of corrugated surfaces are reviewed. It also presents review of Scattering properties dielectric backed strip gratings, dihedral corner reflector and wedges are also reviewed. Literature related to fractals, fractal electrodynamics and fractal arrays are also reviewed.

TABLE OF CONTENTS

- 2.1 Electromagnetic Scattering**
- 2.2 Scattering Properties of Corrugated Surfaces**
- 2.3 Back Scattering Reduction Using Strip Gratings**
- 2.4 Fractals**
- 2.5 Fractal Electrodynamics**
- 2.6 Fractal Arrays**

2.1 ELECTROMAGNETIC SCATTERING

The scattering from various objects is a subject of immense interest in electromagnetics and was studied by many researchers in various frequency ranges of the electromagnetic spectrum for wide variety of applications from radio frequency to optical range [1].

Joseph B Keller presented geometrical theory of diffraction as an extension of geometrical optics which accounts for diffraction [2]. The diffracted rays are produced by incident rays which hit edges, corners, or vertices of boundary surfaces, or which graze such surfaces. Based on electromagnetic theory the mathematical justification of the theory was also done.

R. A Ross presented an analytical formulation suitable for the estimation of radar cross section of rectangular flat plates using scattering theory [3]. Calculations based upon the geometrical theory of diffraction show excellent agreement with measured data except at edge-on aspects. Geometrical diffraction theory provides a significant improvement over conventional physical optics in the estimation of the radar cross section of rectangular flat plates

C A Balanis et al reviewed high frequency diffraction studies of last fifty years illustrating the theories and emphasizing their application in antennas and scattering problems [4]. Physical theory of diffraction, uniform theory of diffraction, geometrical theory of diffraction and their alternatives were discussed. An in depth analysis of scattering by a wedge and backscattering from a trihedral cone were done as an illustration of these theories.

Piergiorgio L. E. Uslenghi presented different conditions for zero backscattering [5]. A body with a relative surface impedance ± 1 which is axially symmetric in terms of both geometric and material properties is considered and the constitutive parameters to ensure a zero backscattered field are derived.

William B. Gordon calculated scatter from surfaces with zero curvature [6]. The reduction of physical optics scattering integral to a contour integral is used for the calculation. Plane surfaces, cylinders and cones were analyzed for the scattering calculations.

The near field backscatter from a flat plate illuminated by a dipole source was analyzed using contour integral evaluated around the boundary of the plate [7]

The same authors presented far field analysis of the fields scattered by a flat metal plate [8]. The surface integral of far field approximation for Kirchhoff-Helmholtz formula of scattered field from a flat metallic plate is reduced to line integral which help in reducing the sampling for numerical calculations.

Hey and Senior made an analysis of electromagnetic scattering by a thin conducting plate [9]. The extension of rigorous theoretical results on infinite edges were used to derive currents in finite edges. Also it was shown that currents in the plates are predominant near the edges.

E Knot et al analyzed backscattering from the edges of a rectangular plate [10]. The contribution of the front edge is analogous to that of a wire illuminated by a plane wave, but the rear edge excitation is almost wholly determined by current waves along the side edges of the plate.

H. Kobayashi and K. Hongo studied the scattering of electromagnetic plane waves by arbitrary shaped conducting plates using the physical theory of diffraction [11]. By applying the stationary phase method of integration, simple asymptotic expressions for arbitrarily shaped convex plates were derived. Based on the derived expressions, physical theory of diffraction solutions for convex and rectangular plates were also presented.

R. Alexander Ross analyzed backscattering from square plates illuminated with vertical polarization [12]. Backscattering from a square flat plate was described as a function of aspect angle. This theory accurately predicts the radar cross section of square plates as small as 3 wavelengths on a side. The approach is suitable for treating arbitrary angles of incidence and observation for rectangular and triangular plates.

Gokhan Apaydin et al developed first order approximation of physical theory of diffraction for the field scattered at a perfectly conducting rectangular plate [13]. Analytical investigation of the fringe waves from all four edges were done. Detailed analysis of scattering and grazing incidence have been demonstrated by comparing experimental data with computed results using method of moments.

V V Liepa and Senior investigated the scattering of a plane electromagnetic wave by a metallic sphere loaded with a circumferential slot in the plane normal to the direction of incidence [14]. In the case of backscattering, numerical results agree well with experimental measurements made using a sphere with an equatorial slot backed by a radial cavity of adjustable width.

C. Mullin, R. Sandburg and C. Velline reported a numerical technique for the determination of scattering cross sections of infinite cylinders of arbitrary geometrical cross section [15]. An infinitely long cylinder of arbitrary cross section is assumed for the scattering calculation using this method. Monostatic and bistatic cross sections were calculated for both circular and elliptical cylinders. For the case of monostatic scattering from circular cylinders a numerical check is possible and the result was in agreement with Mie series calculations to six significant figures.

Adour V. Kabakian and Amit M. Patel presented surface impedance method for backscattering reduction of long thin bodies [16]. In this method long thin bodies were assumed as travelling wave antennas. A modulated impedance coating is applied to radiate the surface waves away from the illumination source, thus eliminating backscattering.

2.1.1 Scattering from Dihedral Corner

E. Knott developed a criteria for the radar cross section reduction of dihedral corners [17]. Corner reflectors are the dominant contributor of monostatic radar cross section in ships and military vehicles. Flat surfaces meeting at right angles will contribute more to the radar cross section and have to be avoided.

P. Corona, G. Ferrara and C. Gennarelli presented a mathematical model for the backscattering from a loaded dihedral corner reflector [18]. For this a generalization of physical optics is considered taking into consideration the lighting of each face by the rays diffracted by the edge of the other one. The inclusion of the currents due to the diffracted fields in the physical optics current distribution has been found relevant in the solution of the referred problem.

T. Griesser and C. Balanis presented an analysis of the dihedral corner reflectors using both physical optics and the physical theory of diffraction [19]. The backscattering cross sections of the dihedral corner reflector in the azimuthal plane for both vertical and horizontal polarizations are considered. Though geometrical optics is simple and readily amenable to computer solutions physical optics can yield significant improvements in accuracy.

They have also predicted the backscattering cross section of a dihedral corner reflector using higher order reflections and diffractions [20]. The uniform theory of diffraction plus an imposed edge theory of diffraction is used in the analysis. Dihedral corners with right, acute and obtuse included angles are considered.

2.1.2 Scattering from a Wedge

S Kameyama et al analyzed the reflected and diffracted fields by one or two wedges and compare the effects that wedge shapes and materials give to the reflected and diffracted fields for horizontal and vertical polarized incidence [21]. The numerical results show that for one or two wedges, wedge shapes, materials and incident polarization don't give significant effect to diffracted fields, but the waves incident close to the wedge surfaces are affected by them.

2.2 SCATTERING PROPERTIES OF CORRUGATED SURFACES

A Hessel and J Schmoys presented Bragg condition as a necessary condition for perfect blazing for both TE and TM polarizations [22]. The Bragg condition is presented as a necessary condition for perfect blazing of infinite, perfectly conducting diffraction gratings that produce only a single diffracted order $n = -1$.

J. L. Roumiguieres, D. Maystre, and R. Petit investigated the possibility of making perfectly conducting rectangular-groove gratings for both TE and TM polarizations [23]. The direction of the diffracted waves were in the $n=-1$ spectral order i.e. in the exact opposite direction of the incident wave. These blazed gratings work in the infrared and microwave regions and can be used in Littrow mount.

E V Jull reported rectangular corrugated surfaces which can convert linearly polarized incident waves to circularly polarized waves [24]. Normal incidence and an incident angle of 45 degree are considered for the design of the corrugated surface.

James W Heath and E V Jull presented total backscattering from conducting rectangular corrugations [25]. For TE or TM polarization or both simultaneously rectangular groove corrugations can completely convert specular reflection from a conducting surface to backscatter.

W. Chen, N. C. Beaulieu, D. G. Michelson, and E. V. Jull presented off-Bragg blazed rectangular groove gratings [26]. Aspect ratio a/d between 0.5 and 0.75 results in off Bragg blazed gratings. Off-Bragg blazing can be used in high efficiency frequency scanning antennas, multiplexers and demultiplexers in quasi-optical millimeter-wave systems.

E V Jull and Gordon R Ebbeson reported corrugated surfaces which can be used for reducing interfering reflections from buildings near airport runways [27]. H polarized plane waves illuminating a rectangular comb grating with grating spacing $h/2 < a < h$ can completely convert specular reflection to backscatter.

James W Heath and E V Jull analyzed perfectly blazed reflection gratings with rectangular grooves [28]. Perfect blazing with arbitrary polarization for near grazing incidence is shown to be possible in principle with deep wide grooves. For narrow groove widths experimental results are compared with theoretical results but is giving good agreement only for TM polarization only.

E V Jull et al presented the triangular groove gratings for the simultaneous TE and TM polarizations [29]. Experimental and numerical verification of the profile is also done and efficiency of 99.9 percent was reported at a frequency of 35 GHz.

Vietti et al presented a numerical validation of the concentric square rings backscattering for reflect array applications [30]. The structures used in the printed reflectarray provide enhanced bandwidth. .

Young-Huang Chou et al analyzed the performance of a grating metal surface with broad and flat backscattering field pattern [31]. Method of moments and Floquet's theorem are used to solve the induced current and backscattered fields of the planar structure. This can be used in vehicular collision avoidance systems at an operating frequency of 77 GHz.

Haijian Hou and Junhong Wang studied the scattering property of a square patch gradient index metasurface [32]. The metasurface designed to transform incident wave to surface wave reduced backscattered RCS by 16dB.

R. A. Hurd and E. V. Jull analyzed the theory of reflection gratings with narrow grooves [33]. Using conformal transformation technique, the scattering of a plane H-polarized wave from a grating composed of narrow grooves in a perfectly conducting surface is investigated theoretically. An exact integral equation is derived and then simplified by applying quasi-static approximations. This analysis can be applied to corrugated surfaces for multipath interference suppression.

S.V. Maly presented the numerical analysis of electromagnetic scattering by arrays that have periodic structures [34]. The proposed technique may be used in ultra wide band applications.

A. Lakhtakia et al presented self-similarity in diffraction by self-similar fractal screen [35]. In problems involving array synthesis use of fractal structures like Sierpinski gasket will ease the process.

2.3 BACK SCATTERING REDUCTION USING STRIP GRATINGS

C.M. Shiao and S.T. Peng presented an analysis of current distribution induced on a metal-strip grating by an incident plane wave [36]. The finite conductivity of the metal strips of the grating are characterized by a complex permittivity with large imaginary part. The mode-matching method is used to formulate the scattering problem to determine the scattering fields everywhere. Numerical results are given to illustrate the effects of the dielectric constant of the

surrounding media, as well as the incident angle and polarization on the current distribution induced by an incident plane wave.

T.L. Zinenko, A.I. Nosich and Y. Okuno presented plane wave scattering by resistive and dielectric strip gratings [37]. The dependences of the transmitted, reflected, and absorbed power fractions on the electrical and material parameters are presented.

K.A. Jose, P. Mohanan, K.G. Nair and N. Sridhar presented the effect of periodic strip structure on reduction of radar cross section of planar surfaces [38]. A numerical analysis to the problem of periodic metallic strips on a dielectric sheet above the ground plane is considered. The numerical results agree well with experimental results and the authors propose the use of this low backscattered surface for RCS reduction applications.

V. Ajaikumar et al reported backscattering reduction of corner reflector using simulated corrugated surface [39]. Stationary Corner reflectors of 900 were the main interest in this study since they are involved in many targets and normally show an enhancement in radar cross section. A typical reduction of 40-50 dB is achieved using this method.

Jose and Nair [40] demonstrated that rectangular corrugations on conducting surfaces can be simulated by strip gratings. Conducting strips of proper spacing gave good results of perfect blazing. For perfect blazing by corrugated surfaces the groove depth have to be equal to $\lambda/4$. This makes it necessary to maintain a minimum thickness which cannot be reduced further. This problem can be solved by the use of strip gratings. Both TE and TM polarizations satisfied the condition for perfect blazing.

Elimination of specular reflection from conducting surfaces at normal and near normal angles were reported by Jose et al [41] using strip gratings which cannot be done by corrugated surfaces. Use of self-complementarity strip gratings which were not possible using conventional metallic corrugated gratings helped to achieve this goal.

D S Stephan et al reported Simulated Corrugated Surface (SCS) gratings with strip width varying in geometric progression giving wide band width [42].

D.S Stephen et al reported simultaneous elimination of specular reflection and backscattered power from a plane metallic surface by simulated corrugated surfaces of constant period and variable strip width for TM polarization [43]. A modified strip grating with dual periodicity for RCS reduction is reported. Elimination of specular reflection for wide range aspect angles for TE polarization is achieved. This overcomes the main disadvantage of conventional strip grating which eliminates specular reflection for a limited angle of incidence only.

Thomaskutty Mathew et al reported the development of a new simulated corrugated surface which eliminates specular reflection and backscattering simultaneously [44]. Non Bragg blazing was achieved for both TE and TM polarizations. This can simulate the performance of 3D metallic corrugations and can be used for radar cross section reduction and frequency scanning.

T Mathew et al reported a trapezoidal strip grating surface that eliminates specular reflection almost over the entire X band of frequencies for TM polarization [45]. This metallo-dielectric structure overcomes the bandwidth limitations of conventional rectangular strip gratings. A reduction of -40 dB is achieved over a wide frequency range of 3.6 GHz using the trapezoidal strip grating. The gradual change in strip width results in a large number of elementary gratings with various width which resonates at different frequencies. This explains the increase in bandwidth.

T Mathew et al presented the development of a V shaped blazed reflection grating giving circularly polarized backscattering [46]. TM polarized electromagnetic waves can be completely backscattered to circularly polarized waves by this grating. Elimination of specular reflection over wide angular range and enhanced bandwidth compared to ordinary rectangular strip gratings were also achieved.

K A Jose et al reported a moment method solution or the radar cross section of a strip grating backed with reflector [47]. The point matching method which is simple and effective for the calculation of reflected and scattered field from periodic strip grating structure is utilized in the analysis. The theoretical results were verified with measured experimental data and strip gratings reduced radar cross section of metallic surfaces effectively.

X. Li et al reported a blazed metasurface gratings as the planar equivalent of a non-planar saw tooth grating [48]. This metasurface can reflect most of the incident power back in the path of incidence and with reduced power reflected in the specular direction. Theoretical results were validated by experimental measurements and this metasurface may find applications from microwave to optical frequencies.

M Memarian et al reported wide band/angle blazed surfaces using multiple coupled blazing resonances [49]. Multiple blazing resonances are combined similar to the case of coupled resonator filters forming a blazing passband between the incident wave and the first grating order. Blazed gratings with single and multiple blazing passbands are fabricated and measured showing increase in band width of specular reflection rejection demonstrated at X band.

All these blazed gratings used Euclidean geometries of metallizations over a dielectric substrate.

2.4 FRACTALS

Mandelbrot explains fractal geometry in the book Fractal geometry of nature [50]. Conventional ideal shapes like triangles, squares, circles, spheres etc. forms the basic building blocks of Euclidian geometry which is the geometry studied in high school mathematics. Shapes in nature like clouds, lightning, coastal lines, waterfalls, mountains etc. cannot be pictured by Euclidian geometry. Fractals emerged as a means of describing these irregular shapes in nature. Mandelbrot defined fractal as a rough or fragmented geometric shape that can be subdivided in parts each of which is a reduced size or copy of the whole

Fractals have the following properties

- (i) Self-similarity (ii) fractal dimension and (iii) formation by iteration.

In Euclidian geometry the dimension is always an integer. Fractals are geometrical objects with non-integer or fractal dimensions. Fractals are created by mathematical formula using iterative techniques.

Munesh Chandra et al presented iterative procedures in generating Sierpinski carpet [51]. The Sierpinski carpet was generated with square as the initiator and then using superior iterations.

2.5 FRACTAL ELECTRODYNAMICS

Dwight L. Jaggard and Xiaoguang Sun considered the problem of scattering from a corrugated surface [52]. In this paper the physical optics approach is used to investigate scattering from perfectly conducting fractal surfaces.

S. Savaidis, P. Frangos, D. L. Jaggard and K. Hizanidis formulated scattering from fractally corrugated surfaces with use of the extended boundary condition method [53]. Generalized Floquet modes were used to expand the fields and analytical closed-form expressions for the scattering amplitudes were obtained for both horizontal and vertical polarization of the incident electromagnetic waves.

C. Puente, J. Romeu, R. Pous and X. Garcia and F. Benitez presented a fractal antenna based on the Sierpinski gasket [54]. A multiband behavior over five bands were reported with the experimental measurements and computational analysis of this fractal antenna.

C. Puente, J. Romeu, R. Bartolemi and R. Pous proposed the Perturbation of the Sierpinski antenna to allocate operating bands [55]. The spacing between the bands of the Sierpinski antenna were modified. Experimental results suggest that the fractal structure can be perturbed to change the log-period keeping the multiband behavior of the antenna.

R Ghathak et al proposed a Perturbed Sierpinski Carpet Antenna with CPW Feed for wireless LAN applications [56]. A modified Sierpinski carpet geometry in planar monopole configuration is used to achieve the desired resonance characteristics. The measured antenna gain of 3.5 dBi at the lower band and 4.5 dBi at the higher band was in close agreement with the simulated results.

Homayoon Oraizi and Shahram Hedayati proposed the combination of two fractal geometries for the design of a fractal monopole antenna [57]. First iteration of Giuseppe Peano fractal and Sierpinski carpet fractal are combined to construct this ultra wideband antenna. The antenna gave omnidirectional radiation pattern and a good gain with high radiation efficiency.

Douglas H. Werner and Suman Ganguly presented an overview of fractal antenna engineering research [58]. The unique properties of fractals can be utilized for multiband behavior with compact size. The application of fractal concepts to the design of antenna arrays is also emphasized. Reconfigurable systems can also make use of fractal concepts.

D.H. Werner et al presented genetically engineered multiband fractal antennas [59]. A size reduction of 30 to 55 percent can be achieved by this method. This study gave an insight into the design of miniaturized multiband fractal antennas.

2.5.1 Sierpinski Carpet Fractals

G.J. Walker and J.R. James introduced the concept of fractal volume antennas [60]. The fractal volume concept was applied to a microstrip patch antenna. This increased the degree of design freedom associated with fractal antenna elements and hence improve their input matching characteristics.

Anupam et al studied metallo-dielectric structure with fractal based metallization for backscattering reduction [61]. Backscattering reduction for both TE and TM polarization is achieved by employing a metallo-dielectric structure with a Sierpinski carpet fractal based metallizations. A reduction in backscattered power of

~30 dB is obtained for normal incidence in the X band with third iterated stage of the fractal geometry.

In [62] scattering behavior of metallo-dielectric structures based on sierpinski carpet fractal geometry with superstrate loading is reported. The frequency for backscattering minimum can be controlled with the superstrate thickness for both TE and TM polarizations.

Anupam et al analyzed the behavior of fractal based metallo-dielectric structures for the control of RCS for various objects [63]. The square Sierpinski carpet structure gave backscattering reduction over a wide range of frequencies compared to other fractal geometries.

Chandran et al. reported radar cross section enhancement of dihedral corner reflector using fractal based metallo-dielectric structures [64].

E. L Barreto et al proposed a new fractal antenna array for wireless application [65]. The simple structure and compact size of this antenna array is its advantage such that it can be easily integrated in miniature devices.

Lehman investigated fractal diffraction gratings built through rectangular domains. In this work the correlation between the method to build fractal gratings and the intensity distribution for diffracted fields in the Fraunhofer region is studied [66].

A theoretical and experimental investigation of an optical fractal antenna using Sierpinski carpet was done by T L Cheng [67].

J.P. Gianvittorio, J. Romeu, S. Blanch and Y. Rahmat-Samii reported a frequency selective surface for multiband and dual polarized applications using fractal iterative techniques [68]. Two or three stop bands were attained depending on the number of iterations utilized for generating the geometry of the cell. Due to the symmetry of the geometry these frequency selective surfaces are dual polarized.

R.V. Hara Prasad, Y. Purushottam, V.C. Misra and N. Ashok proposed a square microstrip fractal patch antenna for three band operation [69]. A gain greater

than 7dB and a return loss better than 10 dB were achieved with this Sierpinski carpet antenna. This microstrip fractal antenna can be used for wireless, satellite and mobile communication.

Zhengwei Du, Ke Gong and J.S. Fu and Baoxin Gao analyzed the above Sierpinski carpet fractal antenna using FDTD method [70]. The multiband frequency operation of the antenna resulted from the driven element and the effect of the parasitic elements is negligible according to the study.

2.6 FRACTAL ARRAYS

S C Patricio et al presented the development of a printed antenna array based on Sierpinski carpet fractal elements [71]. By ensuring the radiation beam maximum direction in the perpendicular plane of the array axis, the array directivity is increased.

D.H. Werner et al presented an efficient recursive procedure for evaluating the impedance matrix of linear and planar fractal arrays [72]. These fast recursive algorithms were developed using the self-similar properties of fractal arrays. The methodology was demonstrated by uniformly exciting a triadic cantor linear fractal array and a Sierpinski carpet planar fractal array.

S. Costanzo and F. Venneri proposed a reduced size reflect array element based on Minkowski fractal [73]. The miniaturization capability of the fractal geometry is used to achieve the smaller interelement spacing. The fractal-shaped X-band reflectarray elements embedded into a $0.3\lambda \times 0.3\lambda$ cell is demonstrated. The experimental validation of the design is done by a 15×15 reflectarray prototype.

D.H. Werner, R.L. Haupt and P.L. Werner presented an overview of fractal antenna engineering emphasizing the design of fractal antenna arrays [74]. The design algorithms mainly depends on the recursive nature of fractals. Some important properties of fractal arrays are introduced. They include the frequency independent multiband characteristics, low side lobe levels and ability to design rapid beam forming algorithms by exploiting the recursive nature of fractals.

Shufeng Zheng et al presented a miniature band pass frequency selective surface (FSS) based on fractal antenna-filter-antenna (AFA) array [75]. Superior frequency selectivity and low profile compared to conventional FSS are the advantages of AFA array.

D.H. Werner, M.A. Gingrich and P.L. Werner presented a self-similar fractal radiation pattern synthesis technique for reconfigurable multiband arrays [76]. The self-similarity of a specified fractal radiation pattern is applied in a generalized Fourier series synthesis in this method. The advantages of this new multiband array design approach are a significantly reduced mutual coupling environment, the fact that a minimal amount of element switching is required, and the ability to easily implement in the form of a reconfigurable aperture.

Xu Liang et al presented the synthesis of fractal patterns from concentric ring arrays [77]. The self-similarity property of the array pattern is used in the analysis.

2.6.1 Sierpinski Carpet Fractal Arrays

Icaro V Soares reported the application of Sierpinski carpet fractal antennas for energy harvesting [78]. A two antenna array is utilized for this purpose. These arrays were optimized in order to get impedance matching, reduced return losses, high gain and bandwidth. The efficiency achieved is about 10 percent.

Dipika et al proposed a modified Geometry Sierpinski carpet fractal antenna array for wireless communication [79]. Third iterated stage of Sierpinski carpet fractal array was designed for achieving high gain and bandwidth. This can be used for wideband/multiband applications. Measured and simulated results were also compared

Yuan Chen et al studied Polarization anisotropic transmission through metallic Sierpinski carpet aperture array [80]. The Sierpinski carpet fractal array achieved polarization dependence and dual band transmission feature simultaneously.

A Karmarkar et al analyzed fractal based antenna array using differential evolution algorithm [81]. A novel method is proposed to compute the Sierpinski carpet array factor in this paper.

A Noor and Z Hu reported a wide band multilayer Sierpinski carpet array radar absorber [82]. 3D printing technology can be used to realize this structure. This absorber gives a reduction of -10 dB from 6 to 40 GHz with a thickness of 7.2mm.

In the present work arrays of different iterated stages of Sierpinski Carpet dielectric backed fractal array based on Sierpinski carpet is investigated to utilize them for backscattering modification of metallic objects.

REFERENCES

- [1] R. J. Wagner and P. J. Lynch, "Theorem on electromagnetic backscatter," *Phys. Rev.*, vol. 131, pp. 21-23, 1963.
- [2] J. B. Keller, "The geometrical theory of diffraction," *Journal of the Optical Society of America*, Vol 52, No 2, February 1962.
- [3] R. A. Ross, "Radar cross section of rectangular flat plates," *IEEE Trans Antennas Propag.*, vol. AP-14, pp. 229-235, May 1966.
- [4] Constantine A. Balanis, Levent Sevgi, Pyotr Ya and Ufimtsev "Fifty Years of High Frequency Diffraction," *International Journal of RF and Microwave Computer-Aided Engineering*, April 2013.
- [5] Piergiorgio L. E. Uslenghi, "Three theorems on zero backscattering" *IEEE Transactions on Antennas and Propagation*, Volume: 44, Issue: 2, Feb 1996.
- [6] W. B. Gordon, "Calculating scatter from surfaces with zero curvature," *IEEE Trans. Antennas Propag.*, vol. 51, no. 9, pp. 2506-2508, 2003.
- [7] William B. Gordon "Contour Integral Representation for near field backscatter from a Flat Plate" *IEEE Transactions on Antennas and Propagation* Volume: 60, Issue: 5, May 2012.

-
- [8] William B. Gordon “Far-field approximations to the Kirchhoff-Helmholtz representations of scattered fields,” IEEE Trans. Antennas Propagat., vol. AP-23, pp. 590–592, 1975.
- [9] J S Hey and Senior “Electromagnetic Scattering by Thin Conducting Plates at Glancing Incidence” Proceedings of the Physical Society, Vol 72, No 6, 1958.
- [10] E. Knott, V. Liepa and T. Senior “Plates and Edges”, IEEE Transactions on Antennas and Propagation, Vol 19, No 6, November 1971.
- [11] H. Kobayashi and K. Hongo, “Scattering of electromagnetic plane waves by conducting plates,” Electromagnetics, vol. 17, no. 6, pp. 573-587,1997.
- [12] R. A. Ross, “Backscattering from square plates illuminated with vertical polarization,” IEEE Trans. Antennas Propag., vol. 54, no. 1, pp. 272-275, Jan. 2006.
- [13] Gökhan Apaydin, Feray Hacivelioglu, Levent Sevgi, William B. Gordon, Pyotr Ya Ufimtsev, “Diffraction at a Rectangular Plate: First-Order PTD Approximation” IEEE Transactions on Antennas and Propagation, Volume: 64, Issue: 5, May 2016.
- [14] V. V. Liepa and T. B. A. Senior, "Modification of the scattering behavior of a sphere by loading", Proc. of IEEE, Vol. 53, pp. 1004-1011, Aug 1965.
- [15] C. Mullin, R. Sandburg and C. Velline, “A numerical technique for the determination of scattering cross sections of infinite cylinders of arbitrary geometrical cross section,” IEEE Transactions on Antennas and Propagation ,Volume: 13 , Issue: 1 , Jan 1965.
- [16] Adour V. Kabakian and Amit M. Patel, “Backscatter reduction of long thin bodies by surface impedance modulation” IEEE International Symposium on Antennas and Propagation July 2016.
- [17] E F Knott “Radar Cross Section” Its Prediction, Measurement and Reduction, Artech House 1985.

-
- [18] P. Corona, G. Ferrara and C. Gennarelli “Backscattering by loaded and unloaded dihedral corners” IEEE Transactions on Antennas and Propagation, Vol 35 , No 10, October 1987.
- [19] T. Griesser and C. Balanis “Backscatter analysis of dihedral corner reflectors using physical optics and the physical theory of diffraction”, IEEE Transactions on Antennas and Propagation Vol 35, Issue: 10, October 1987.
- [20] T. Griesser and C. Balanis “Dihedral corner reflector backscatter using higher order reflections and diffractions” IEEE Transactions on Antennas and Propagation Volume: 35, Issue: 11, November 1987.
- [21] Saki Kameyama, Jiro Iwashige, Motohiko Iwaida and Yuki Isayama “Diffracted Fields by the Edge of Wedge and Reflected Fields from Surface of Wedge” International Conference on Complex, Intelligent, and Software Intensive Systems (CISIS), 2013.
- [22] A. Hessel, J. Schmoys, and D. Y. Tseng “Bragg-angle blazing of diffraction gratings” Journal of the Optical Society of America Vol. 65, Issue 4, 1975.
- [23] J. L. Roumiguieres, D. Maystre and R. Petit “On the efficiencies of rectangular-groove gratings” Journal of the Optical Society of America Vol. 66, Issue 8, pp. 772-775 (1976)
- [24] E V Jull “Reflection from circular polarizers” Electronics Letters Volume: 15, Issue: 14, July 1979.
- [25] J W Heath and E V Jull “Total Backscatter from Conducting Rectangular Corrugations” IEEE Transactions on Antennas and Propagation, VOL. AP-21, NO. 1, January 1979.
- [26] W. Chen, N. C. Beaulieu, D. G. Michelson, and E. V. Jull “Off-Bragg Blazed Rectangular Groove Gratings for High Diffraction Efficiency Devices” IEEE Transactions on Antennas and Propagation Volume: 61 , Issue: 4 , April 2013.

-
- [27] E V Jull “Reduction of interference from large reflecting surfaces” IEEE Transactions on Antennas and Propagation, Volume: 25, Issue: 4, July 1977.
- [28] James W. Heath and Edward V. Jull “Perfectly blazed reflection gratings with rectangular grooves” Journal of the Optical Society of America Vol. 68, Issue 9 September 1978.
- [29] E. V. Jull, N. C. Beaulieu, and D. C. W. Hui “Perfectly blazed triangular groove reflection gratings” Journal of the Optical Society of America, Vol. 1, Issue 2, 1984.
- [30] G. C. Vietti, M. Mussetta, P. Pirinoli and M. Orefice “Validation of concentric square rings backscattering for reflectarray applications” Proceedings of the 5th European Conference on Antennas and Propagation April 2011.
- [31] Young-Huang Chou, Shew-Jon Lin, Shyh-Jong Chung “Analysis of a grating metal structure with broad back-scattering field pattern for applications in vehicle collision avoidance system” IEEE Transactions on Vehicular Technology, Volume: 51, Issue: 1, Jan 2002.
- [32] Haijian Hou and Junhong Wang, “Study on the scattering property of square patch gradient index metasurfaces” IEEE 5th Asia-Pacific Conference on Antennas and Propagation, July 2016.
- [33] R. A. Hurd and E. V. Jull, “Theory of a reflection grating with narrow grooves” Radio Science, Volume 16, Number 3, pages 271-277, May-June 1981.
- [34] S.V. Maly “The numerical technique for analysis of the electromagnetic scattering by complicated periodic structures” VI th International Conference on Mathematical Methods in Electromagnetic Theory Proceedings. September 1996.
- [35] A. Lakhtakia, N. Holter, and V. Varadan “Self-Similarity in Diffraction by a Self-similar Fractal Screen” IEEE Transactions on Antennas and Propagation Volume: 35, Issue: 2, Feb 1987.

-
- [36] C.M. Shiao and S.T. Peng “Distribution of current induced on metal-strip gratings by plane wave” IEEE Transactions on Microwave Theory and Techniques, Volume: 46, Issue: 6, Jun 1998.
- [37] T.L. Zinenko, A.I. Nosich and Y. Okuno “Plane wave scattering and absorption by resistive-strip and dielectric-strip periodic gratings” IEEE Transactions on Antennas and Propagation Volume: 46, Issue: 10, Oct 1998
- [38] K.A. Jose, P. Mohanan, K.G. Nair and N. Sridhar “Effect of periodic strip structure on reduction of radar cross section of planar surfaces” Digest on Antennas and Propagation Society International Symposium June 1989.
- [39] V. Ajaikumar, K. A. Jose, C. K. Aanandan, P. Mohanan, and K. G. Nair “Backscattering reduction of corner reflectors using SCS techniques”, Microwave and Optical Technology Letters Vol 5, No 11, October 1992.
- [40] K.A. Jose and K.G. Nair, “Reflector-backed perfectly blazed strip gratings simulate corrugated reflector effects,” Electronics Letters, Vol 23, No 2, January 16, 1987.
- [41] K.A. Jose, C.K. Aanandan and K.G. Nair “Low backscattered TM-polarised strip gratings, Electronics Letters, Vol 23 , No 17 , August 1987.
- [42] D. Saji Stephen, Thomaskutty Mathew, P. Mohanan, and K. G. Nair “A modified strip grating for dual periodicity for RCS reduction, “Microwave and Optical Technology Letters, Vol7, No 7, May 1994.
- [43] D. S. Stephen, T. Mathew, K. A. Jose, C. K. Aanandan, P. Mohanan and K. G. Nair, “New Simulated corrugated Scattering Surface giving wideband characteristics,” Electronic Letters, Voi.29, No 4, February 1993.
- [44] Thomaskutty Mathew, D. Saji Stephen, K. A. Jose, C. K. Aanandan, P. Mohanan and K. G. Nair “The performance of a novel simulated corrugated surface for the reduction of radar cross section” Microwave and Optical Technology Letters, Vol. 6, No. 10, August 1993.

- [45] T. Mathew, D.S. Stephen, C.K. Aanandan, P. Mohanan and K.G. Nair “Wideband trapezoidal strip grating for elimination of specular reflection” *Electronics Letters*, Volume: 30, Issue: 13, 23 Jun 1994.
- [46] T. Mathew, S.D. Saji, C.K. Aanandan, P. Mohanan and K.G. Nair “Development of a blazed reflection grating with enhanced bandwidth and angular range giving circularly polarised backscattering” *IEEE Antennas and Propagation Society International Symposium*. June 1995.
- [47] K A Jose, C K Aanandan, P Mohanan and K G Nair “Moment method solution for the RCS of a strip grating backed with reflector” *Antennas and Propagation Society Symposium* June 1991.
- [48] Xiaqiang Li, Mohammad Memarian, Kirti Dhvaj and Tatsuo Itoh “Blazed Metasurface Grating: The Planar Equivalent of a Sawtooth Grating” *IEEE MTT-S International Microwave Symposium (IMS)* May 2016.
- [49] Mohammad Memarian, Xioquiang Li, Yasuo Morimoto and Tatsuo Itoh, “Wideband /angle blazed surfaces using Multiple coupled Blazing resonances, “*Nature scientific reports* 7, February 2017.
- [50] Mandelbrot, B. “*The Fractal Geometry of Nature*” W. H. Freeman and Co.: New York, 1982.
- [51] Munesh Chandra, Sanjay M. Shah “Iterative Procedures in Generating Fractal Carpets” *International Conference on Computational Intelligence and Communication Networks* October 2011.
- [52] Dwight L. Jaggard and Xiaoguang Sun “Scattering from fractally corrugated surfaces,” *Journal of the Optical Society of America*, Vol. 7, Issue 6, June 1990.
- [53] S. Savaidis, P. Frangos, D. L. Jaggard, and K. Hizanidis “Scattering from fractally corrugated surfaces with use of the extended boundary condition method” *Journal of the Optical Society of America*, Vol. 14, No 2, 1997.

- [54] C. Puente, J. Romeu, R. Pous, X. Garcia and F. Benitez “Fractal multiband antenna based on the Sierpinski gasket,” *Electronics Letters*, Volume: 32 , No 1 , January 1996.
- [55] C. Puente, J. Romeu, R. Bartolemi and R. Pous “Perturbation of the Sierpinski antenna to allocate operating bands,” *Electronic Letters* Vol 32, No 24 November 1996.
- [56] Rowdra Ghatak, Rabindra K. Mishra and Dipak R. Poddar, “Perturbed Sierpinski Carpet Antenna with CPW Feed for IEEE 802.11 a/b WLAN Application,” *IEEE Antennas and Wireless Propagation Letters*, Volume: 7, August 2008.
- [57] Homayoon Oraizi and Shahram Hedayati, “Miniaturized UWB Monopole Microstrip Antenna Design by the Combination of Giuseppe Peano and Sierpinski Carpet Fractals,” *IEEE Antennas and wireless Propagation Letters*, Vol. 10, January 2011.
- [58] Werner D. H and Ganguly S “An Overview of Fractal Antenna Engineering Research” *IEEE Antennas Propagation. Magazine*, Vol 45, 2003.
- [59] D.H. Werner, P.L. Werner and K.H. Church “Genetically engineered multiband fractal antennas” *Electronics Letters* Volume: 37, Issue: 19, 13 Sep 2001.
- [60] G.J. Walker and J.R. James, “Fractal volume antennas”, *Electronic Letters*, Vol. 34, No. 16, August 1998.
- [61] Chandran AR, Mathew T, Aanandan C K, Mohanan, P, and Vasudevan K. “Low backscattered dual-polarised metallo-dielectric structure based on Sierpinski carpet”, *Microwave Opt. Technol. Letters*, Vol 40, No 3, pp. 246–248, 2004.
- [62] Chandran A.R, T. Mathew, C K.Aanandan, P.Mohanan, and K Vasudevan, “Frequency tunable metallo-dielectric structure for backscattering reduction,” *IEE Electronics Letters*, Vol. 40, No. 20, 1245–1246, 2004.

- [63] A R Chandran, M Gopikrishna, C K Aanandan, P Mohanan and K Vasudevan, “Scattering behavior of fractal based metallo-dielectric structures”, Progress in Electromagnetics Research, Vol. 69, pp 323-339, 2007.
- [64] A R Chandran, M Gopikrishna, C K Aanandan, and K Vasudevan “Radar cross-section enhancement of dihedral corner reflector using fractal-based metallo-dielectric structures,” Electronics Letters, Volume, 42, No 20, September 2006.
- [65] E. L Barreto et al “A New Triple Band Microstrip Fractal Antenna for C-band and S-band Applications” Journal of Microwaves, Optoelectronics and Electromagnetic Applications, September 2016.
- [66] Lehman, M. “Fractal diffraction gratings built through rectangular domains,” Optics Communications, Volume 195, No 4, August 2001.
- [67] Francesco De Nicola et al “Multiband Plasmonic Sierpinski Carpet Fractal Antennas,” ACS Photonics, March 2018.
- [68] J.P. Gianvittorio, J. Romeu, S. Blanch and Y. Rahmat-Samii, “Self-Similar Prefractal Frequency Selective Surfaces for Multiband and Dual-Polarized Applications,” IEEE Transactions on Antennas and Propagation, Vol 51, No 11, November 2003.
- [69] R.V. Hara Prasad, Y. Purushottam, V.C. Misra and N. Ashok “Microstrip fractal patch antenna for multi-band communication,” Electronics Letters, Volume 36, Issue 14, July 2000.
- [70] Zhengwei Du, Ke Gong, J.S. Fu and Baoxin Gao, “Analysis of microstrip fractal patch antenna for multi-band communication,” Electronics Letters, Vol 37, No 13, June 2001.
- [71] S. C. Patrício, M. Carleti, Arismar Cerqueira S. Jr. and J. A. J. Ribeiro “Development of a Printed Antenna Array based on Sierpinski Carpet Fractal Elements” International Microwave and Optoelectronics Conference November 2015.

- [72] D.H. Werner, D. Baldacci and P.L. Werner, “An efficient recursive procedure for evaluating the impedance matrix of linear and planar fractal arrays,” *IEEE Transactions on Antennas and Propagation*, Vol 52, No 2, February 2004.
- [73] S. Costanzo and F. Venneri “Miniaturized Fractal Reflectarray Element Using Fixed-Size Patch” *IEEE Antennas and Wireless Propagation Letters* Vol 13, July 2014.
- [74] Douglas H. Werner, Randy L. Haup and Pingjuan L. Werner “Fractal Antenna Engineering: The Theory and Design of Fractal Antenna Arrays” *IEEE Antennas and Propagation Magazine* Volume: 41, Issue: 5, Oct 1999.
- [75] Shufeng Zheng, Yingzeng Yin, Jun Fan, Xi Yang, Biao Li, Weixing Liu “Analysis of Miniature Frequency Selective Surfaces Based on Fractal Antenna–Filter–Antenna Arrays” *IEEE Antennas and Wireless Propagation Letters* March 2012.
- [76] Douglas H. Werner, Mark A. Gingrich, and Pingjuan L. Werner “A Self-Similar Fractal Radiation Pattern Synthesis Technique for Reconfigurable Multiband Arrays” *IEEE Transactions on Antennas and Propagation* (Volume: 51, Issue: 7, July 2003).
- [77] Xu Liang, Wu Zhensen and Wang Wenbing “Synthesis of fractal patterns from concentric-ring arrays” *Electronics Letters* Volume: 32, Issue: 21, 10 Oct 1996.
- [78] Icaro v. Soares, Ursula C. Resende, Sandro and M. Goncalves “Sierpinski Carpet Fractal Microstrip Arrays for Energy Harvesting Applications,” *IEEE Conference on Electromagnetic Field Computation*, November 2016.
- [79] Rahul Batra, P. L. Zade and Dipika Sagne, “Design and Implementation of Sierpinski Carpet Fractal Antenna for Wireless Communication,” *International Journal of Scientific Research Engineering & Technology*, Vol 1, No 3, July 2012.

- [80] Yuan Chen et al “Polarization anisotropic transmission through metallic Sierpinski-Carpet aperture array, “Optics Express, February 2014.
- [81] Anirban Karmakar, Rowdra Ghatak, R.K. Mishra & D.R. Poddar Sierpinski carpet fractal-based planar array optimization based on differential evolution algorithm, Journal of Electromagnetic Waves and Applications, 29:2, 247-260, January 2015.
- [82] A Noor and Z Hu “Wideband multilayer Sierpinski carpet array radar absorber,” IEE Electronics Letters, Vol.52, No. 19, September 2016.

3 METHODOLOGY

The methodology of the research work is explained in this chapter. The chapter begins with description of overview of instrumentation for scattering measurements. Vector Network Analyzer, Anechoic chamber and Arch method are explained. Design process, fabrication steps and measurement procedure are also presented. It also presents different objects used in scattering studies such as flat metallic plates, dihedral corner reflectors and

TABLE OF CONTENTS

- 3.1 Overview of Instrumentation for Scattering Measurements**
 - 3.2 Subsystems used in Scattering Measurements**
 - 3.3 Measurement Procedure**
 - 3.4 Design and fabrication of fractal arrays**
 - 3.5 Flat Metallic Plate Loaded with Dielectric Backed SCF Arrays**
 - 3.6 Non Planar Structures**
-

3.1 OVERVIEW OF THE INSTRUMENTATION FOR SCATTERING MEASUREMENTS

Scattering measurements are done using a Vector Network Analyzer (VNA) in an anechoic environment. The structures are mounted on a dielectric stand placed at the center of an arch. The arch and surroundings are inside an anechoic chamber to avoid unwanted reflections from the walls and ceilings of the enclosed room. The main subsystems in the instrumentation are

- (i) Anechoic Chamber

- (ii) Arch method
- (iii) Vector Network Analyzer

3.2 SUBSYSTEMS USED IN SCATTERING MEASUREMENTS

3.2.1 Anechoic Chamber

Measurements of scattering must be unaffected by its surrounding environment. The anechoic chamber provides an environment free of echo or other radiated signals to reduce the effects of undesirable signals [1-4]. Reflected electromagnetic waves are absorbed completely by an anechoic chamber. Unwanted reflections and external noise has to be eliminated to avoid measurement errors. The interior surface of RF anechoic chamber are covered with radiation absorbent material (RAM). The RF absorbers are made of lossy material. The RF absorbers are shaped in such way that the incoming electromagnetic waves penetrate into it with minimal reflections. Once the electromagnetic energy travels inside the material, the RF energy transforms into thermal energy and dissipates into the surrounding air. Basically there are two types of anechoic chamber design: rectangular and pyramidal. Geometrical optics is used to design anechoic chamber and is used to reduce specular reflection. Free space conditions are simulated by rectangular chamber which will maximize the volume of the quiet zone inside a chamber. But at large angles of incidence significant specular reflections can occur in a rectangular chamber.

Pyramidal shaped absorbers are used to avoid unwanted reflections in the test area.

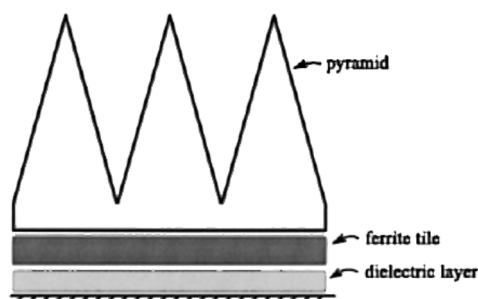


Fig 3.1 Pyramidal absorbers in the wall of an anechoic chamber

As the electromagnetic wave passes into the pyramid many small reflections are created and these reflections tend to cancel out. The cancellation of the reflections will be effective only if the length of the pyramid is at least half the wavelength of the lowest frequency of interest. Carbon mixed polyethylene foam is used for the construction of the pyramidal structure. But the wavelength of the electromagnetic wave is shorter than the free space wavelength when it passes through the pyramidal structure. The wavelength is reduced by a factor

$$\lambda_f = \lambda / \sqrt{\epsilon_r} \quad \text{where}$$

ϵ_r is the relative permittivity of the absorbing material and λ_f is the wavelength inside the pyramidal absorber.

3.2.2 Arch Method

Arch method is used to measure power scattered in various angles by the target of interest. A wooden arch shaped table is used to fix both transmitting and receiving horn antennas which can be freely moved over the arch as shown in figure 3.2.

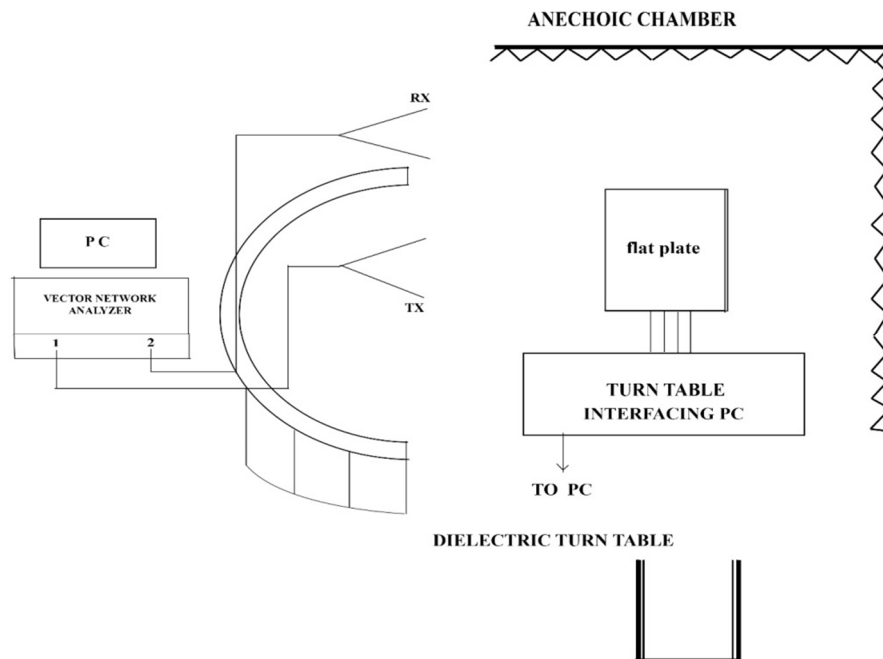


Fig 3.2 Schematic diagram of the Arch Method

A turn table is placed at the center of the arch which carries a dielectric holder or dielectric stand to fix the metallic surface over which the dielectric backed fractal arrays are loaded. The turn table is placed in an anechoic chamber. The turn table can be rotated by using a stepper motor controlled by the PC which is interfaced with the Vector Network analyzer. When moved along the arch, the transmitting and receiving antennas are at a constant distance from the turn table. The scattered power from the target can be measured through an angle of 180° . Both transmitting and receiving antennas are placed on wooden carriages which are free to move over the arch such that scattered power at any angle can be measured by properly placing the receiving antenna. For measurements of blazing angle of incidence must be varied. For this the target mounted on the turn table can be rotated by using a stepper motor interfaced through a microcontroller to the PC. Python software is used for interfacing programming and data acquisition through the Vector Network Analyzer which is used for measurement of the scattered fields.

A photograph of the arch method is shown below



Fig 3.3 Photograph of Arch method

3.2.3 Vector Network Analyzer

Vector Network analyzer measures both magnitude and phase of the transmission and reflection coefficients. The unique feature of the Vector Network Analyzer is that it contains both source used to generate a known stimulus signal, and

a set of receivers used to determine changes to this stimulus caused by device under test.

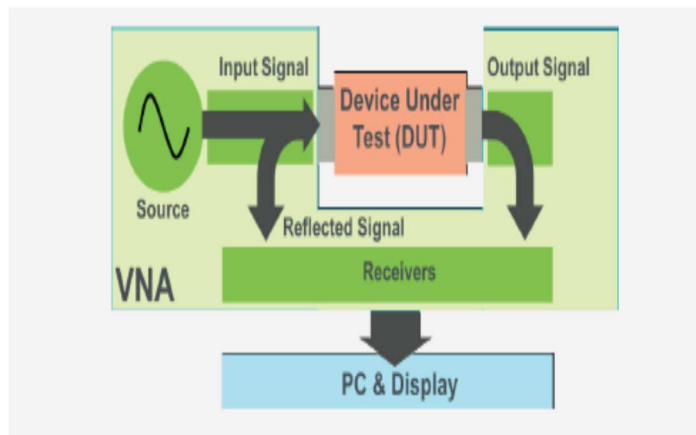


Fig 3.4 Working of a VNA

Ports 1 and 2 of the four port VNA is used for S_{12} measurements. The device under test can be connected to either port in either direction because the instrument has the capability of reversing the signal flow so that the reflections at both ports (S_{11} and S_{22}), as well as the forward and reverse transmissions (S_{21} and S_{12}), can be measured. The four key specifications of a VNA are frequency range, dynamic range, trace noise, and measurement speed.

Dynamic range is the measurable attenuation range from max to min for a specified frequency range. Trace noise measures how much random noise is generated by the VNA and passes into the measurement. It is typically measured in milli-dB (0.001 dB). Measurement speed is the time it takes to perform a single sweep or measurement.



Fig 3.5 Rhode & Schwartz ZVB 20 used in measurement

The Rhode & Schwartz ZVB 20 can span over a range of 10 MHz to 20GHz. It is a four-port models. Its wide dynamic range of 140 dB, low trace noise of 0.004 dB (RMS) and high output power of up to +13 dBm, which can be adjusted electronically in a range of 90 dB, provide fast and accurate measurements. The R&S ZVB20 VNA combines high measurement accuracy with exceptional speed – better than 5 μ s per point. They feature excellent temperature and long-term stability, which ensures reliable measurements over several days without having to recalibrate the units.

For backscattering measurements S_{12} is taken on the Vector Network analyzer after calibrating it. The results can be displayed in linear or logarithmic format. By applying in built time domain gating signal processing technique undesired responses can be avoided. The analyzer is interfaced with a PC and data can be stored in the computer for analysis.

3.3 MEASUREMENT PROCEDURE

A flat metal plate is mounted on the dielectric stand over the turn table at the center of the Arch placed in the anechoic chamber. Two identical X band Horn antennas are fixed on the wooden carriage running over the arch. Both transmitting and receiving antennas are placed very close normal to the dielectric stand fixed over the turn table. Antennas are connected to the two ports of VNA through lossless high frequency cables. The vertical positions of the horn antennas and the dielectric stand are adjusted such that the flat metal plate is made normal to the antennas with same height from ground level.

X band frequency range of 8 to 12 GHz is selected in the VNA. Proper sampling rate and averaging are applied. By applying time gate to Vector Network Analyzer unwanted responses from the surroundings are eliminated. The VNA is calibrated with the plane plate to give 0 dB flat response over the X band.

First iterated stage of the Sierpinski carpet array is loaded over the flat metal plate on the dielectric stand and the response on the VNA is recorded. Without

disturbing the setup the dielectric thickness of the Sierpinski carpet array is varied. Measurements are recorded for various dielectric thickness of the fractal array.

After completing the measurements for the first stage of the Sierpinski carpet array the procedure is repeated for second and third iterated stages of the Sierpinski carpet array. Response for each dielectric thickness variation on the VNA is recorded in the computer interfaced to it.

For measuring variations of relative backscattered power with angle of incidence for frequency corresponding to minimum backscattered power, the turn table is rotated with dielectric backed fractal array loaded metallic structure for 360° . The pattern is plotted in the PC interfaced to the computer using python software.

Scattered power at various angles for the frequency with minimum backscattered power in normal incidence, are measured by moving the receiving antenna along the arch.

3.4 DESIGN AND FABRICATION OF FRACTAL ARRAYS

Backscattering measurements are planned for the X band. A flat metallic plate of dimension $10\lambda \times 10\lambda$ ($30\text{ cm} \times 30\text{ cm}$) is used for the backscattering study, where λ is the wavelength corresponding to the center frequency.

4×4 Sierpinski carpet arrays are designed to cover $30\text{ cm} \times 30\text{ cm}$ flat metal plate. Each element in the Sierpinski Carpet array have a dimension $7.5\text{cm} \times 7.5\text{cm}$. Design of the fractal array is done using CST Microwave studio CAD software. By using photo etching, fabrication of the fractal arrays of different dielectric thickness are completed.

3.4.1 Sierpinski Carpet and Sierpinski Carpet Array

The figure shows the difference between a Second iterated stage of Sierpinski carpet and Sierpinski carpet array fabricated for backscattering studies.

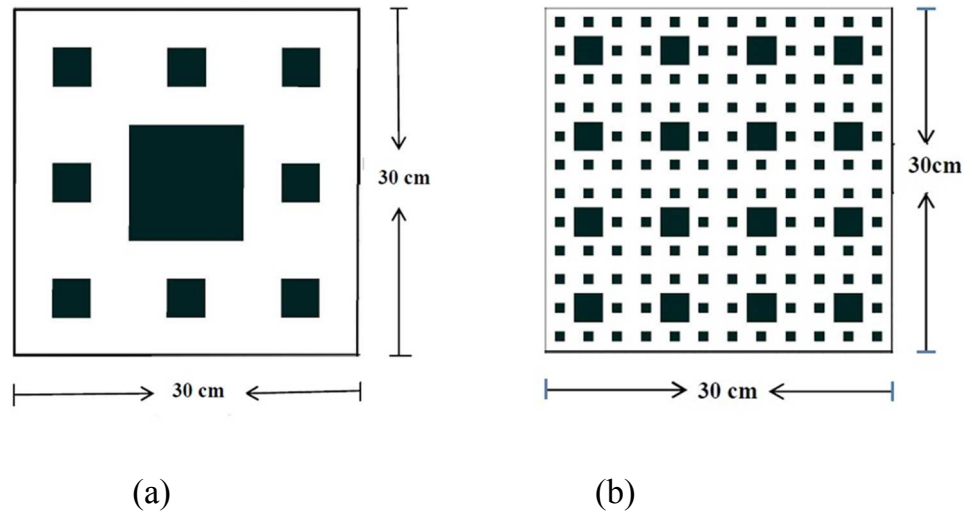


Fig 3.6 Second iterated stage of (a) Sierpinski Carpet (b) Sierpinski Carpet Array

The corresponding first and third iterations are also shown below

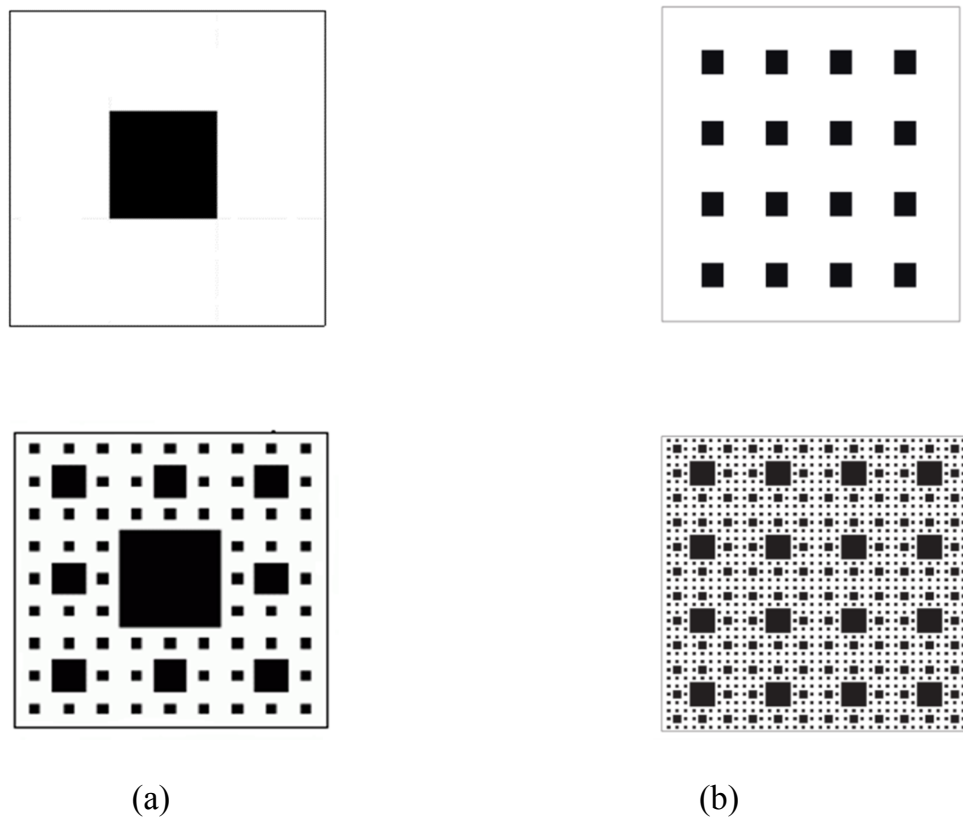


Fig 3.7 First and third iterated stages of (a) Sierpinski Carpet (b) Sierpinski Carpet Array

3.5 FLAT METALLIC PLATE LOADED WITH DIELECTRIC BACKED SCF ARRAYS

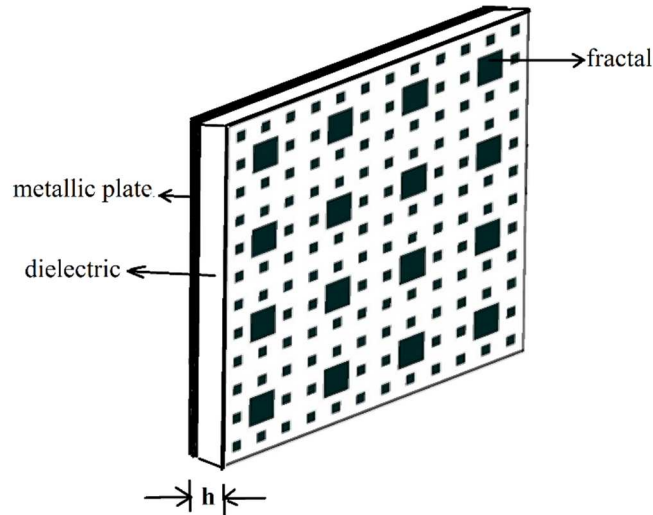


Fig 3.8 Flat metallic plate loaded with dielectric backed second stage of SCF Array

Figure shows a flat metallic plate loaded with dielectric backed second stage of the SCF array. The fractal arrays are fabricated on FR 4 dielectric substrate ($\epsilon_r = 4.4$) with thickness h . The value of dielectric thickness is varied over a range of 0.8mm to 6 mm.

3.5.1 Various iterated stages of the SCF arrays

First, second and third iterated stages of the Sierpinski carpet arrays are loaded over the flat metal plate with various dielectric thickness h with dielectric constant $\epsilon_r = 4.4$. The dielectric thickness variations are from 0.8mm to 6 mm.

The first, second and third iterated stages of the Sierpinski carpet array are also fabricated with dielectric thickness varying between 0.8mm to 6 mm.

3.5.2 Stacking of SCF Arrays for Backscattering Reduction

Two layers of fractal arrays are stacked with an intermediate dielectric layer to obtain backscattering reduction. The thickness of the dielectric layer is varied from

1mm to 6 mm. A layer of PMMA (poly methyl methacrylate) with $\epsilon_r = 2.5$ is used for dielectric separation between the fractal arrays as shown in figure.

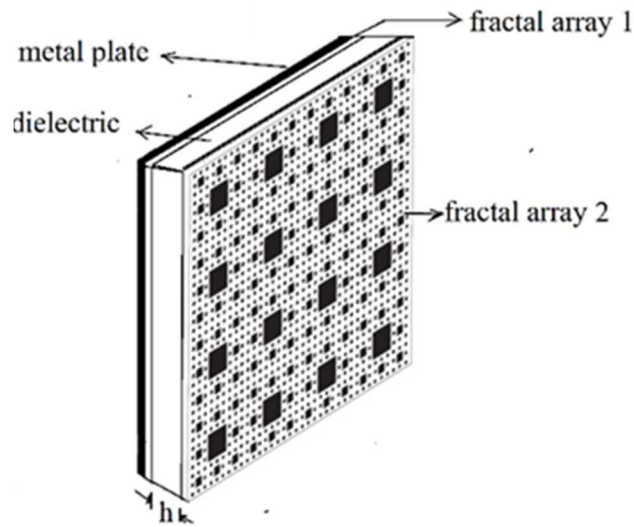


Fig 3.9 Stacked SCF arrays over flat plate

3.5.3 Interleaving of second and third iterated stages of SCF Arrays for Backscattering reduction

Interleaving of second and third iterated stages of the Sierpinski carpet array can be used for backscattering reduction from flat metal plates.

Fully interleaved structures, horizontally and vertically interleaved structures have been designed and fabricated on FR 4 substrate with a thickness of 0.8 mm. Second and third iterated stages of the Sierpinski carpet array are used for interleaving.

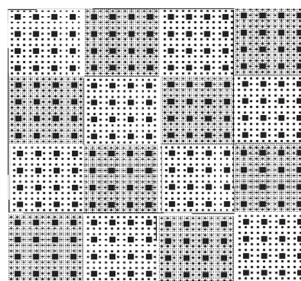


Fig 3.10 Fully interleaved structure

3.6 NON PLANAR STRUCTURES

3.6.1 Dihedral Corner Reflector

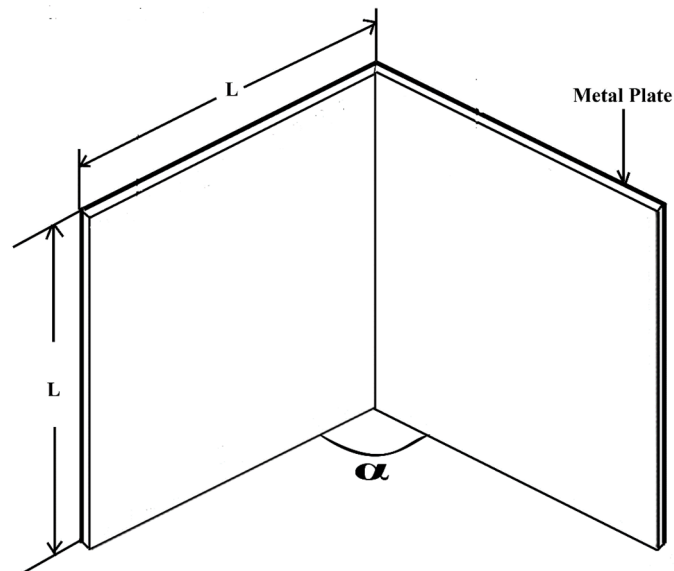


Fig 3.11 Plane dihedral corner reflector

Dihedral corner reflectors are very important in backscattering studies. Backscattering is maximum from dihedral corners compared to metallic surfaces of other shapes.

Dihedral corner reflector is fabricated using two flat metallic plates of $30\text{cm} \times 30\text{cm}$ dimension connected by a hinge to vary the angle between the plates. A 90° dihedral corner reflector was also fabricated using by gluing two flat metallic plates at 90° included angle. A dielectric stand is used to fix the dihedral corner reflector over the turn table at the centre of the arch.

3.6.2 Wedge

Two flat metal plates of $30\text{cm} \times 30\text{cm}$ dimension are connected by a hinge to form a metallic wedge. By varying the including angle, using the hinge the angle of the wedge can be adjusted. The wedge is mounted on a dielectric stand over the

centre of the arch on the turn table. The VNA is calibrated for 0 dB with a flat metallic plate.

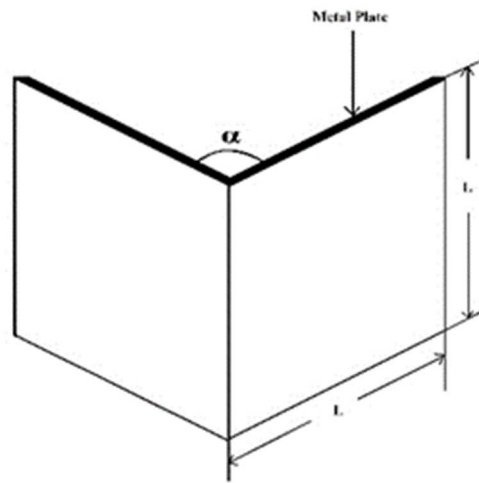


Fig 3.12 Plane metallic wedge

The faces of the wedge directed towards the transmitting and receiving antenna are loaded with dielectric backed fractal arrays. Measurements from the VNA are recorded on a computer interfaced to the VNA.

Different iterated stages of the Sierpinski carpet array are loaded and measurements are recorded. The wedge angle is varied over a range from 80 degree to 120 degree and measurements are recorded .

REFERENCES

- [1] L.H. Hemming, “Electromagnetic Anechoic Chambers”, IEEE Press, Wiley Interscience, Hoboken, NJ.
- [2] Evaluation of RCS and Receive Wall Reflectivity of Anechoic Chambers, Emerson & Cuming Microwave Products N.V, 2004.
- [3] Irina Munteanu and I. Munteanu “Simulation Methodology for the Assessment of Field Uniformity in a Large Anechoic Chamber” IEEE Transactions on Magnetics, Volume: 50 , No 2 , February. 2014.

- [4] H. Togawa, K. Hatakeyama and K. Yamauchi, “Reflectivity measurements in anechoic chambers in the microwave to millimeter range” IEEE Transactions on Electromagnetic Compatibility ,Volume: 47 , No 2 , May 2005.
- [5] E F Knott “Radar Cross Section” Its Prediction, Measurement and Reduction, Artech House 1985.
- [6] K. Hoffmann and Z. Skvor “A novel vector network analyzer”, IEEE Transactions on Microwave Theory and Techniques ,Volume: 46 , No 12 , December 1998.”
- [7] Ulrich Stumper and Thorsten Schrader “Calibration Method for Vector Network Analyzers Using One or Two Known Reflection Standards”, IEEE Transactions on Instrumentation and Measurement ,Volume 63 , No 6 , June 2014.

4 BACKSCATTERING REDUCTION OF A FLAT METAL PLATE USING DIELECTRIC BACKED FRACTAL ARRAYS

In this chapter backscattering reduction of a flat metal plate using dielectric backed fractal arrays are discussed. Simulated and measured results of various iterated stages of SCF arrays loaded over the flat metal plate with different thickness are presented. This chapter also presents the wide angle elimination of specular reflection with dielectric backed SCF array. The results of the investigations on stacked SCF arrays for backscattering reduction is also presented. Finally, the measured results for backscattering reduction of flat plate with dielectric backed interleaved SCF array is also elaborated

TABLE OF CONTENTS

- 4.1 Introduction
- 4.2 Simulated Results of Backscattering Reduction of Flat Metal Plate Loaded with Dielectric Backed SCF Array
- 4.3 Measured Results
- 4.4 Wide Angle Elimination of Specular Reflection with Dielectric backed SCF array
- 4.5 Stacked SCF Arrays for Backscattering Reduction
- 4.6 Interleaved SCF array for Backscattering Reduction
- 4.7 Conclusion

4.1 INTRODUCTION

Scattering from complex targets like aircrafts, missiles, ships etc. can be modelled by a combination of simple shapes such as flat plates, corner reflectors,

cones and wedges. Backscattering from metallic objects is a measure of its monostatic radar cross section. Reduction in radar cross section decreases the detectability of a target and there are different methods employed to achieve this. Metallic corrugated surfaces were effectively used for the reduction of backscattering, but were bulky and difficult to fabricate[1]. It is already established that dielectric backed planar strip gratings simulate the effects of corrugated surfaces[2]. This simple and effective technique offers advantages of easy fabrication, low production cost, light weight over conventional methods. Dielectric backed strip gratings of various shapes based on Euclidian geometry were reported and were investigated for backscattering reduction [3-5].

Metallic fractal structures can be effectively used for achieving radar cross section reduction. Sierpinski gasket and Sierpinski carpet are two simple planar structures in fractal geometry and were used by several researchers for backscattering reduction studies. Anupam et al[6-8] reported radar cross section reduction using Sierpinski carpet based metallo-dielectric structure. In all these works single fractal element with different iterated stages are investigated for backscattering reduction. Use of arrays of Sierpinski Carpet Fractal (SCF) structures for backscattering reduction applications has not been reported. This chapter presents the results of the investigations of backscattering reduction of flat metal plate using dielectric backed SCF arrays. The backscattering reduction studies are carried out in the X band frequency range on a flat metal plate loaded with dielectric backed SCF array.

4.2 SIMULATED RESULTS OF BACKSCATTERING REDUCTION OF FLAT METAL PLATE LOADED WITH DIELECTRIC BACKED SCF ARRAYS

A $10\lambda \times 10\lambda$ flat metallic plate is selected for backscattering study at X band. Simulation studies were performed in CST microwave studio frequency domain solver.

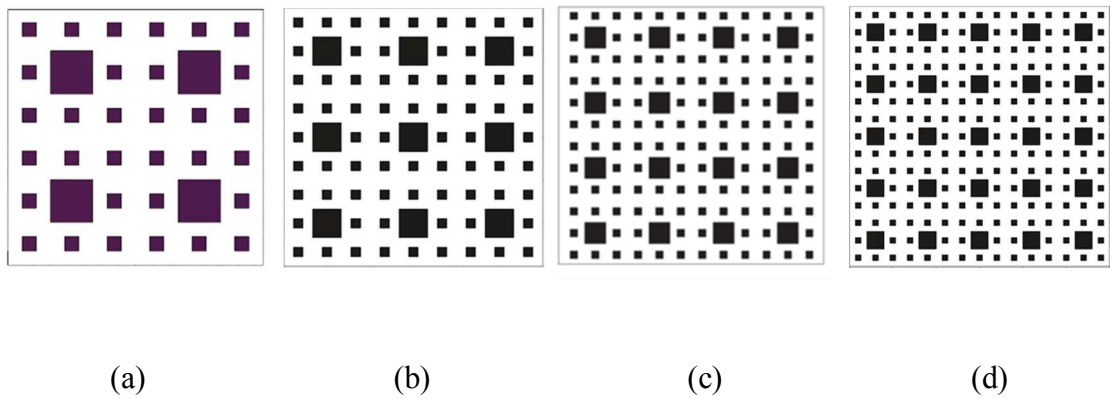


Fig 4.1 Different sizes of SCF arrays investigated

(a) 2×2 array, (b) 3×3 array, (c) 4×4 array, (d) 5×5 array

Backscattering from a flat plate loaded with Second iterated stage of SCF arrays of order 2×2 , 3×3 , 4×4 and 5×5 were analysed. The 4×4 array gave a -10 dB backscattering reduction over the entire X band and is selected for backscattering reduction study.

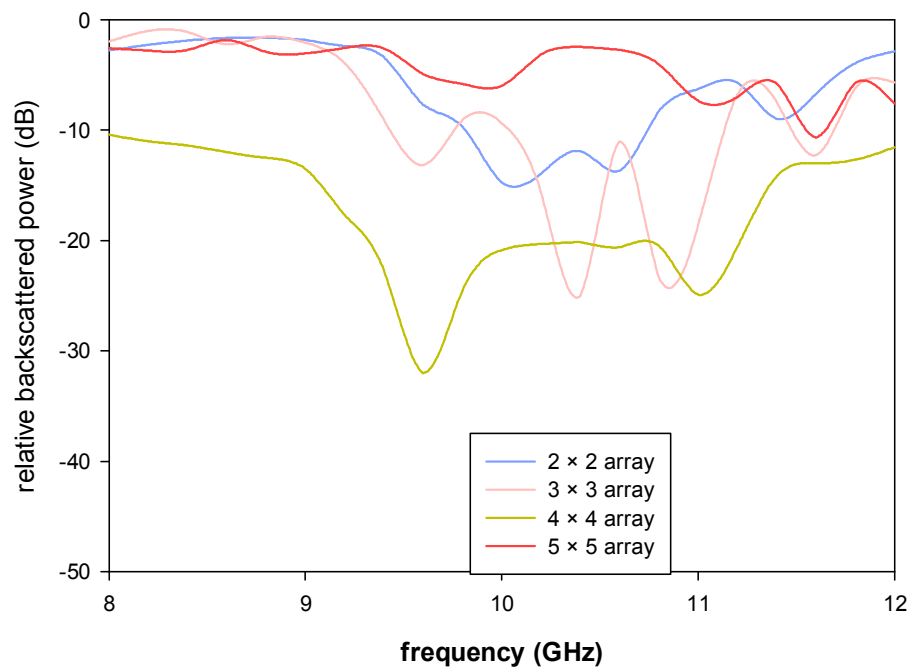


Fig 4.2 Variation of relative backscatterd power with frequency for second iterated stage SCF array for different combinations

The simulated frequency response plot for the backscattering of second iterated stages of SCF arrays of different combinations is shown in figure 4.2.

From the figure, it is evident that backscattering reduction is below -10 dB for the entire X band for the 4×4 SCF array. A maximum reduction of -32.1dB is obtained for the frequency 9.5 GHz.

From the simulation studies the 4×4 SCF array gives better backscattering reduction over a wide band. The 4×4 SCF array is fabricated and measurements were done over the X band.

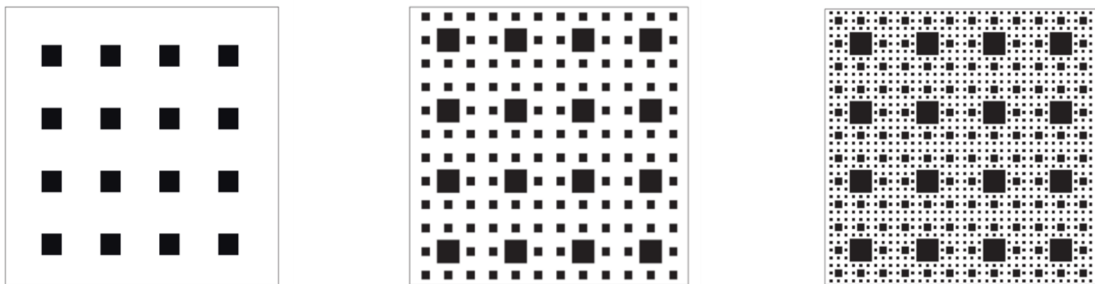


Fig 4.3 Different iterated stages of the SCF 4×4 array

4.3 MEASURED RESULTS

The flat metallic plate is vertically mounted on a the turn table at the centre of the arch placed in an anechoic chamber as explained in Chapter 3. The transmitting and receiving antennas are kept side by side to approximate monostatic measurement. The vector Network Analyzer ZVB 20 is given proper gating and transmitted power is selected. The VNA is then calibrated for 0 dB return loss for the normal incidence of the metallic plate.

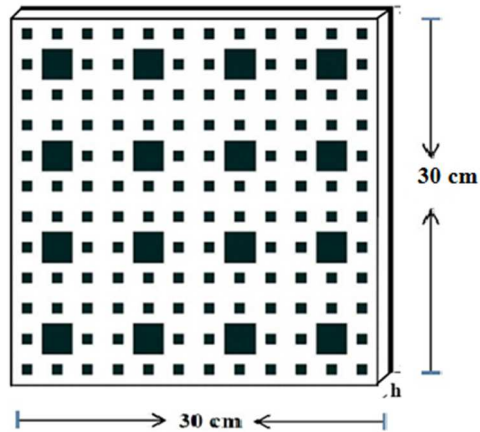


Fig 4.4 Schematic diagram of Flat metal plate loaded with SCF array backed with dielectric

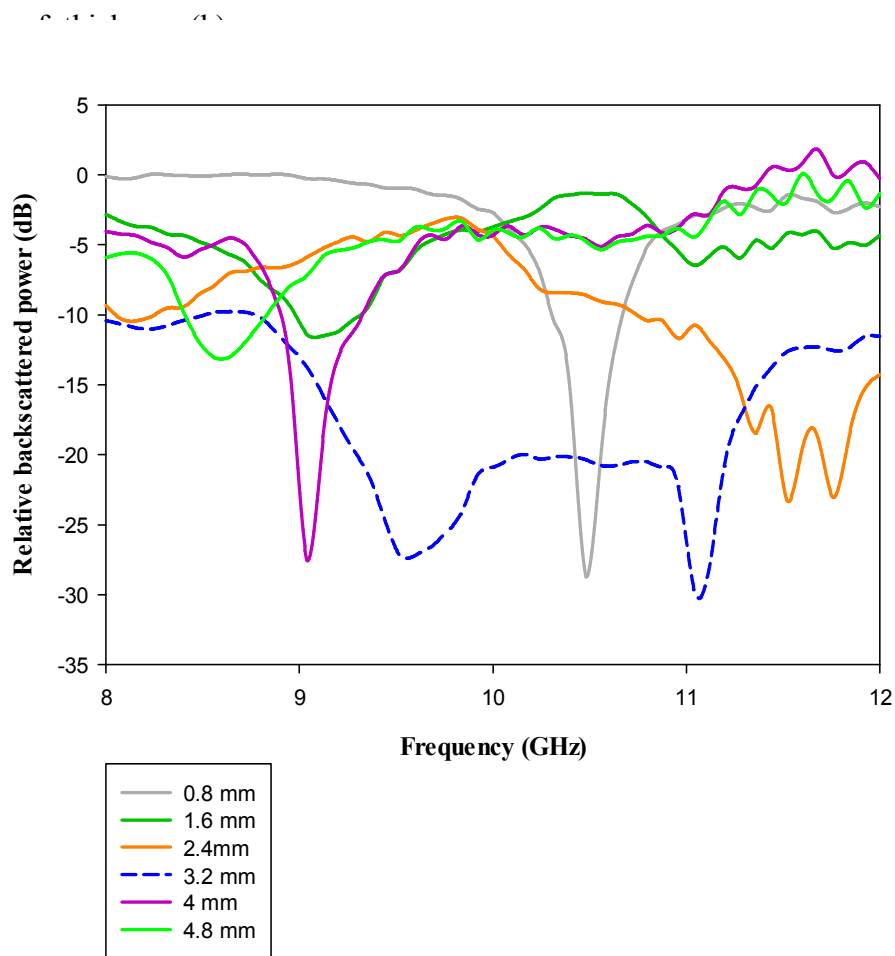


Fig 4.5 Variations of relative backscattered power for metallic plate loaded with 2nd iterated stage of SCF array with different dielectric thickness

The fractal structure based on SCF array was realized by photo etching metallization on a $30 \times 30 \text{ cm}^2$ FR-4 substrate ($\epsilon_r = 4.4$) of thickness h as shown in figure 4.4.

The dielectric backed SCF array is loaded over the flat metal plate. Thickness h is varied and measurements are repeated for the different iterated stages of the SCF array. Figure 4.5 shows variations of relative backscattered power for metallic plate loaded with second iterated stage of SCF array with different dielectric thickness. Maximum reduction in backscattering is obtained for a dielectric thickness of $h=3.2 \text{ mm}$.

Backscattering reduction obtained at normal incidence for the different iterations in the X band are shown in figure 4.6.

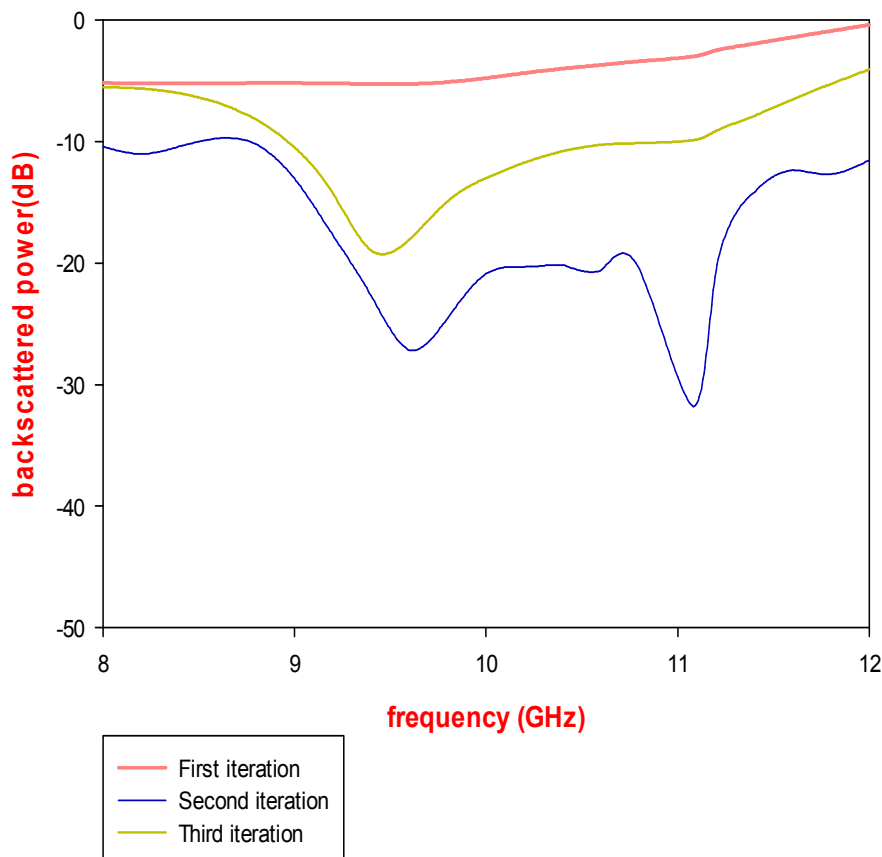


Fig 4.6 Variation of relative backscattered power with frequency for various iterated stage of dielectric backed Sierpinski carpet array with thickness $h=3.2\text{mm}$

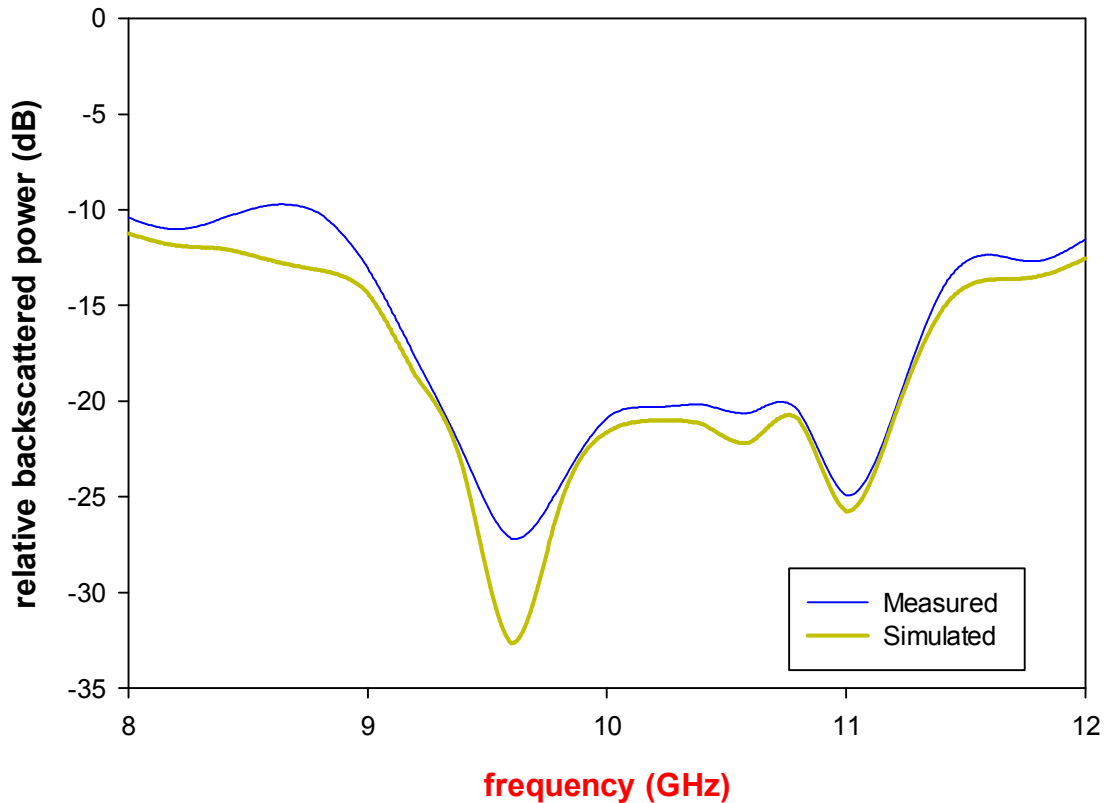


Fig 4.7 Variation of backscattered power with frequency response for the second iterated stage of dielectric backed 4×4 SCF array

From figure 4.6 it can be seen that the second iterated stage of the SCF array give good reduction in backscattering with a -10 dB reduction over the entire X band. The first iteration give an almost flat response below -5 dB and scattered power increases for higher frequencies of X band. At 9.48 GHz a maximum reduction of 20 dB is obtained for the third iterated stage of the Sierpinski Carpet array. But the -10 dB bandwidth obtained is only less than 1 GHz. A maximum reduction of 31.7 dB is obtained at 11.08 GHz for this structure. At 9.5 GHz a reduction of 28 dB is also attained. The reduction is more than 20 dB for a significant portion of the band.

Figure 4.7 shows the comparison between simulated and measured results for the second iterated stage of the dielectric backed SCF array. It is evident from the graph that simulated and measured results are in reasonably good agreement

.The slight discrepancies between simulated and measured results are due to fabrication errors.

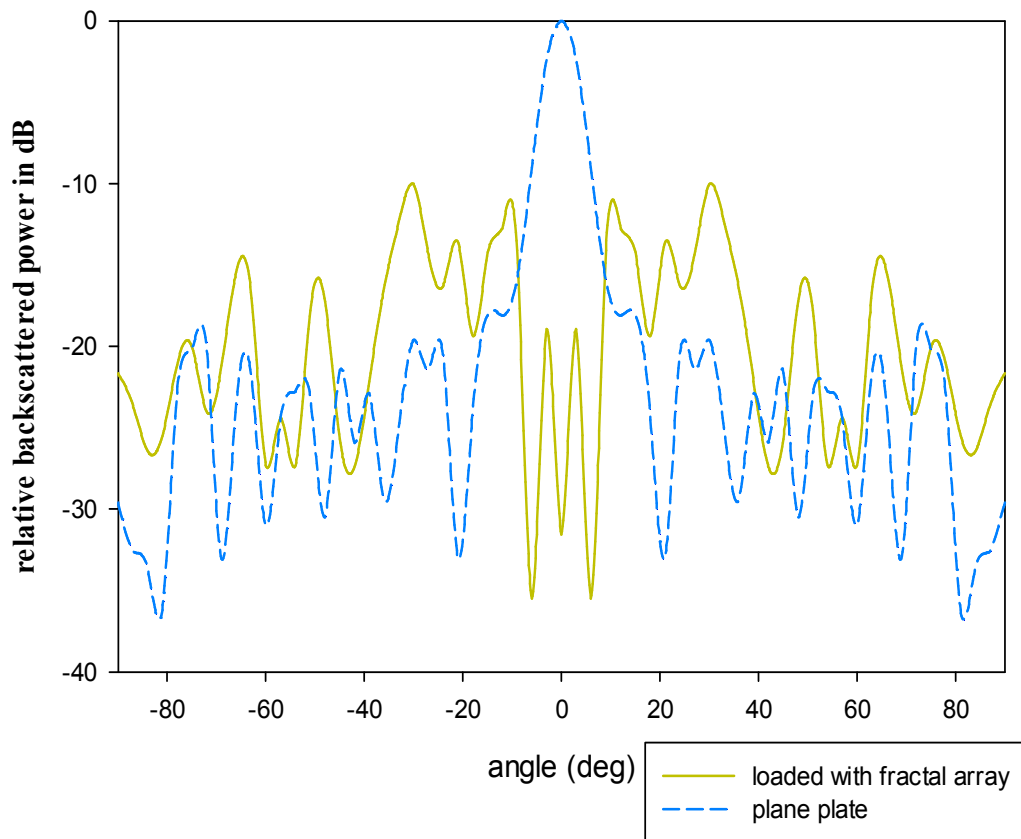


Fig 4.8 Variations of relative backscattered power with angle of incidence at $f=11.08$ GHz for second iterated stage of SCF array and thickness $h=3.2$ mm

Figure 4.8 shows variation of relative backscattered power with angle of incidence for second iterated stage of SCF array and a flat metal plate of same dimensions. It can be seen that the backscattered power is reduced significantly at normal incidence compared to flat plate. It is observed that the backscattering is high for angle of incidence ± 29 degrees which is due to blazing effects at these angles of incidence.

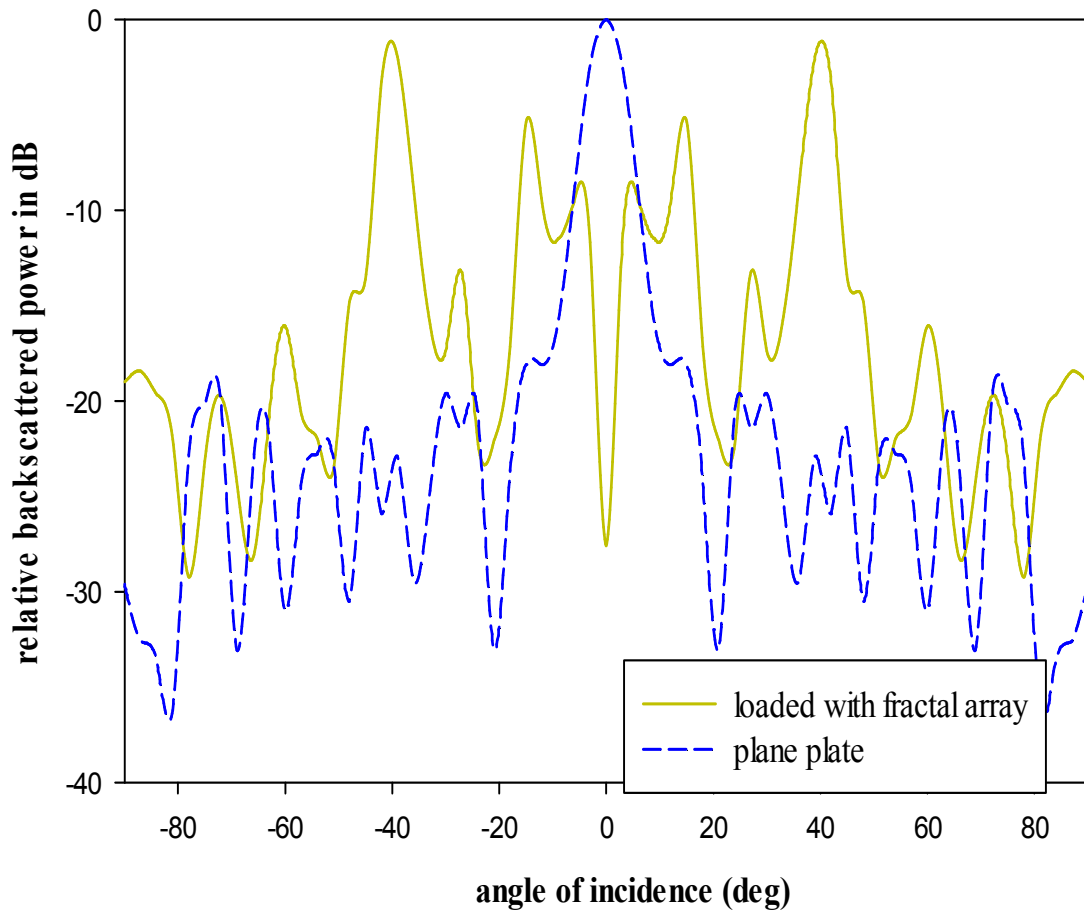


Fig 4.9 Variations of relative backscattered power with angle of incidence for frequency $f=9.5$ GHz for second iterated stage of SCF array ($h=3.2$ mm.)

Figure 4.9 shows variations of relative backscattered power with angle of incidence at 9.5 GHz for the second iterated stage of the SCF array. In this case also the backscattered power is reduced significantly compared to flat metal plate at normal incidence. For this frequency it is noted that backscattered power is maximum at ± 39 degrees, which is due to blazing effects at these angle of incidence.

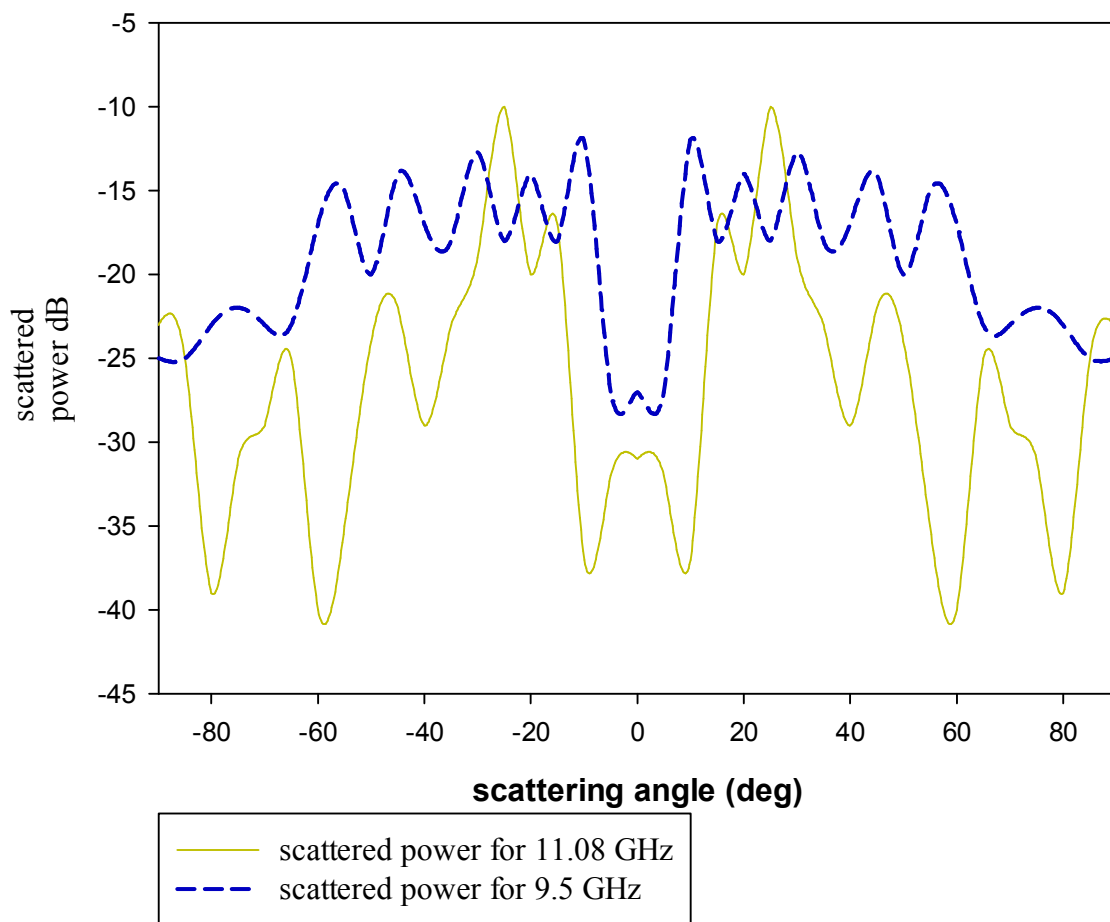


Fig 4.10 Variation of scattered power with scattering angle at 11.08 GHz and 9.5 GHz for the second iterated stage of the SCF array with thickness $h=3.2\text{mm}$ at normal incidence

The measured variations of scattered power for different scattering angles at frequencies 11.08 GHz and 9.5 GHz at normal incidence are shown in fig 4.10.

At a frequency of 11.08 GHz the scattered power is maximum at scattering angle of 25° and for frequency 9.5 GHz the scattered power is maximum at scattering angle of 10° .

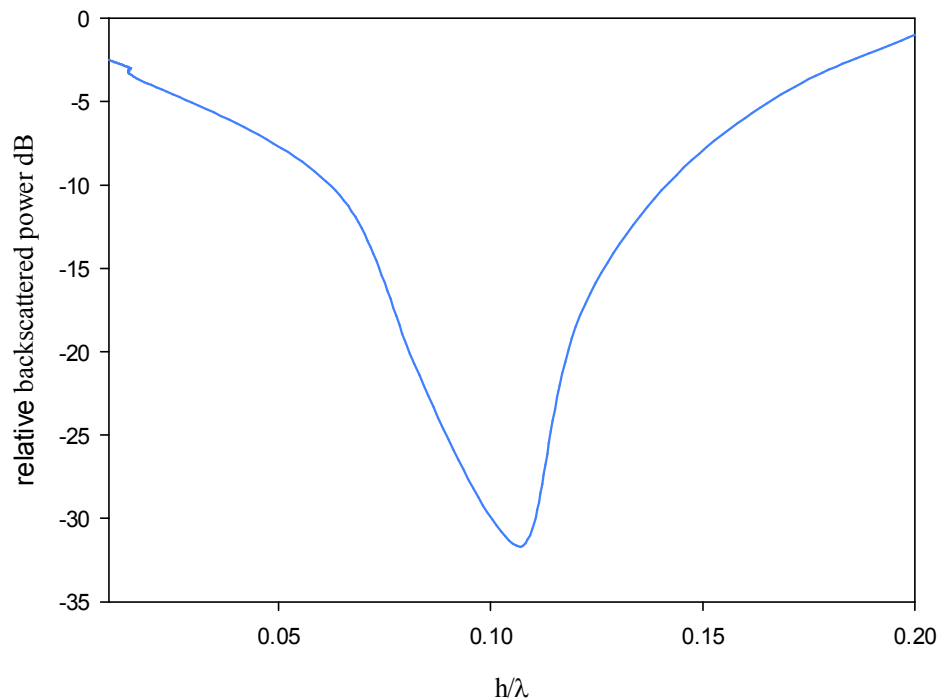


Fig 4.11 Variation of relative backscattered power with dielectric thickness for second iterated stage of the SCF array for frequency of 11.08

The effect of variation of dielectric thickness on relative backscattered power is also considered. Dielectric thickness is normalized using the mean value of wavelength in the band of study. Backscattered power variations with h/λ is plotted in figure 4.11. The minimum value of backscattered power at normal incidence is obtained for $h=0.107\lambda$.

4.4 WIDE ANGLE ELIMINATION OF SPECULAR REFLECTION WITH DIELECTRIC BACKED SCF ARRAY

An incident electromagnetic wave can be scattered into different diffraction orders by a reflection grating. The period (d) is the important parameter which determines the scattering behavior of the grating.

According to Bragg's law of diffraction

$$\sin \theta_n = \sin \theta_i + n\lambda/d$$

where θ_i is the angle of incidence and θ_n is the angle of diffraction and $n = 0, \pm 1$ and λ is the wavelength.

When $n = 0$, specular reflection takes place while $n = -1$ corresponds to blazing.

This happens when an oblique incident electromagnetic wave gets reflected in the direction of incidence. Most of the structures reported for attaining blazing used Euclidian geometry. This section presents the results of investigations on flat metal plate loaded with SCF array for achieving blazing and thereby achieving elimination of specular reflection.

The fractal array is fabricated by photoetching a 30 cm \times 30 cm single side claded FR-4 substrate ($\epsilon_r = 4.4$) with thickness $h_1 = 0.8$ mm. For optimising the performance, another dielectric sheet ($\epsilon_r = 2.5$) of thickness h_2 is inserted between the metal plate and the fractal structure as shown in figure 4.12.

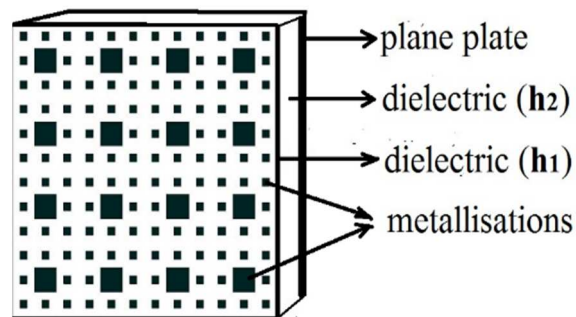


Fig. 4.12 Schematic diagram of the dielectric backed 4 \times 4 SCF array

The dielectric backed SCF array structure is illuminated at different angles of incidence and the corresponding specular reflected power ($\theta_r = \theta_i$) is measured by placing the receiver at $\theta_r = \theta_i$ and the results are plotted in figure 4.13.

For measurements at 9.8 GHz from figure 4.13 it is found that the specular reflection power is below -10 dB over a wide angular range of 0° - 58° . Maximum reduction in reflected power of -34.5 dB is observed for an angle of incidence of 26°

and -25 dB for $\theta_i = 39^\circ$. The reduction in specular reflection is obtained because of the scattering of incident power to different angles. When the power is scattered back to the source it is called blazing. This is verified by measuring the backscattered power for different angles of incidence.

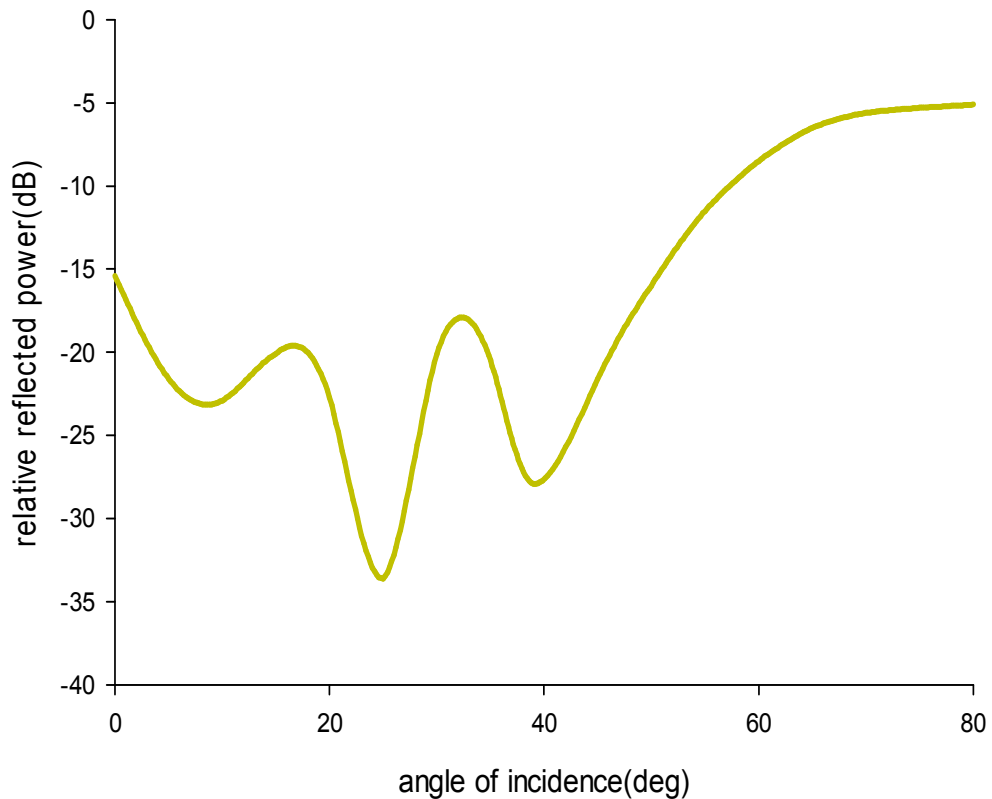


Fig.4.13 Variation of relative reflected power with angle of incidence for the SCF array at 9.8 GHz. ($h_1=0.8\text{mm}$ & $h_2=4.5\text{mm}$)

Figure 4.14 shows the variations of relative backscattered power with angle of incidence for the dielectric backed SCF array at 9.8 GHz. It is evident from the graph, the backscattered power is maximum with -4dB at angle of incidence $\theta_i = 39^\circ$. This corresponds to blazing satisfying Bragg's condition.

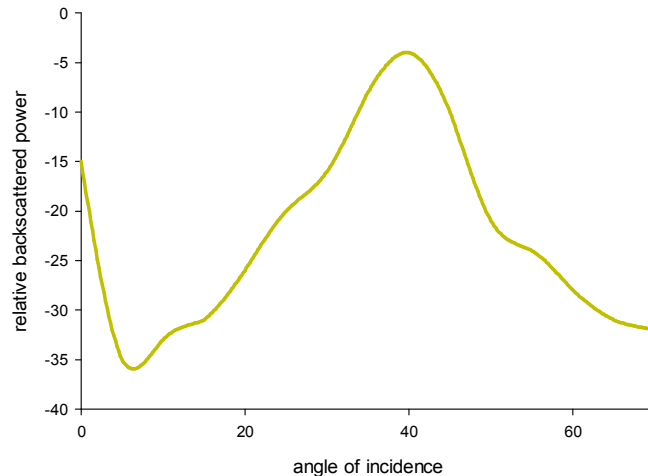


Fig 4.14 Variation of relative backscattered power with angle of incidence for the SCF array at 9.8 GHz .($h_1=0.8\text{mm}$ & $h_2=4.5\text{mm}$)

Figure 4.15 illustrate the measured variations of relative reflected power with frequency for angles of incidence $\theta_i = 26^\circ$ and 39° respectively. Reduction of relative reflected power below -10 dB is achieved for a frequency band of 1.72 GHz for $\theta_i = 26^\circ$ and 1.9 GHz for $\theta_i = 39^\circ$. From figure 4.15 it can be seen that for angle of incidence $\theta_i = 39^\circ$ the reduction of specular reflection below -10 dB is obtained over a frequency band of 1.9 GHz, with a maximum reduction of -27 dB at 9.8 GHz.

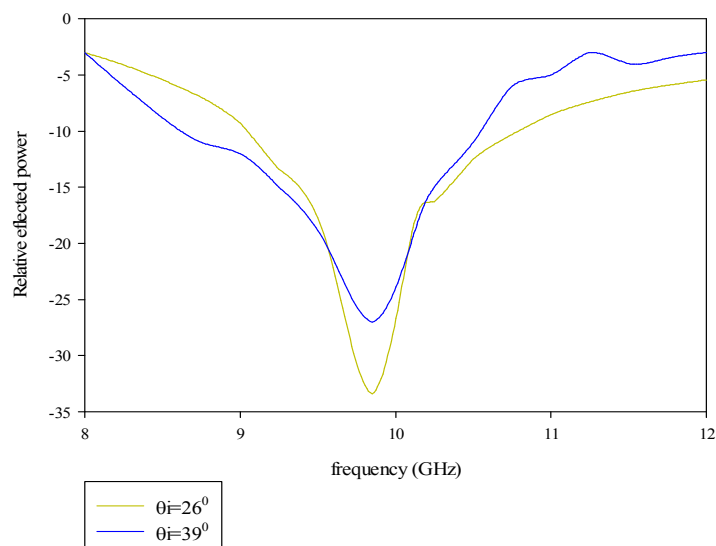


Fig.4.15 Variation of relative reflected power with frequency for the second iterated stages of the SCF arrays for $\theta_i = 26^\circ$ and $\theta_i = 39^\circ$.($h_1=0.8\text{mm}$ & $h_2=4.5\text{mm}$)

Figure 4.16 shows the relative backscattered power with frequency for angles of incidence 26° and 39° respectively. For $\theta_i=39^{\circ}$ a relative backscattered power of -4 dB is obtained at 9.8 GHz while for $\theta_i=26^{\circ}$ the backscattered power remains low throughout the X band. The above measurement results show that the proposed dielectric backed SCF array structure is effective in wide angle elimination of specular reflection over a wide frequency band.

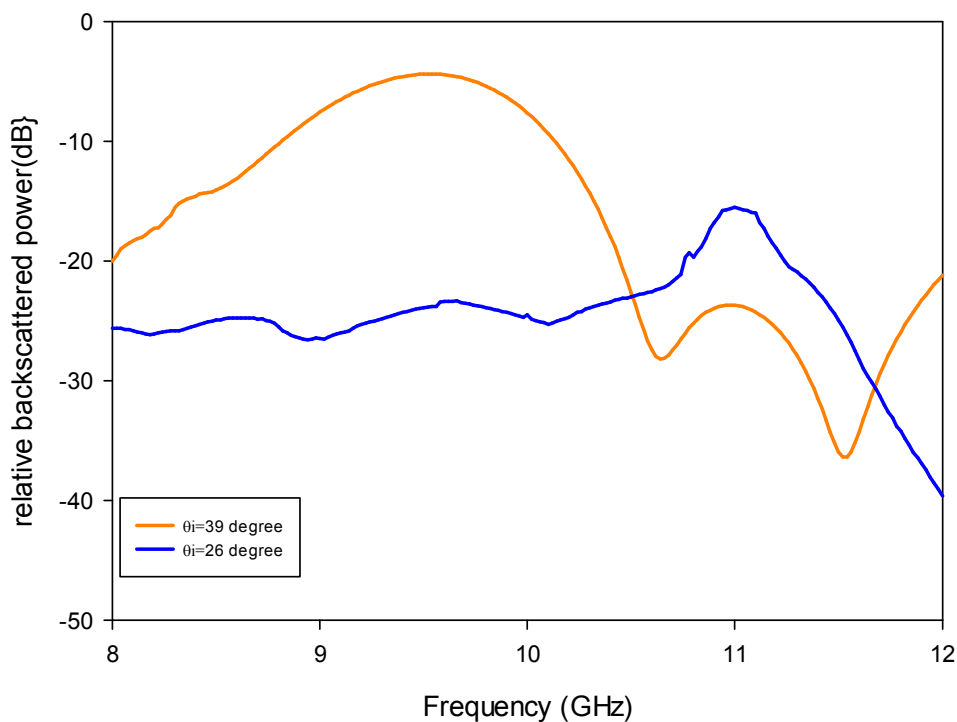


Fig.4.16 Relative backscattered power with frequency at angle of incidence $\theta_i=39^{\circ}$ and $\theta_i=26^{\circ}$ for the second iterated stage of SCF array. ($h_1=0.8\text{mm}$ & $h_2=4.5\text{mm}$)

Figure 4.17 shows the variation of relative reflected power with dielectric thickness for the second iterated stage of the structure at an angle of incidence $\theta_i=26^{\circ}$. The dielectric thickness h_2 is varied from 0 to 0.2λ . From the figure it is found that specular reflection is minimum for $h_2/\lambda=0.14$.

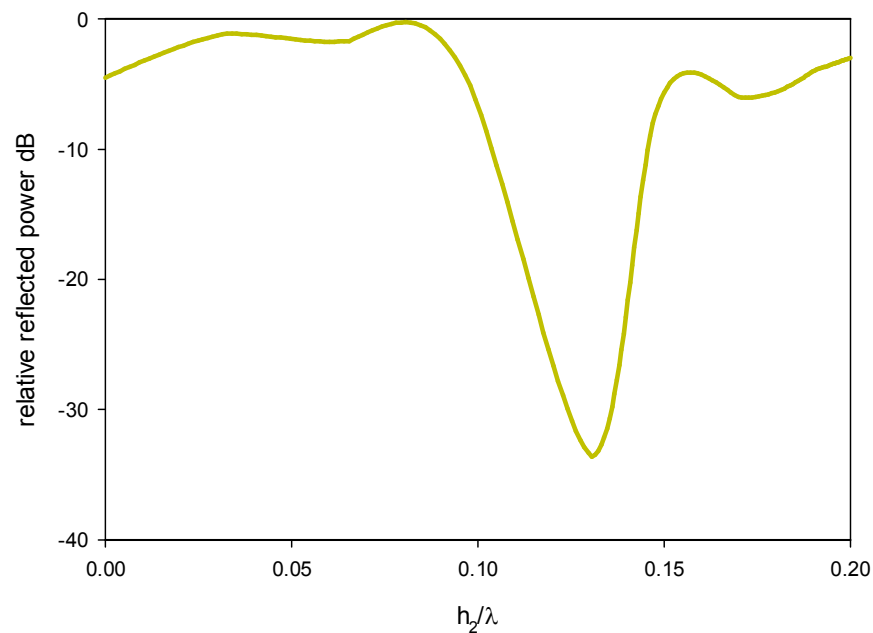


Fig.4.17 Variation of relative reflected power with dielectric thickness (h_2) for the second iterated stage of the SCF array with $h_1=0.8\text{mm}$

From the above discussions it can be seen that the second iterated stage of the 4×4 SCF array can be effectively used for eliminating specular reflection over wide angular range with broad band characteristics. Elimination of specular reflection below -10 dB is achieved over an angular range of $0^\circ - 58^\circ$ at 9.8 GHz. These surfaces may find applications in RCS control and in frequency scanned reflectors.

4.5 STACKED SCF ARRAYS FOR BACKSCATTERING REDUCTION

Scattering studies on flat plates loaded with dielectric backed multilayer SCF arrays is described in this section. Different iterated stages of the SCF arrays stacked with intermediate dielectric sheets on a metal plate and are used in the investigation. Experiments conducted at X band shows a good backscattering reduction over a wide frequency range.

For the experimental studies SCF arrays are etched on 0.8mm FR4 sheets. These arrays are stacked with low loss dielectric sheets of PMMA (poly

methyl methacrylate) of thickness (h) in between as shown in fig 4.18. Experiment is done in X band

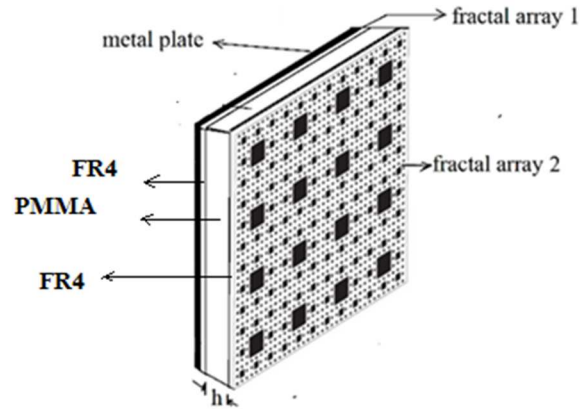


Fig. 4.18 Stacking of two different iterated stages of SCF array

For reducing the overall thickness, stacking of only two fractal structures are considered at a time. The order of stacking is important because backscattered power varies when stacking order is reversed. Measurements are repeated by varying dielectric thickness separating the two stacking fractal arrays. Backscattered power in various angles are also measured by rotating the stacked structure loaded plane plate.

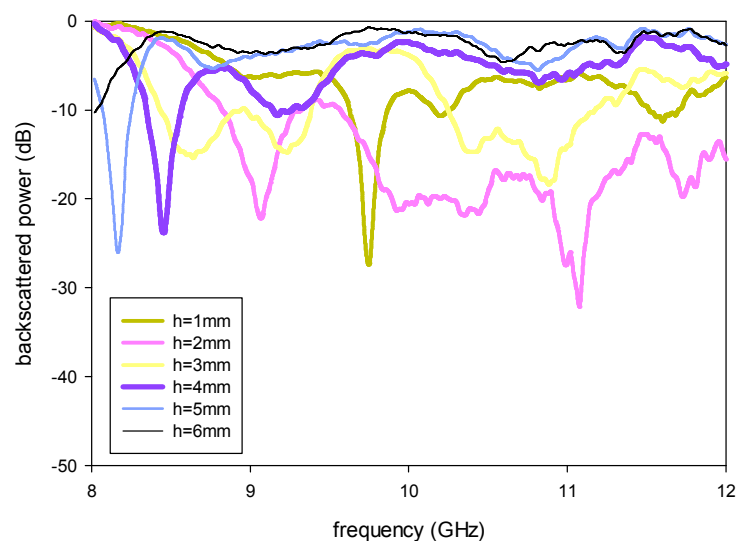


Fig 4.19 Variation of backscattered power with frequency for different dielectric thickness

The thickness (h) of the dielectric separating the two fractal structures are varied and frequency response is plotted in figure 4.19. From the figure it can be seen that backscattered power is minimum over a wide band for a dielectric thickness of $h=2\text{mm}$ with a minimum value of of 32 dB at 11.08 GHz.

Variation of relative backscatterd power with dielectric thickness is plotted in figure 4.20. The backscatterd power reduces to a minimum at $h=2$ mm and then increases as dielectric thickness increases.

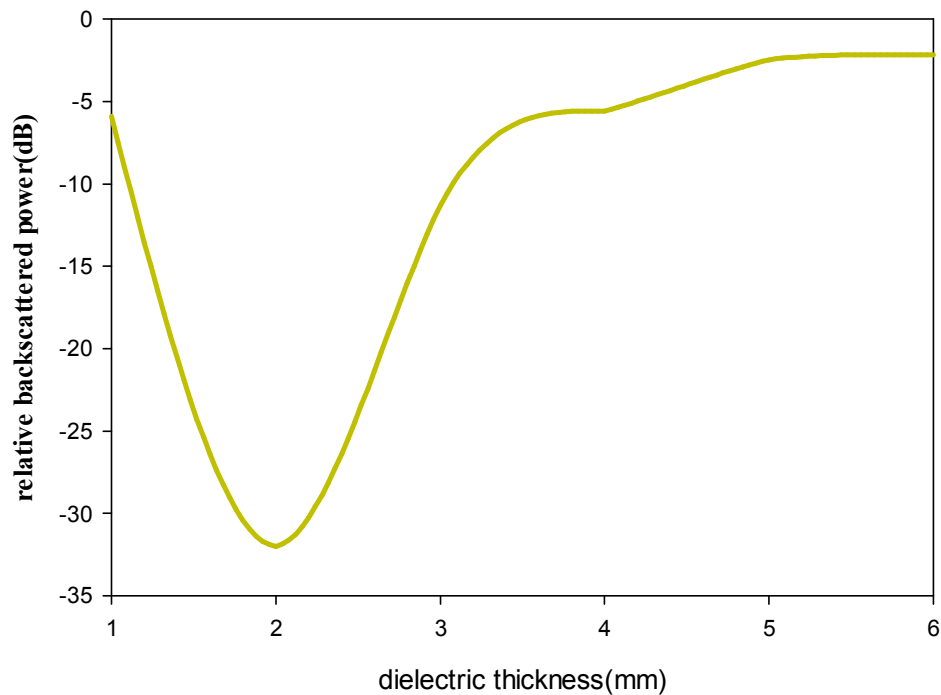


Fig 4.20 Variation of backscattered power with dielectric thickness at $f=11.08$ GHz

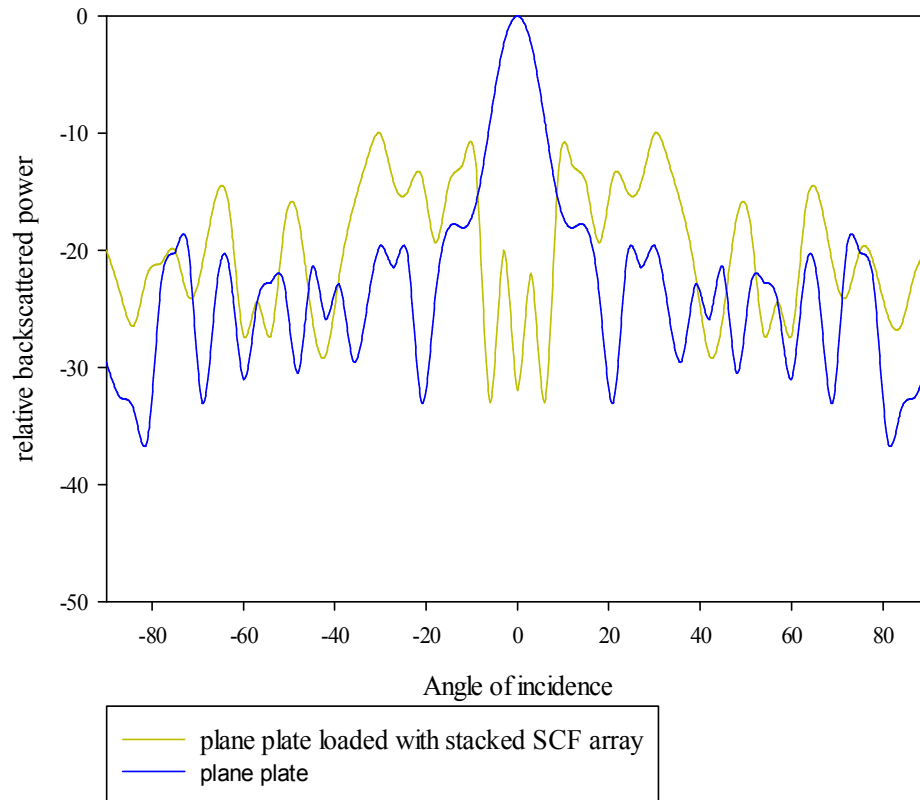


Fig 4.21 Variation of relative backscattered power with angle of incidence at $f=11.08$ GHz for stacked SCF array

Figure 4.21 illustrates the Variation of relative backscattered power with angle of incidence at $f=11.08$ GHz for stacked SCF array. It can be seen that the backscattered power is reduced significantly compared to flat plate.

For normal incidence power scattered in various directions are measured by placing the receiving antenna at various scattering angles of the arch. The received power variations at frequency 11.08 GHz is plotted in figure 4.22. The scattered power is maximum at a angle of 22° .

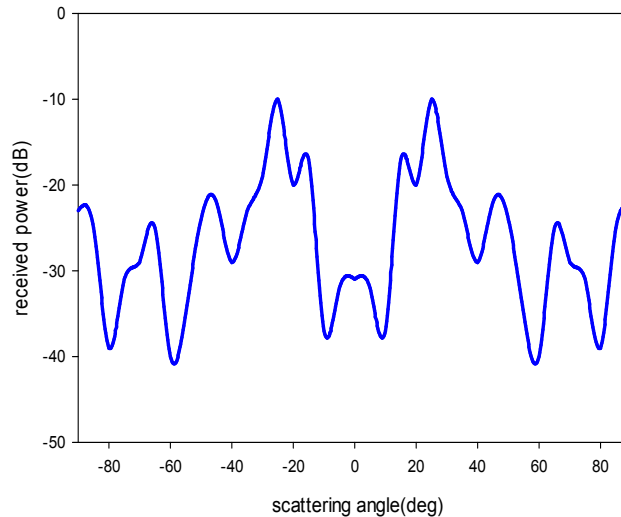


Fig 4.22 Variation of received power with scattering angle at normal incidence for $f = 11.08$ GHz

4.6 INTERLEAVED SCF ARRAY FOR BACKSCATTERING REDUCTION

The fabrication of stacked array is a complicated process, and also it is bulky. So modification on the single fractal arrays is investigated. Here different iterated stages on the same plane are used as array element. Different stages are interleaved as shown in figure 4.23(a), (b) and (c).

Interleaving element by element rowwise (horizontal) or columnwise (vertical) are shown in figure 4.23.

Figure 4.23(c) is the 90° rotated version of 4.20(b).

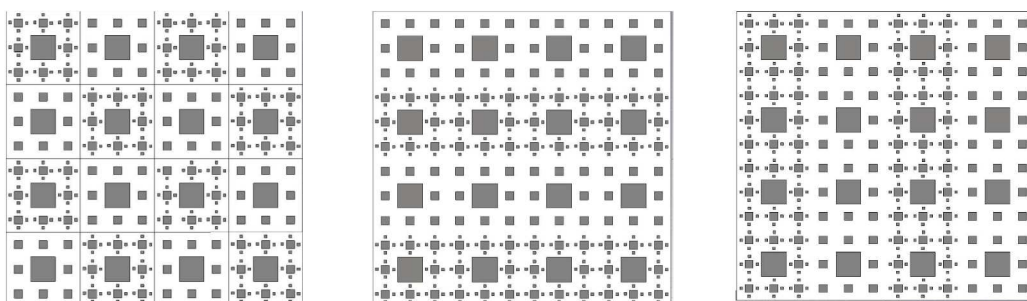


Fig 4.23 (a) Fully interleaved (b) horizontal interleaved (c) vertical interleaved

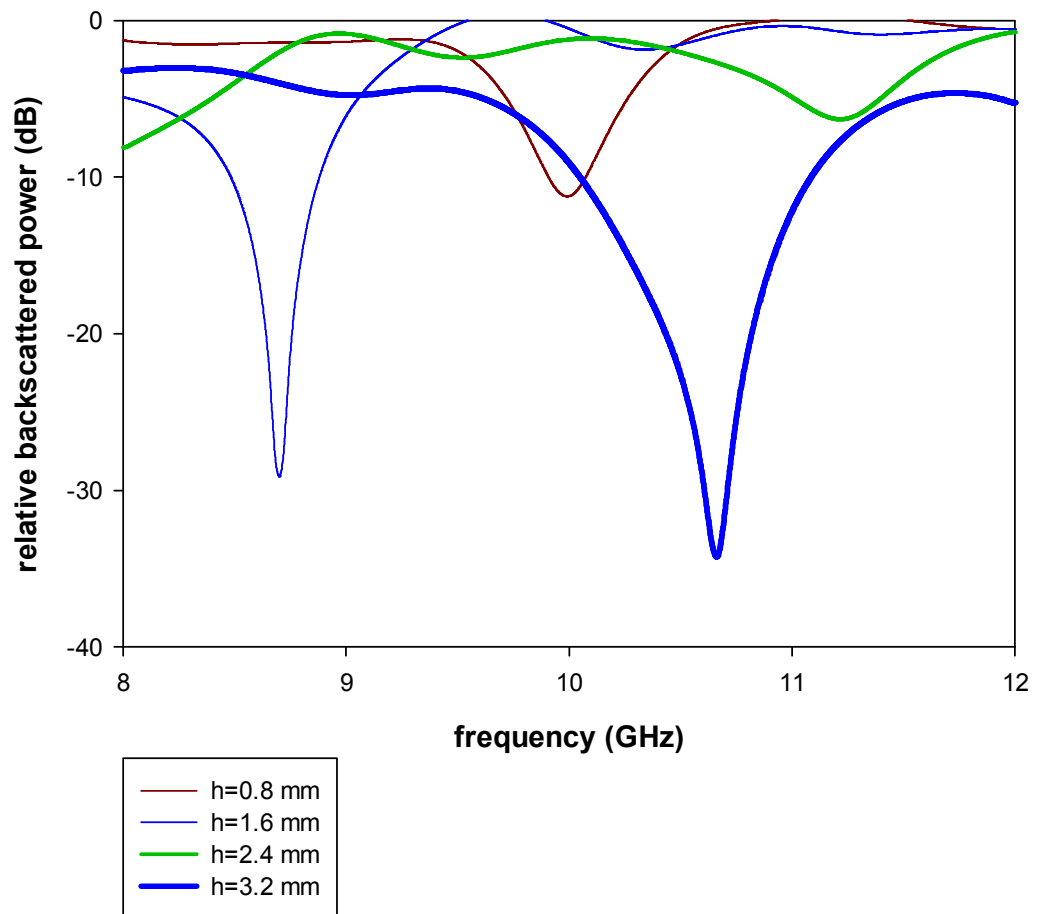


Fig 4.24 Variation of relative backscattered power with frequency for the fully interleaved structure

From figure 4.24 it can be seen that backscattered power is minimum when the fully interleaved structure is of 3.2 mm dielectric thickness. The minimum backscattered power obtained is -35.4 dB at a frequency of 10.66 GHz.

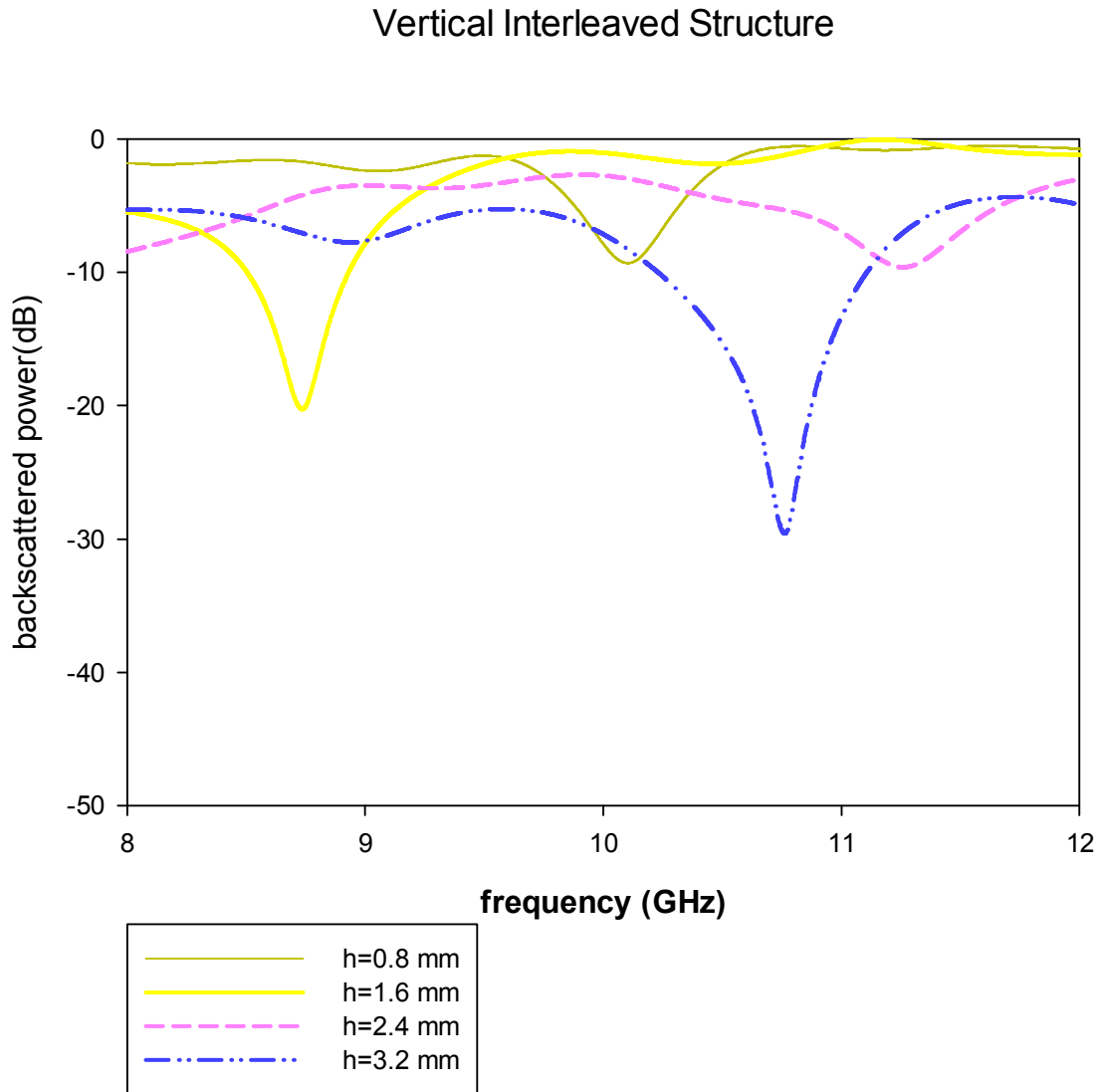


Fig 4.25 Variation of relative backscattered power with frequency when loaded with vertical interleaved structure

When loaded over the flat metal plate with vertical interleaved structure a minimum backscattered power of -30 dB is obtained at a frequency 10.76 GHz. The backscattered power reached a minimum value when the dielectric thickness of the FR-4 substrate is 3.2 mm.

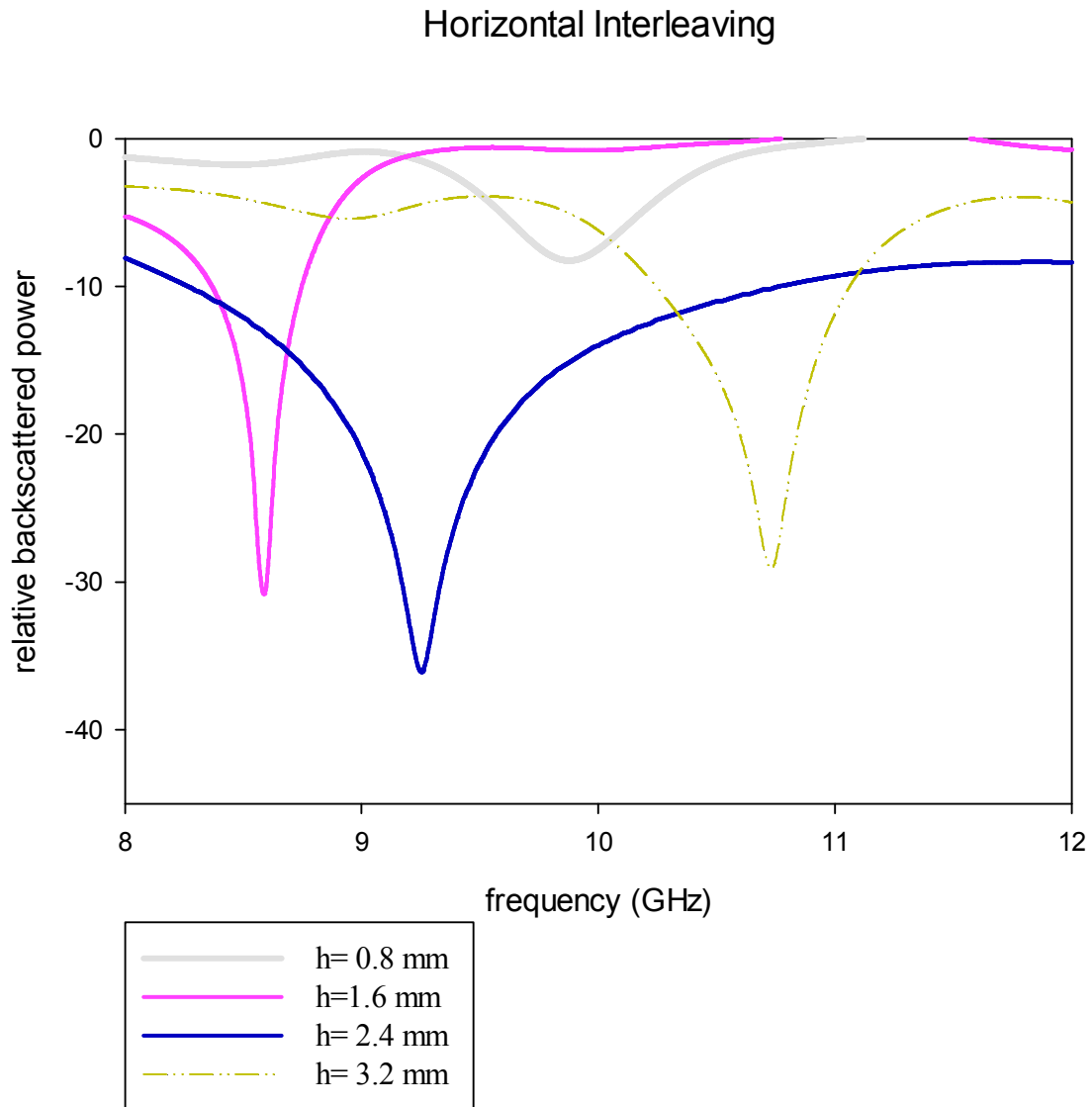


Fig 4.26 Variation of relative backscattered power with frequency when loaded with horizontal interleaved structure

From figure 4.26 it can be seen that for dielectric backed horizontally interleaved structure with a dielectric thickness of 2.4 mm, the backscattered power reached a minimum value of -36 dB at 9.26 GHz. The -10 dB band width is also maximum when the horizontal interleaving structure is used.

A maximum reduction in backscattering over wide band width is obtained when using horizontal interleaving.

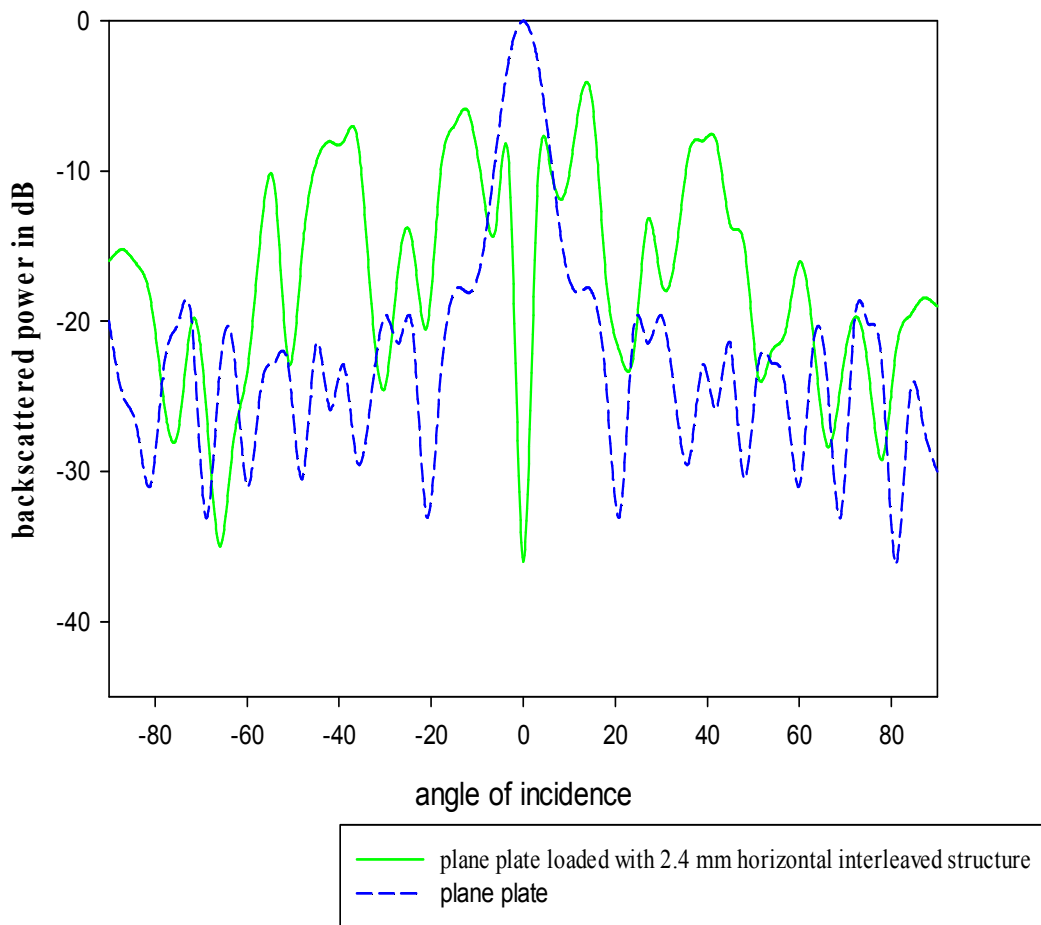


Fig 4.27 Variation of relative backscattered power with angle of incidence of the horizontally interleaved SCF array loaded over the flat plate with a dielectric thickness of 2.4 mm

Variation of relative backscattered power with angle of incidence of the horizontally interleaved SCF array loaded over the flat plate with a dielectric thickness of 2.4 mm is shown in figure 4.27

The backscattered power is maximum at an angle of incidence 19° .

4.7 CONCLUSION

Backscattering reduction of more than 10 dB is attained over the entire X band by loading the second iterated stage of the 4×4 SCF array with a dielectric thickness of 3.2 mm. A maximum reduction of 31.7 dB is obtained at 11.08 GHz for this

structure. At 9.5 GHz a reduction of 28 dB is also attained. The reduction is more than 20 dB for a significant portion of the band. Thus it is established that wideband RCS reduction is obtained using SCF array technique.

At a frequency of 11.08 GHz the received power is maximum at an angle of 25° and for frequency 9.5 GHz the received power is maximum at an angle of 10° . This means that the backscattering reduction is achieved by the scattering of incident power in other directions. The minimum value of backscattered power at normal incidence is obtained for $h=0.107\lambda$.

Blazing effect is observed using SCF arrays. Blazing can produce wide angle elimination of specular reflection from a flat metal plate. The elimination of specular reflection below -10 dB occurs over a wide angular range of 0° - 58° for the present structure. Maximum reduction in reflected power of 34.5 dB is observed at an angle of incidence of 26° . Here the specular reflection is reduced and backscattering is increased in this angular range.

Reduction of reflected power below -10 dB is achieved for a frequency band of 1.72 GHz for an angle of incidence 26° . This is observed for other angles also. For angle of incidence 39° the reduction of specular reflection below -10 dB is obtained over a frequency band of 1.9 GHz, with a maximum reduction of -27 dB at 9.8 GHz. Thus the 4×4 fractal structure is very effective in wide angle elimination of specular reflection over a wide frequency band.

By stacking different iterated stages of SCF arrays a 10 dB reduction in backscattering is obtained over 80 percent of the X band. The maximum backscattering reduction obtained is 32 dB at 11.08 GHz.

The effect of interleaving different iterated stages of the fractal arrays are also considered. Different types of interleaved structures were constructed and measured results show dielectric backed interleaved structure gives good backscattering reduction. For a dielectric thickness of 2.4 mm, the backscattered power reached a minimum value of -36 dB at 9.26 GHz. The -10 dB band width is also better when the horizontal interleaved structure is used.

REFERENCES

- [1] E. V. Jull, N. C. Beaulieu, and D. C. W. Hui “Perfectly blazed triangular groove reflection gratings” *Journal of the Optical Society of America*, Vol. 1, Issue 2, 1984.
- [2] K.A. Jose and K.G. Nair, “Reflector-backed perfectly blazed strip gratings simulate corrugated reflector effects,” *Electronics Letters*, Vol 23, No 2, January 16, 1987.
- [3] D. Saji Stephen, Thomaskutty Mathew, P. Mohanan, and K. G. Nair “A modified strip grating for dual periodicity for RCS reduction,” *Microwave and Optical Technology Letters*, Vol7, No 7, May 1994.
- [4] Thomaskutty Mathew, D. Saji Stephen, K. A. Jose, C. K. Aanandan, P. Mohanan and K. G. Nair “The performance of a novel simulated corrugated surface for the reduction of radar cross section” *Microwave and Optical Technology Letters*, Vol. 6, No. 10, August 1993.
- [5] T. Mathew, D.S. Stephen, C.K. Aanandan, P. Mohanan and K.G. Nair “Wideband trapezoidal strip grating for elimination of specular reflection” *Electronics Letters*, Volume: 30, Issue: 13, 23 Jun 1994.
- [6] Chandran AR, Mathew T, Aanandan C K, Mohanan, P, and Vasudevan K. “Low backscattered dual-polarised metallo-dielectric structure based on Sierpinski carpet”, *Microwave Opt. Technol. Letters*, Vol 40, No 3, pp. 246–248, 2004.
- [7] Chandran A.R, T. Mathew, C K.Aanandan, P.Mohanan, and K Vasudevan, “Frequency tunable metallo-dielectric structure for backscattering reduction,” *IEE Electronics Letters*, Vol. 40, No. 20, 1245–1246, 2004.
- [8] A R Chandran, M Gopikrishna, C K Aanandan, P Mohanan and K Vasudevan, “Scattering behavior of fractal based metallo-dielectric structures”, *Progress in Electromagnetics Research*, Vol. 69, pp 323-339, 2007.

5 SCATTERING BEHAVIOUR OF DIHEDRAL CORNER REFLECTOR LOADED WITH DIELECTRIC BACKED FRACTAL ARRAYS

This chapter presents the results of the scattering measurements of dihedral corner reflectors with corner angles 80° , 90° , 100° , 110° and 120° by loading different iterated stages of the dielectric backed SCF array. Backscattering reduction is achieved for 80° and 90° corners while enhancement in backscattering is observed for higher corner angles.

TABLE OF CONTENTS

- 5.1 Introduction**
 - 5.2 80° Dihedral Corner Reflector Loaded With Dielectric Backed SCF Array**
 - 5.3 90° Dihedral Corner Reflector Loaded With Dielectric Backed SCF Array**
 - 5.4 100° Dihedral Corner Reflector Loaded With Dielectric Backed SCF Array**
 - 5.5 110° Dihedral Corner Reflector Loaded With Dielectric Backed SCF Array**
 - 5.6 120° Dihedral Corner Reflector Loaded With Dielectric Backed SCF Array**
 - 5.7 Conclusions**
-

5.1 INTRODUCTION

Corner reflectors contribute a major portion of backscattering from complex metallic objects. Backscattering from a corner reflector varies with the corner angle.

A detailed study of backscattering from a corner reflector is presented in this chapter. Dielectric loaded Sierpinski Carpet Fractal (SCF) arrays of different iterations are loaded on the internal reflecting surfaces of the corner. The thickness of the dielectric is varied for optimum performance. Measurements are taken for 80° , 90° , 100° , 110° and 120° corner angles.

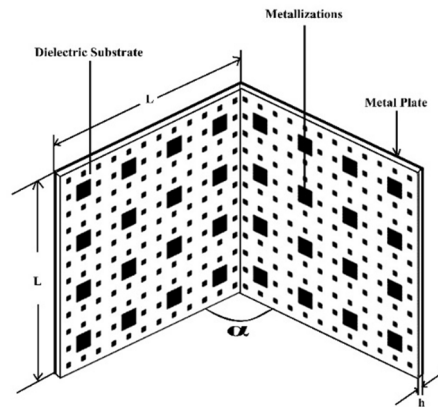


Fig 5.1 Schematic diagram of the dihedral corner reflector loaded with second iterated stage of the SCF array

Figure 5.1 shows a right angled dihedral corner reflector loaded with dielectric backed SCF array of second iteration. FR-4($\epsilon_r = 4.4$) is used as the substrate material with thickness h .

A dihedral corner reflector is constructed by joining two $30\text{ cm} \times 30\text{ cm}$ flat metal plates using a hinge. The corner angle can be varied by using the hinge. The dihedral corner reflector is placed over a dielectric stand on the turn-table at the center of the arch in the anechoic chamber. Measurements are performed using the Rohde & Schwartz ZVB20 VNA. The backscattering from the plane metallic corner is normalized and frequency response is plotted for X band.

5.2 80° DIHEDRAL CORNER REFLECTOR LOADED WITH DIELECTRIC BACKED SCF ARRAY

The hinge is adjusted to have 80° as the corner angle. Dielectric backed SCF arrays of different iterated stages are loaded over the Dihedral Corner Reflector. Backscattering measurements are repeated by varying the dielectric thickness and presented in figure 5.2.

It can be seen that backscattering reduction is achieved for the entire X band by using the first iterated stage of the dielectric backed SCF array. A maximum reduction of -29.1dB is obtained at a frequency of 10.1 GHz when loaded with first iterated stage of the SCF array backed with a dielectric thickness of 2.4 mm.

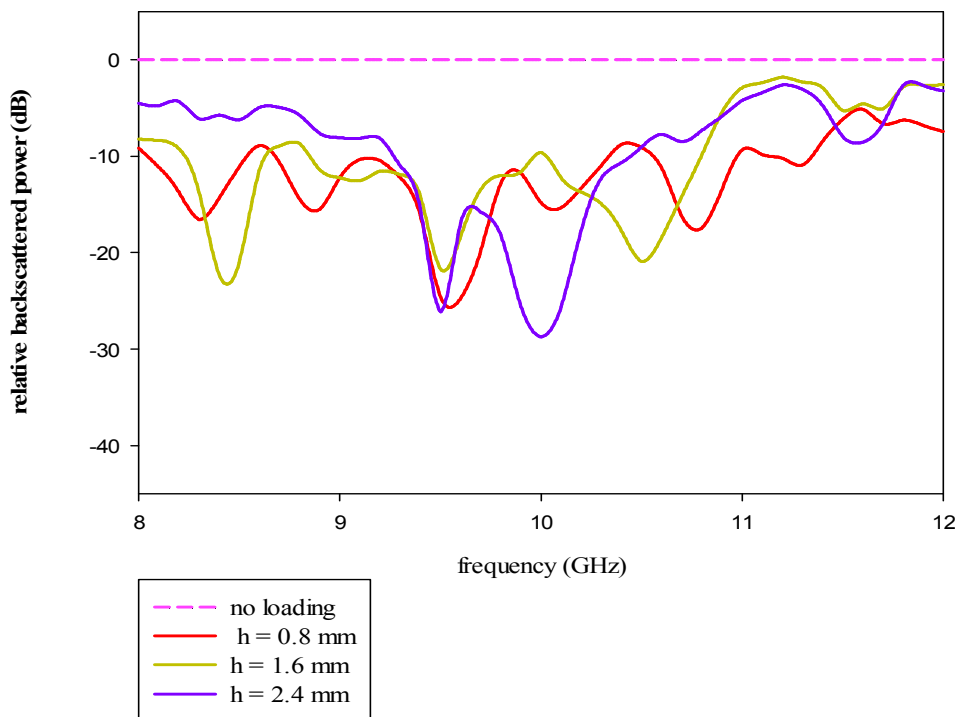


Fig 5.2 Variation of backscattered power with frequency for the 80° dihedral corner loaded with dielectric backed first iterated SCF array of different dielectric thickness (h)

The effect of second iterated stage of the SCF array loading over the 80° corner is studied and the response is shown in figure 5.3. Backscattering reduction is obtained for most portions of the X band by using the second iterated stage. The

maximum reduction obtained is -33.33 dB at a frequency 11.29 GHz when the dielectric thickness of the FR4 substrate is 2.4 mm.

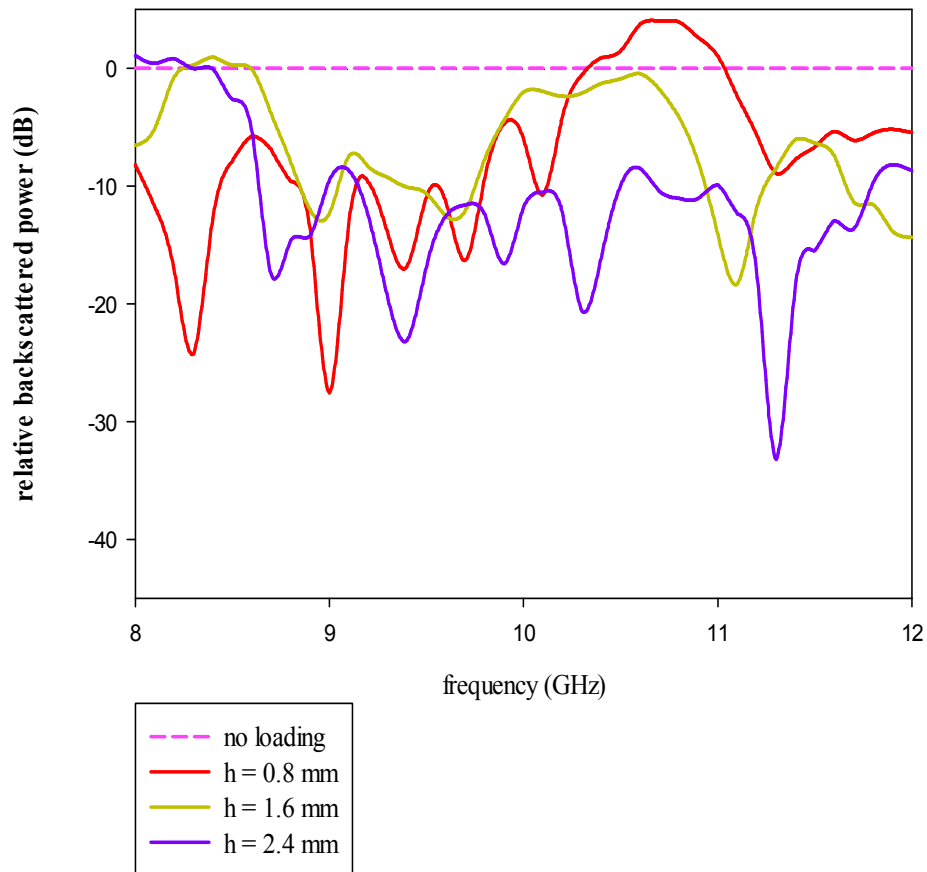


Fig 5.3 Variation of backscattered power with frequency for the 80° dihedral corner loaded with dielectric backed second iterated SCF array of different dielectric thickness (h)

Figure 5.4 shows the frequency response for the 80° corner reflector loaded with dielectric backed SCF array of third iteration with varying substrate thickness. Dielectric thickness of 2.4 mm gives backscattering reduction for the entire X band with a maximum reduction of -30.32 dB at a frequency of 11.29 GHz.

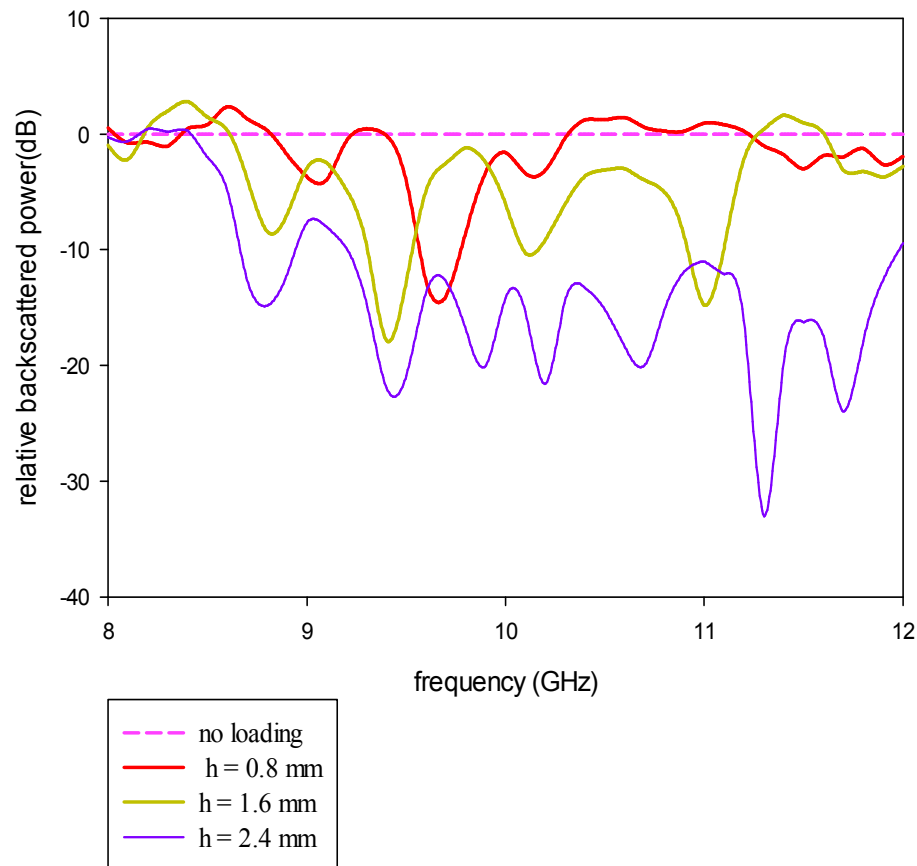


Fig 5.4 Variation of backscattered power with frequency for the 80° dihedral corner loaded with dielectric backed third iterated SCF array of different dielectric thickness (h)

By comparing the three iterated stages with varying dielectric thickness, it is found that a maximum reduction of -33.33 dB is achieved by using 2.4 mm FR4 backed second iterated stage of the SCF at a frequency 11.29 GHz.

5.3 90° DIHEDRAL CORNER REFLECTOR LOADED WITH DIELECTRIC BACKED SCF ARRAY

A right angled corner reflector provides a large back scattering over a wide angular range in a plane normal to its wedge. The effect of loading the three different iterated stages of the SCF array with varying dielectric thickness over the right angled corner is studied.

Figure 5.5 shows variation of backscattered power with frequency at normal incidence for the X band, when the right angled dihedral corner is loaded by dielectric backed first iterated stage of the SCF array.

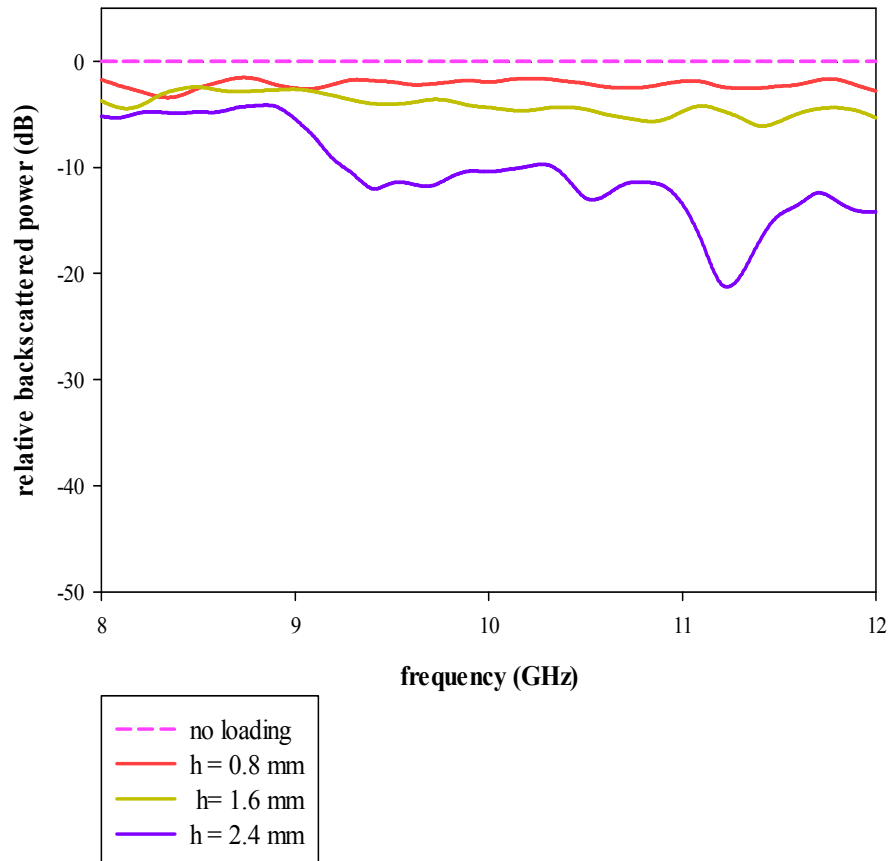


Fig 5.5 Variation of backscattered power with frequency for the 90° dihedral corner loaded with dielectric backed first iterated SCF array of different dielectric thickness (h)

A Maximum reduction of -21.2 dB is obtained when the dielectric thickness is 2.4mm at a frequency 11.24 GHz.

Figure 5.6 shows backscattering from the right angled corner with different dielectric thickness loaded with the second iterated stage of the SCF array.

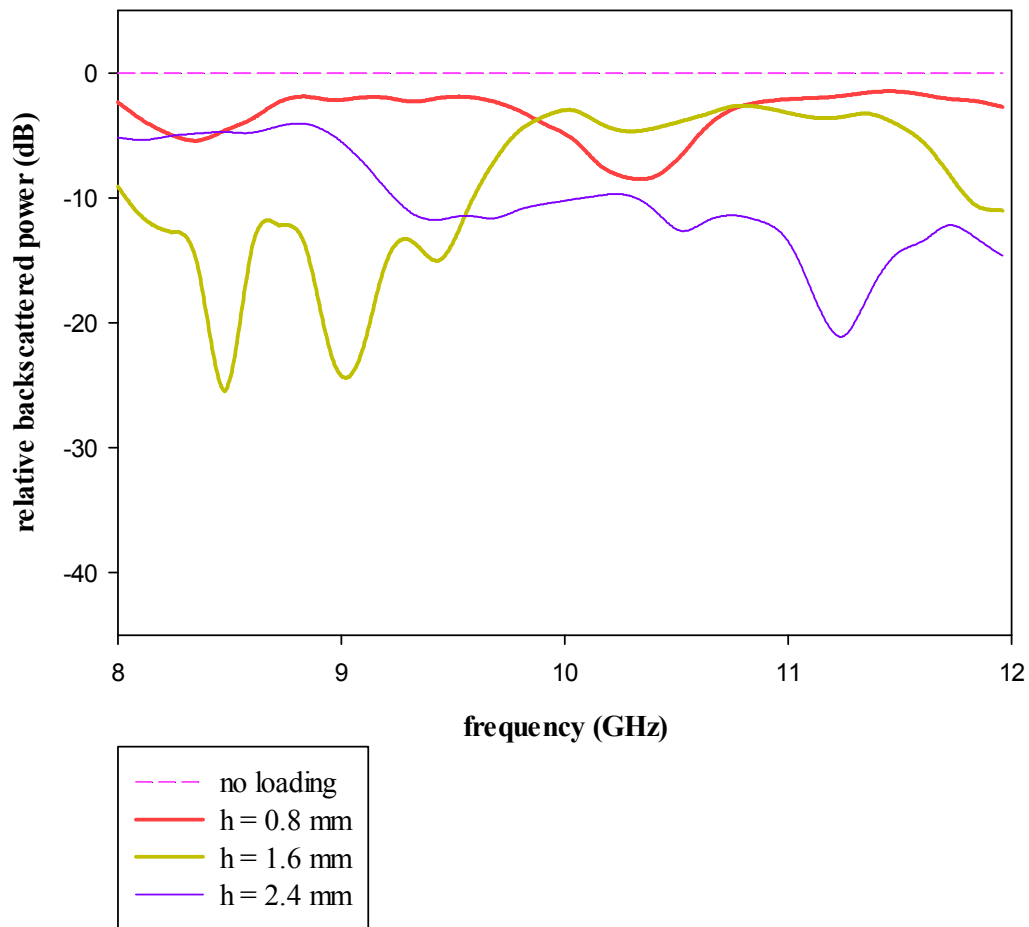


Fig 5.6 Variation of backscattered power with frequency for the 90° dihedral corner loaded with dielectric backed second iterated SCF array of different dielectric thickness (h)

The maximum reduction obtained is -25.39dB at a frequency 8.48 GHz for a thickness of 1.6 mm.

Study is repeated for the third stage and the response is shown in Figure 5.7. Maximum backscattering reduction of -29.7dB is obtained for 2.4 mm substrate thickness at a frequency 11.64 GHz.

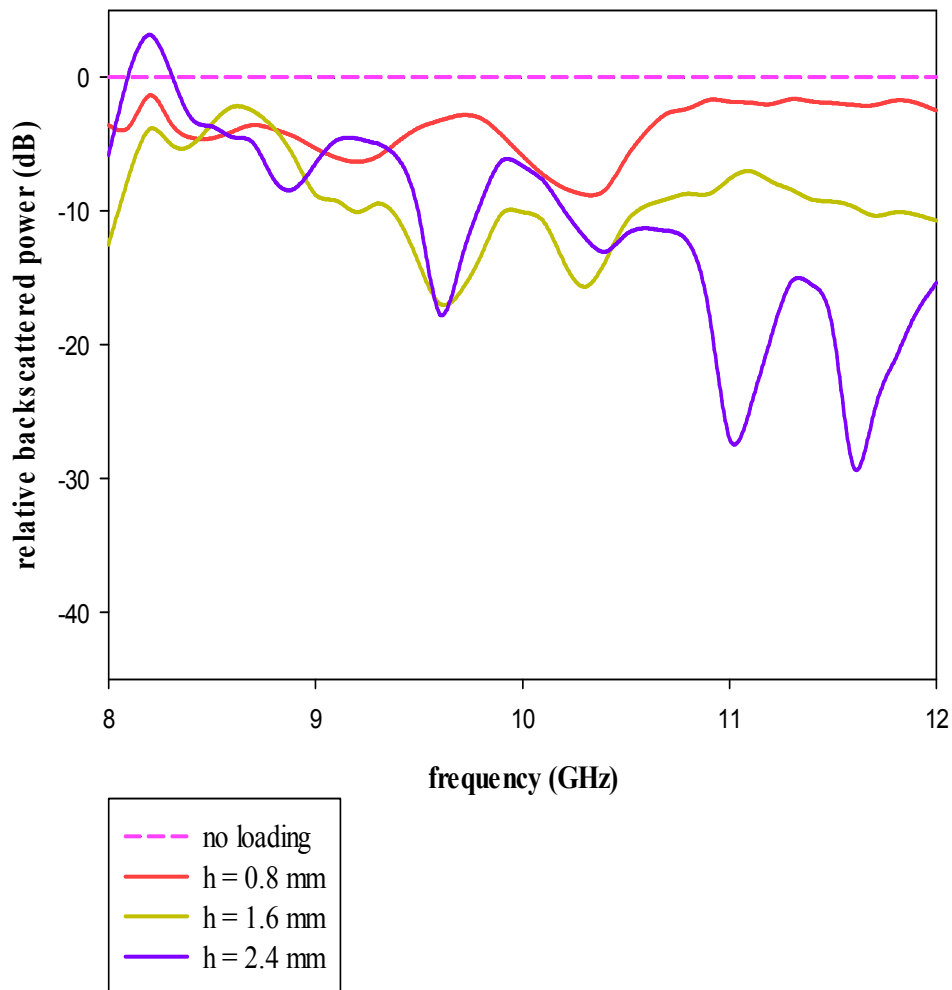


Fig 5.7 Variation of backscattered power with frequency for the 90° dihedral corner loaded with dielectric backed third iterated SCF array of different dielectric thickness (h)

Figure 5.8 shows the scattering pattern in the azimuth angular range for the 90° metallic dihedral corner reflector loaded with 2.4 mm FR4 backed SCF array of third iteration. The pattern plotted for plane corner reflector is also shown in the figure for the sake of comparison. It can be seen from the graph that, the reduction in backscattering is effective over a wide azimuth angular range.

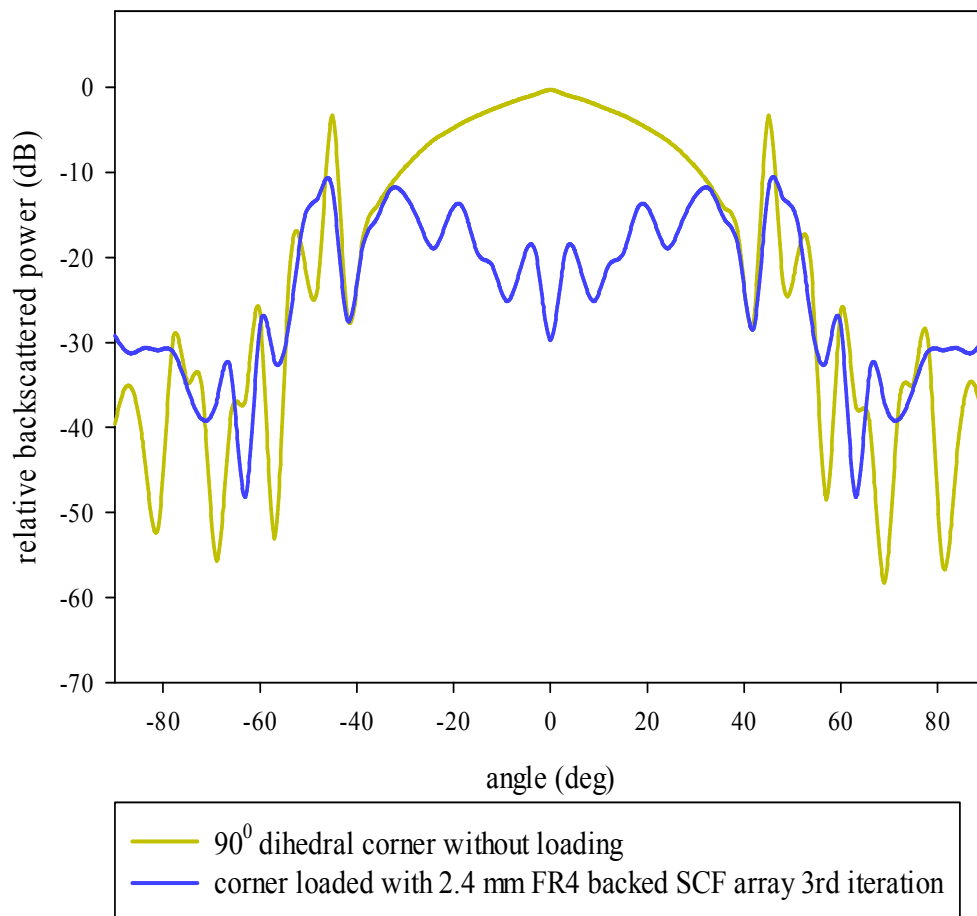


Fig 5.8 Scattering pattern for the 90° metallic corner and the dielectric backed SCF array loaded corner for frequency 11.64 GHz

5.4 100° DIHEDRAL CORNER REFLECTOR LOADED WITH DIELECTRIC BACKED SCF ARRAY

Figure 5.9 shows the frequency response plot for the 100° corner reflector loaded with dielectric backed first iterated stage of SCF array. Backscattering increases when the corner is loaded with first iterated stage of the SCF array with substrate thickness 0.8 mm and 2.4 mm while backscattering is obtained for a portion of the X band when the array is loaded with a substrate thickness of 1.6 mm.

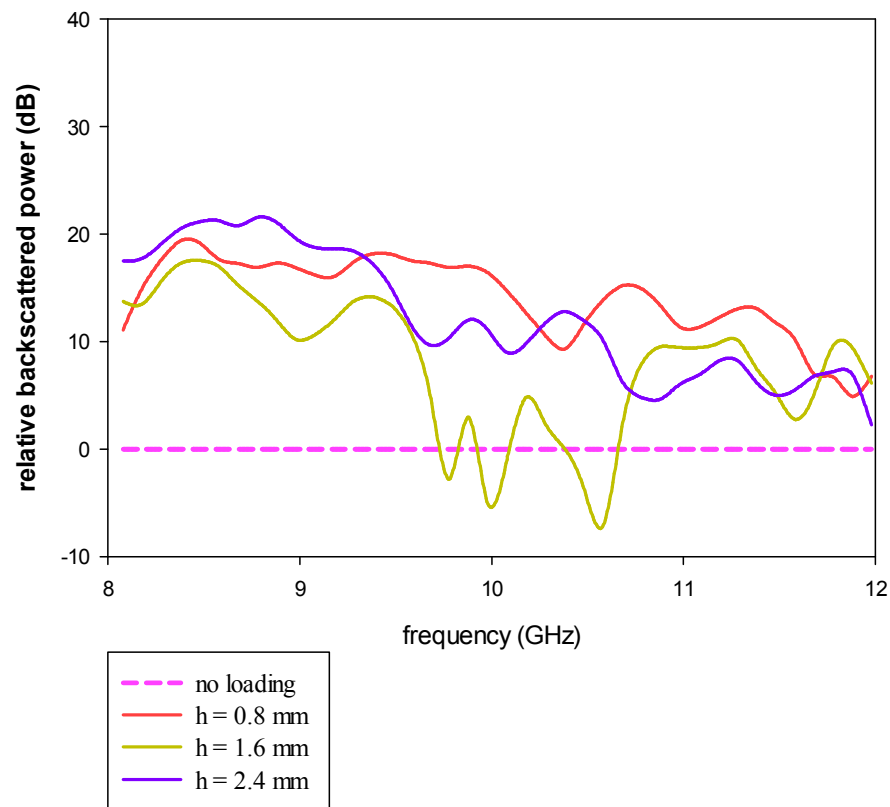


Fig 5.9 Variation of backscattered power with frequency for the 100° dihedral corner loaded with dielectric backed first iterated SCF array of different dielectric thickness (h)

Maximum reduction of -9.18 dB is measured at a frequency of 10.56 GHz when the dielectric substrate thickness is 1.6 mm.

The first iterated stage with 2.4 mm dielectric thickness give a maximum backscattering enhancement of 21.5 dB at 8.81 GHz.

Figure 5.10 shows the variation in backscattering with frequency for a 100° corner reflector loaded with dielectric backed second iterated stage of SCF array. Reduction of backscattering is obtained for the frequency band 11.34 GHz to 12 GHz. A maximum reduction of -19.88 dB is attained at a frequency 11.7 GHz.

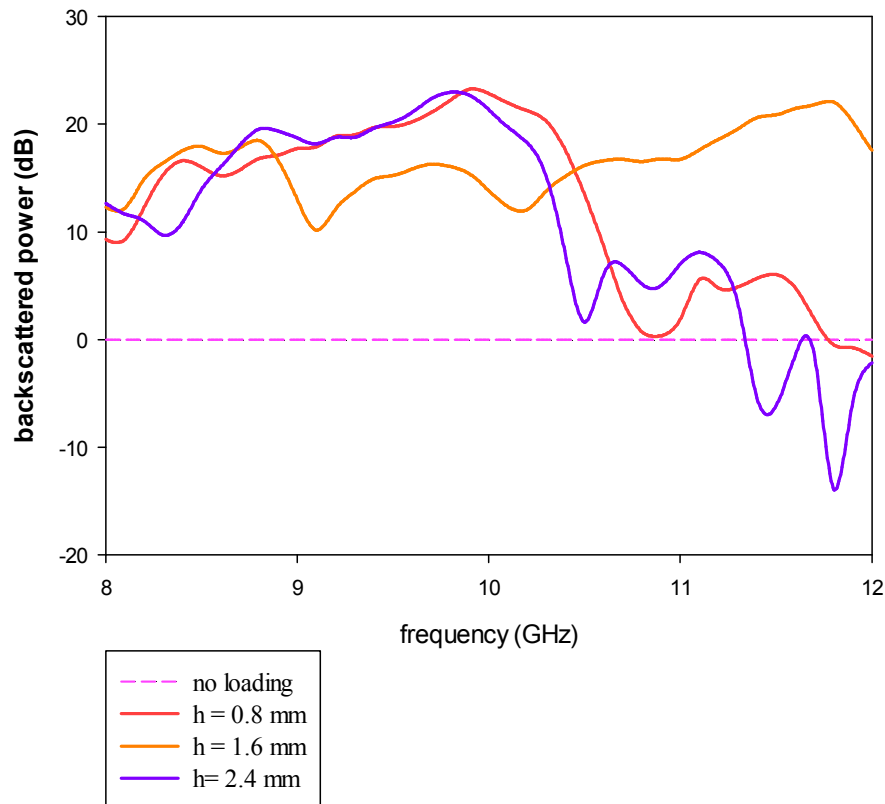


Fig 5.10 Variation of backscattered power with frequency for the 100° dihedral corner loaded with dielectric backed second iterated SCF array of different dielectric thickness (h)

Dielectric thickness of 0.8mm and 1.6mm give enhancement in backscattering over the full X band with the second iterated stage for the 100° corner reflector. Maximum enhancement of 22.9 dB is measured at frequency 9.86 GHz when the corner is loaded with the second iterated stage of the SCF array of dielectric substrate thickness 2.4 mm.

Figure 5.11 shows the variation in backscattering with frequency when the 100° corner reflector is loaded with dielectric backed SCF of third iteration. It can be seen that backscattering reduction is achieved for the upper frequency band while backscattering gets increased at the lower frequencies. Reduction in backscattering is obtained from 10.41 GHz to 12 GHz with a maximum reduction of -21.66 dB at

11.45 GHz when the 100° corner reflector is loaded with 2.4 mm FR4 substrate backed third iterated stage of the SCF array.

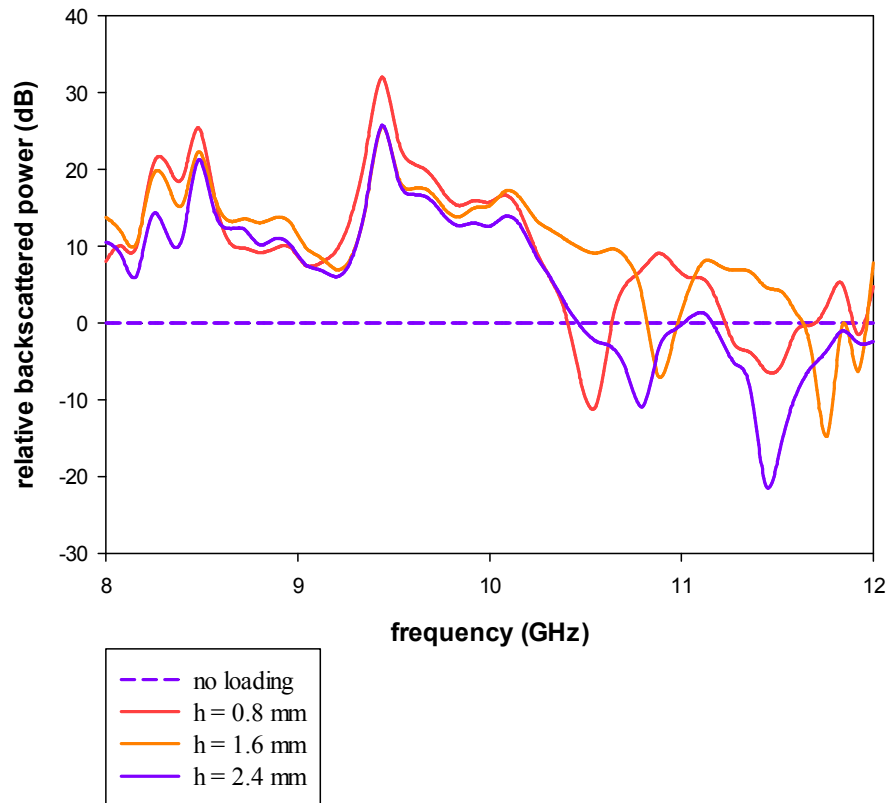


Fig 5.11 Variation of backscattered power with frequency for the 100° dihedral corner loaded with dielectric backed third iterated SCF array of different dielectric thickness (h)

Backscattering gets increased at the lower frequencies with a maximum enhancement of 31.32 dB at 9.42 GHz when the fractal array is loaded with 0.8 mm dielectric thickness.

5.5 110° Dihedral Corner Reflector loaded with dielectric backed SCF array

Figure 5.12 shows the frequency response plot for 110° corner reflector, loaded with dielectric backed first iterated stage of SCF array. Backscattering reduction is obtained for frequency bands 8.76 GHz to 9.08 GHz and 9.46 GHz to 11.42 GHz.

Maximum reduction is obtained for the frequency 11.42 GHz and is measured as -21.9 dB with 2.4 mm dielectric thickness.

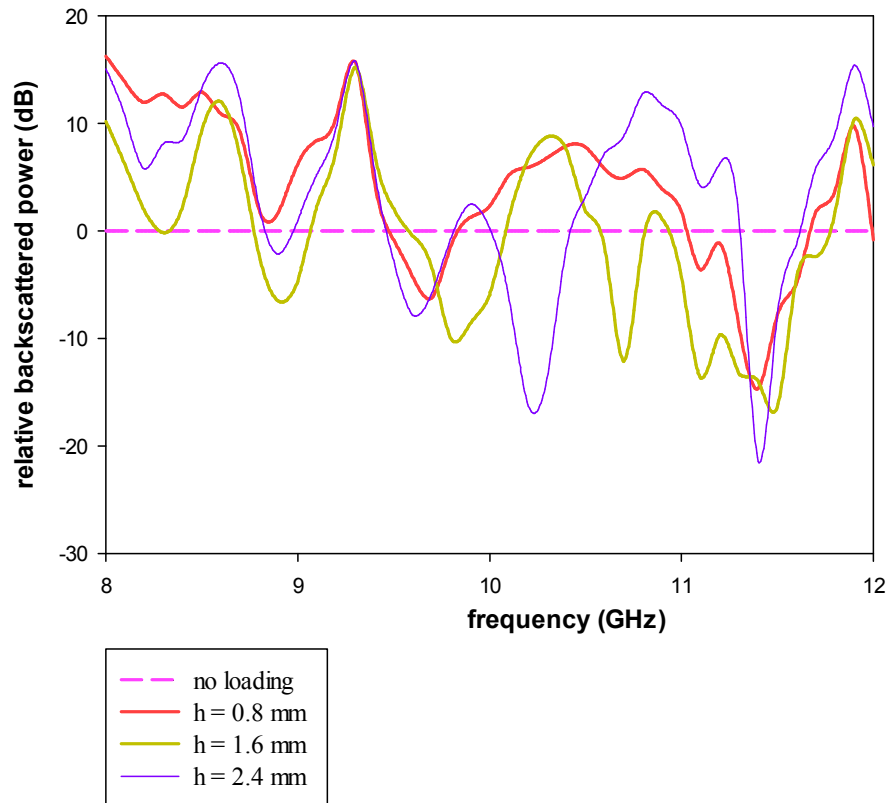


Fig 5.12 Variation of backscattered power with frequency for the 110° dihedral corner loaded with dielectric backed first iterated SCF array of different dielectric thickness (h)

The frequency bands 8 GHz to 8.76 GHz, 9.08 GHz to 9.46 GHz and 11.42 to 12 GHz of the X band showed enhancement in backscattering when the 110° corner reflector was loaded by dielectric backed first iterated stage of the SCF array. Enhancement in backscattering reached a maximum of 15.12 dB at 9.28 GHz when the dielectric substrate thickness is 2.4 mm.

Relative backscattered power is plotted in figure 5.13 for frequencies of the X band when 110° corner reflector is loaded with dielectric backed second iterated stage of the SCF array.

Reduction in backscattering is only in a negligible portion of the X band. Maximum enhancement in backscattering is measured as 24.56 dB at 11.17 GHz for a dielectric thickness of 2.4 mm.

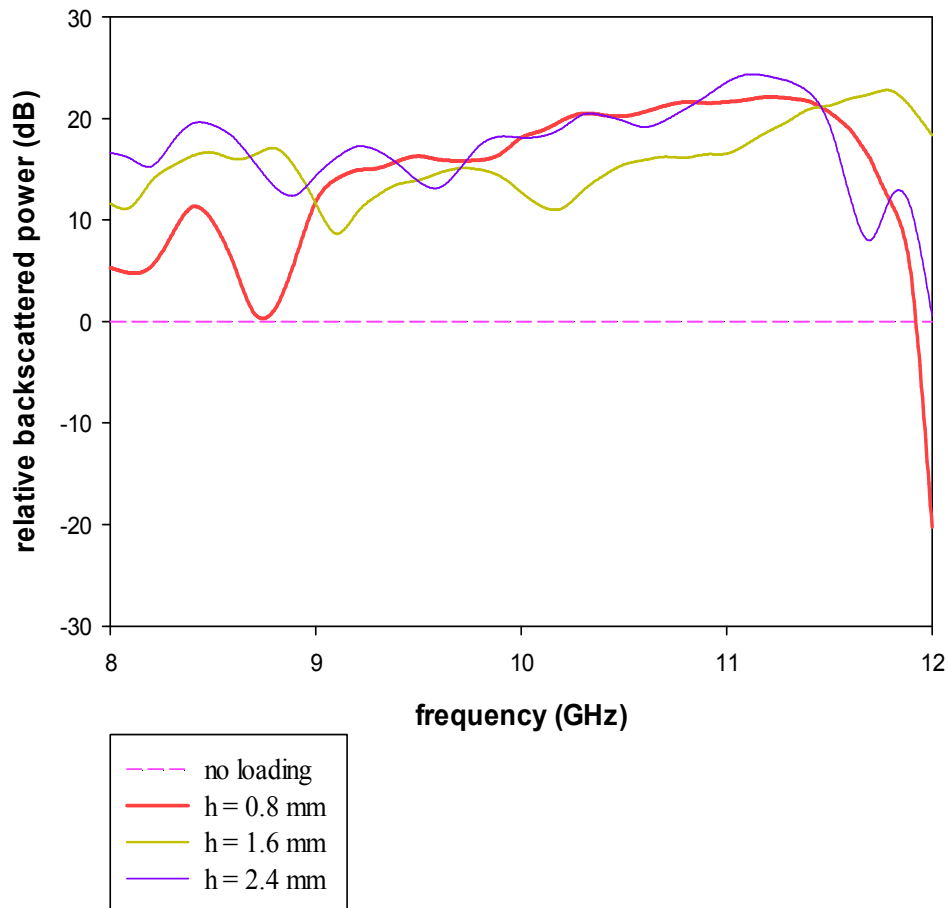


Fig 5.13 Variation of backscattered power with frequency for the 110° dihedral corner loaded with dielectric backed second iterated SCF array of different dielectric thickness (h)

Relative backscattered power variation with frequency is shown in figure 5.14 when the 110° corner reflector is loaded with dielectric backed third iterated stage of SCF array. Significant portion of the X band shows enhancement in backscattering with the maximum measured value of 21.18 dB at 9.86 GHz.

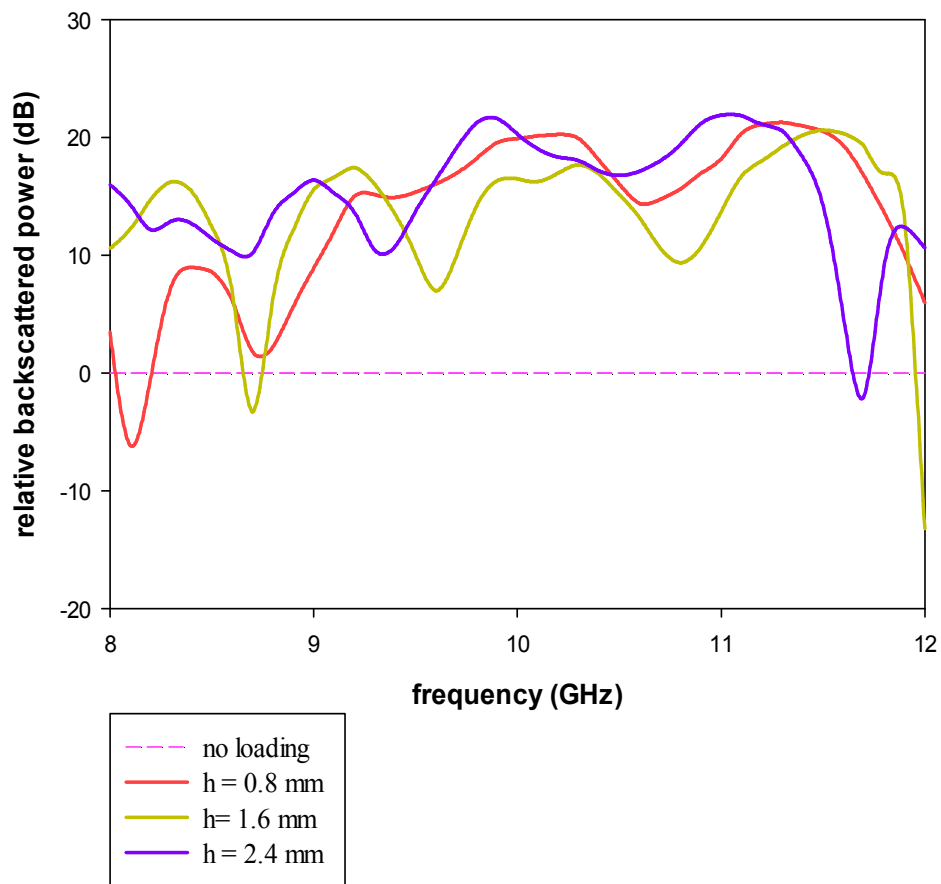


Fig 5.14 Variation of backscattered power with frequency for the 110° dihedral corner loaded with dielectric backed third iterated SCF array of different dielectric thickness (h)

Backscattering reduction is also shown for three very small band widths with a maximum reduction of -6.28 dB at 8.1 GHz when the substrate thickness is 0.8 mm.

For the 110° corner reflector backscattering reduction is achieved for a significant portion of the X band by using first iterated stage of the dielectric backed SCF array. With 2.4 mm dielectric thickness the backscattering reduction is maximum using first iterated stage of the SCF array at a frequency 11.42 GHz and is measured as -21.9 dB.

5.6 120° DIHEDRAL CORNER REFLECTOR LOADED WITH DIELECTRIC BACKED SCF ARRAY

Figure 5.15 shows variation of backscattered power with frequency for the first iterated stage of 120° dielectric backed SCF array. Backscattering reduction is achieved for the frequency bands 8.16 GHz to 9.21 GHz, 9.69 to 10.41 GHz, 10.64 to 10.96 and 11.4 to 12 GHz. Maximum reduction of -21.95 dB is measured at a frequency of 11.61 GHz when the corner is loaded with SCF array of substrate thickness 1.6mm.

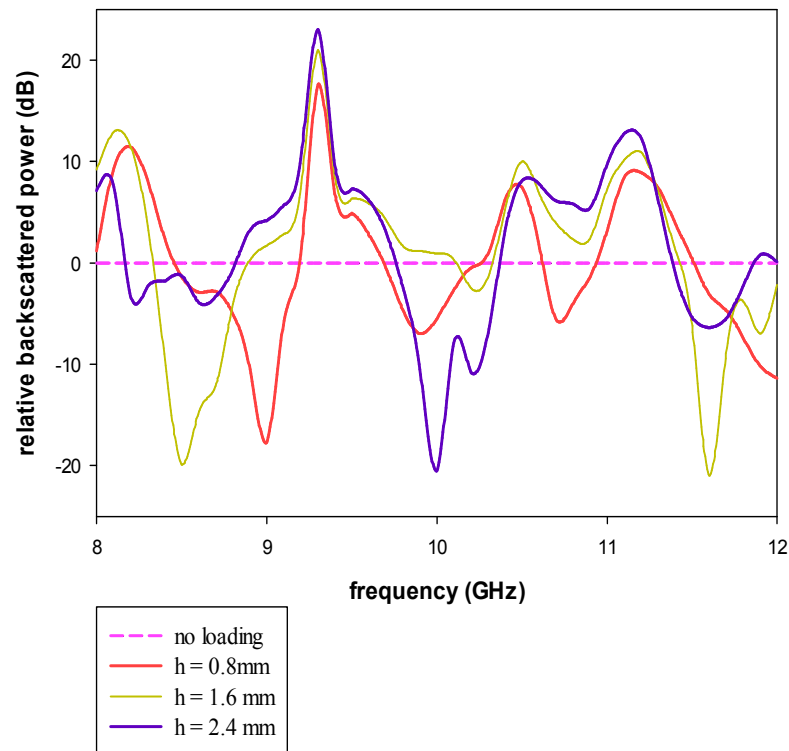


Fig 5.15 Variation of backscattered power with frequency for the 120° dihedral corner loaded with dielectric backed first iterated SCF array of different dielectric thickness (h)

Enhancement in backscattering is obtained mostly when the dielectric thickness is increased to 2.4 mm. A maximum enhancement of 23.1 dB is obtained for the frequency 9.29 GHz.

Figure 5.16 is a plot of variation in backscattered power with frequency when the 120° dihedral corner is loaded with the second iterated stage of the SCF array of different thickness. Backscattering reduction is obtained only for three small bands with a maximum reduction of -18.8 dB at 9.11 GHz for a dielectric thickness of 2.4 mm.

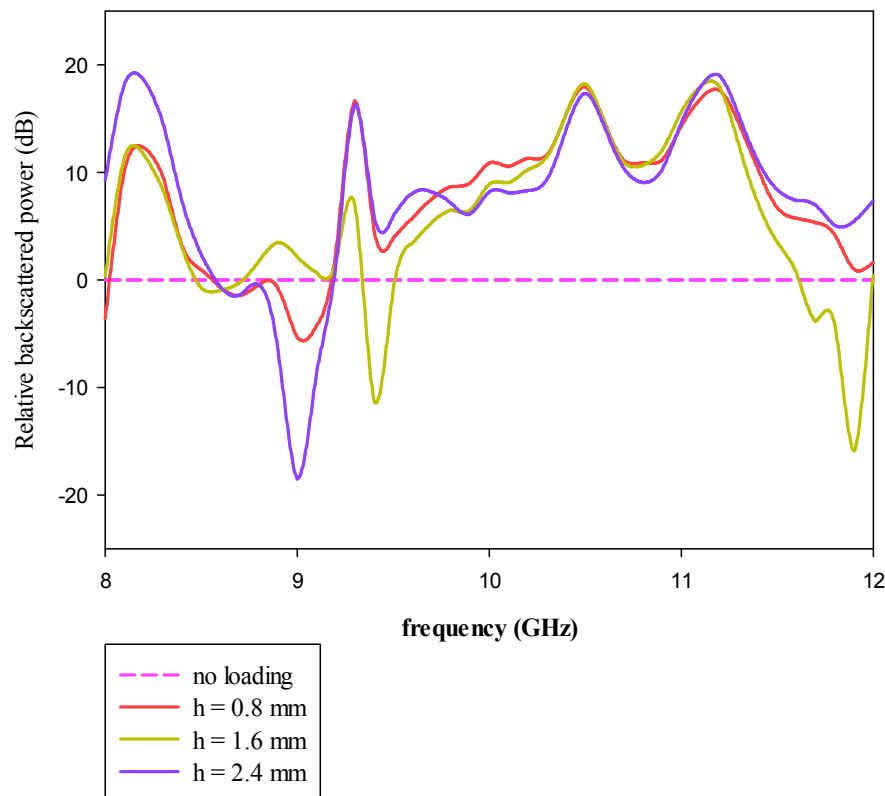


Fig 5.16 Variation of backscattered power with frequency for the second iterated stage of 120° dielectric backed SCF array

Enhancement in backscattering is obtained for almost the entire X band with a maximum enhancement of 19.5 dB at 8.16 GHz for a substrate thickness of 2.4 mm.

Figure 5.17 shows variation of backscattered power with frequency when the dihedral corner is loaded with the third iterated stage dielectric backed SCF array. Reduction in backscattering is achieved for the frequency band 8 GHz to 9.21GHz. Maximum reduction of -15.1 is obtained at a frequency 8.97 GHz.

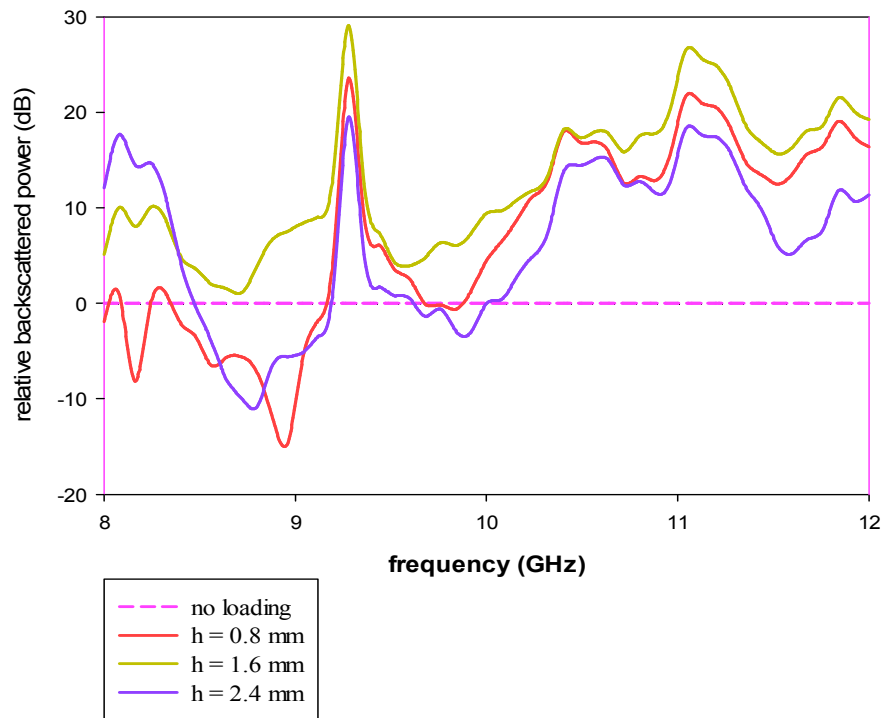


Fig 5.17 Variation of backscattered power with frequency for the third iterated stage of 120° dielectric backed SCF array

From figure 5.17 it is observed that enhancement in backscattering can be achieved by loading third iterated stage of the dielectric backed SCF array for the entire X band. Maximum increase in backscattering is measured as 28.81 at 9.28 GHz.

For the 120° corner reflector backscattering reduction is achieved for a large range of frequency in the X band when loaded with the first iterated stage of the SCF array. The second and third iterated stages of the SCF arrays when loaded over the 120° dihedral corner reflector give enhancement in backscattering.

5.7 CONCLUSIONS

Reduction in backscattering is achieved for the entire X band for 80° and 90° corner reflectors by loading dielectric backed SCF arrays. Backscattering reduction can be achieved only over a small band for the 100° dihedral corner reflector. By

proper selection of substrate thickness and the iterated stage of SCF array reduction in backscattering can be achieved for about 50 percent of the X band.

110° Dihedral corner reflector gives an enhancement in backscattering when loaded with dielectric backed SCF arrays. For the 120° corner reflector enhancement in backscattering is obtained for almost the entire X band with a maximum enhancement of 19.5 dB at 8.16 GHz for a substrate thickness of 2.4 mm.

6 ENHANCEMENT OF BACKSCATTERING FROM A METALLIC WEDGE USING DIELECTRIC BACKED FRACTAL ARRAYS

This chapter presents the results of the investigations on the enhancement of backscattering metallic wedges using dielectric backed fractal arrays. Metallic wedges with angles 80° , 90° , 100° , 110° and 120° are loaded with dielectric backed SCF array and the measured results of backscattering are presented.

TABLE OF CONTENTS

- 6.1 Introduction**
 - 6.2 80° Metallic wedge loaded with dielectric backed SCF array**
 - 6.3 90° Metallic wedge loaded with dielectric backed SCF array**
 - 6.4 100° Metallic wedge loaded with dielectric backed SCF array**
 - 6.5 110° Metallic wedge loaded with dielectric backed SCF array**
 - 6.6 120° Metallic wedge loaded with dielectric backed SCF array**
 - 6.7 Conclusion**
-

6.1 INTRODUCTION

Wedge shaped parts of aircrafts like lower fuselage and drooped wingtips contribute to backscattered power in radar detection. Very large trailing edge wedge is common in aircrafts. Enhancement of backscattered power is important in

commercial aircrafts. The radar cross section and thus the detectability of the aircrafts can be increased by enhancing the backscattering from wedges.

This chapter presents the results of the investigations on of backscattering from metallic wedges of different angles and modifying the behavior by loading the surfaces with dielectric backed fractal arrays.

Wedges of angles 80° , 90° , 100° , 110° and 120° are constructed using two identical flat metal plates connected by a hinge. The metallic plates are of dimension $30\text{ cm} \times 30\text{ cm}$. The wedge with angle 80° is placed on the rotating platform kept inside an anechoic chamber. Two identical X band horn antennas connected to the two ports of a Vector Network Analyzer (VNA) ZVB 20 are placed side by side to measure the backscattered power from the wedge over the X band. The wedge is then loaded with first iterated stage of the Sierpinski carpet array structure fabricated on an FR-4 substrate with thickness 0.8mm as shown in figure 6.1. Backscattered power is again measured to see the effect of loading. Measurements are repeated after loading the wedge with second and third iterated stages of the Sierpinski carpet array. The procedure is also repeated for different thickness.

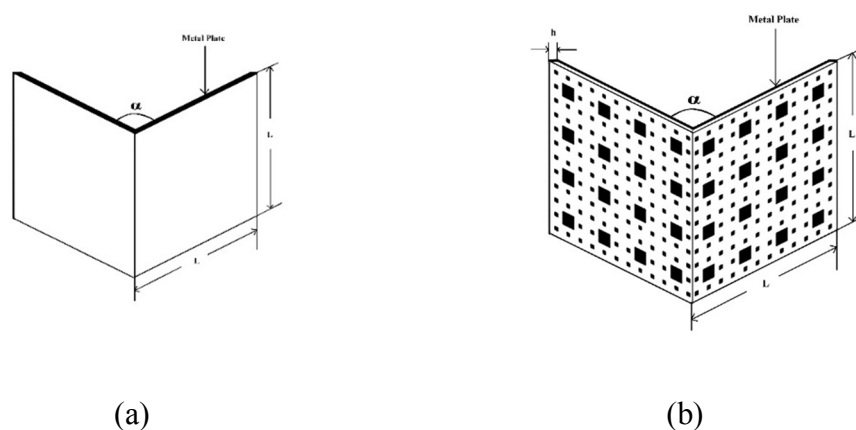


Fig 6.1 Schematic diagram of (a) plain wedge (b) wedge loaded with second iterated stage of SCF array with dielectric thickness h with wedge angle α

The hinge between metal plates is adjusted to produce wedges with angles 90° , 100° , 110° and 120° . Backscattering measurements are repeated.

6.2 80° METALLIC WEDGE LOADED WITH DIELECTRIC BACKED SCF ARRAY

Figure 6.2 shows variation of relative backscattered power with frequency when loaded with first iterated stage of SCF array for different substrate thickness. Enhancement of backscattering is achieved from 10.04 GHz to 12 GHz when loaded with 0.8 mm FR4 backed SCF array. Better enhancement in backscattering is for the entire band when the thickness is increased to 1.6 mm with a maximum enhancement of 3.1 dB.

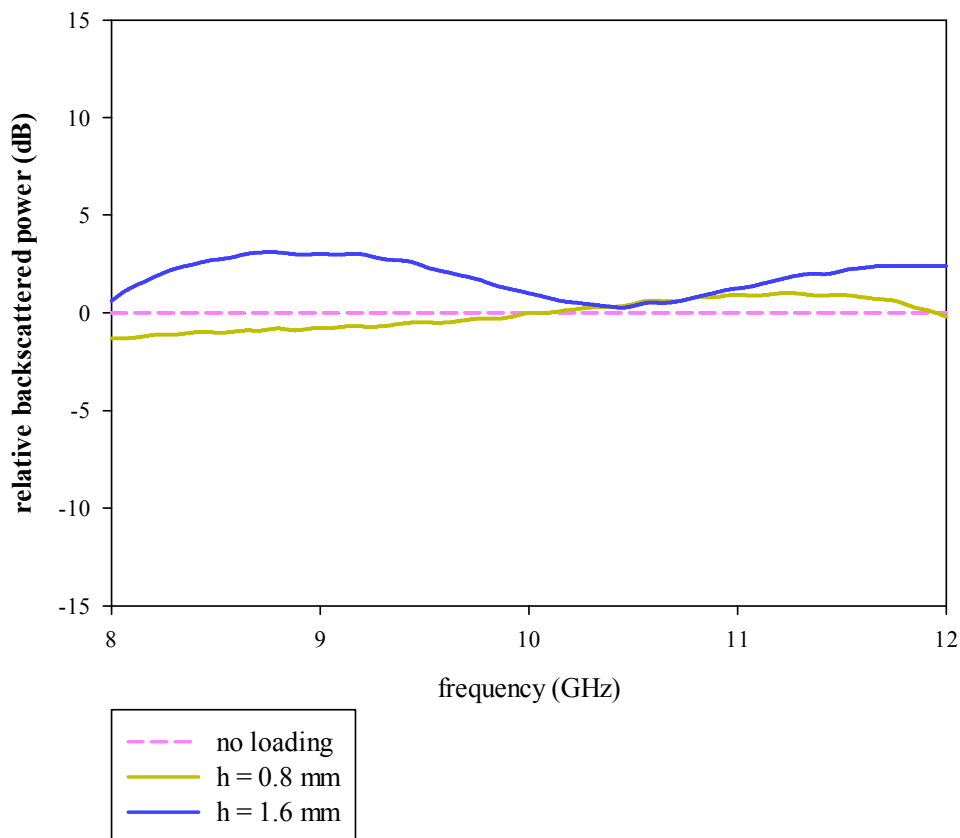


Fig 6.2 Measured variation of relative backscattered power with frequency for 80° wedge loaded with first iterated SCF array

Results of backscattering experiments with second iterated stage of SCF array is given in figure 6.3. Here backscattering enhancement over entire X band is obtained for $h=0.8$ mm. As the thickness is increased enhancement is obtained at the higher end of the X band.

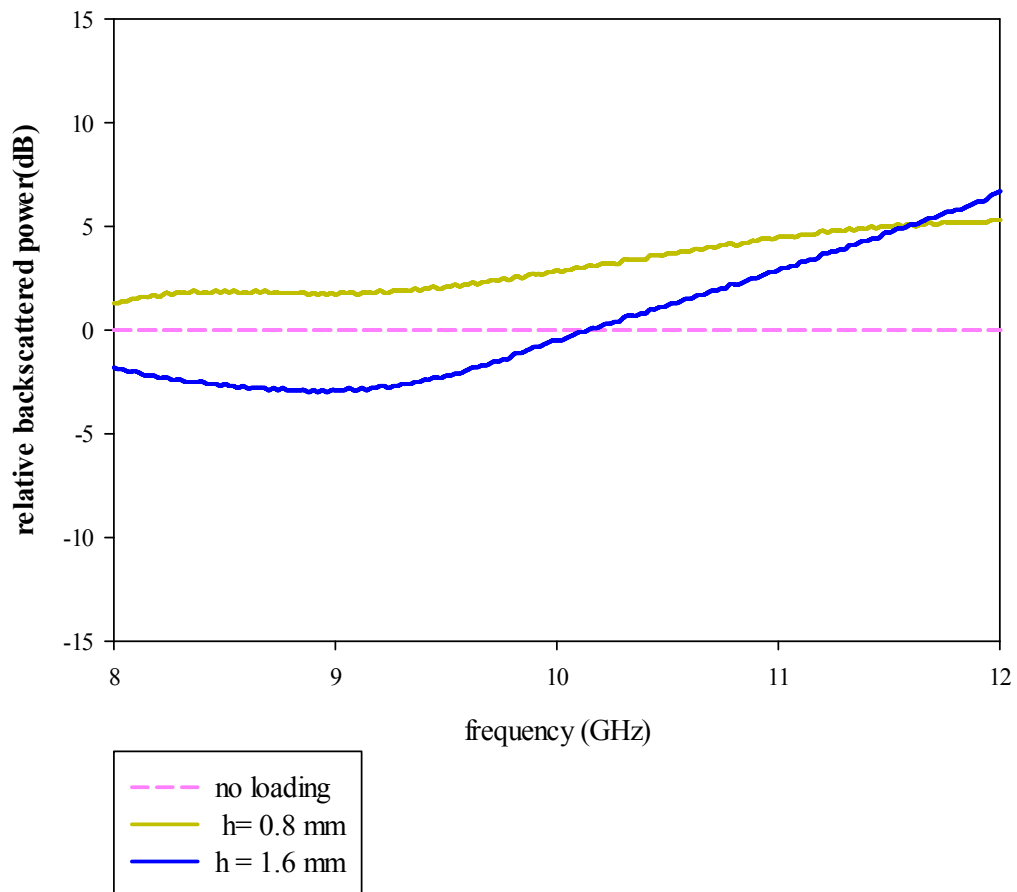


Fig 6.3 Measured variation of relative backscattered power with frequency for 80° wedge loaded with second iterated SCF array

Results for third iterated stage is given in Figure 6.4.

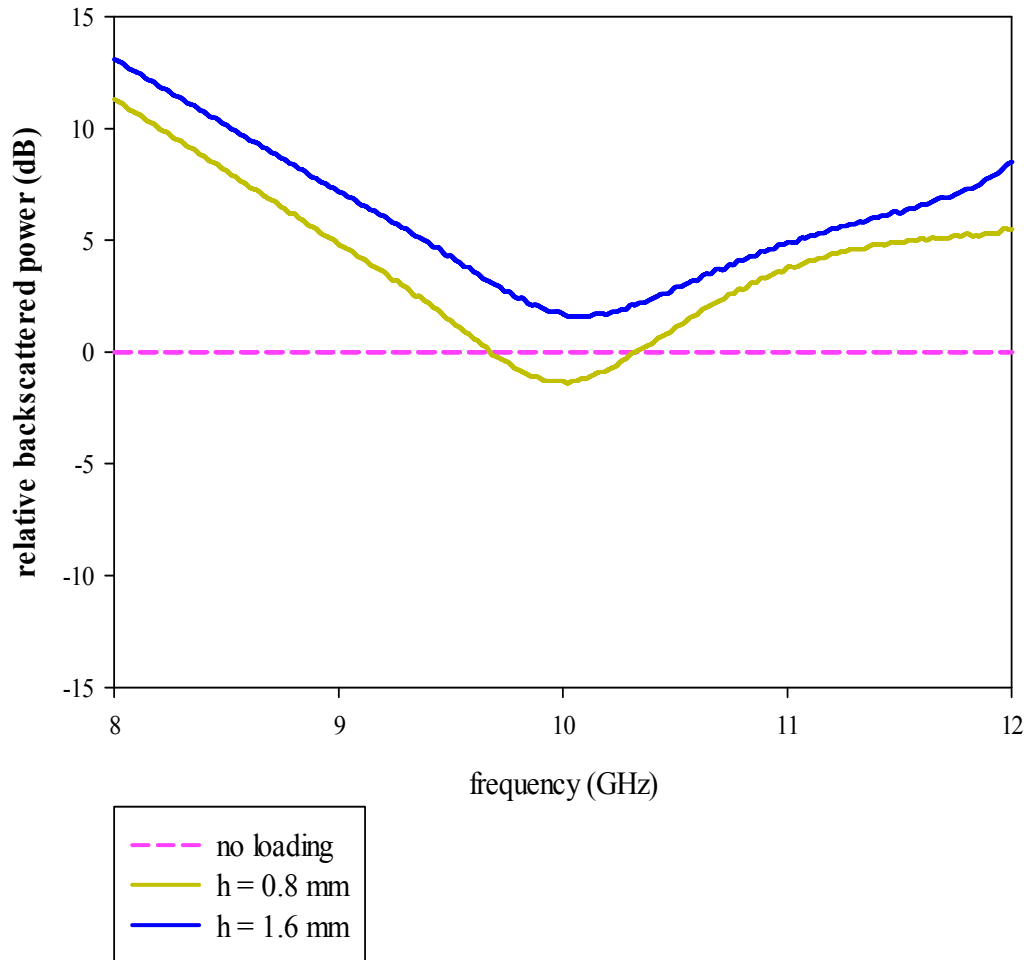


Fig 6.4 Measured variation of relative backscattered power with frequency for 80° wedge loaded with third iterated SCF array

From 6.3 and 6.4 it is found that the second iterated stage of SCF array with $h = 0.8\text{mm}$ and third iterated stage of SCF array with $h = 1.6\text{ mm}$ give enhanced backscattering from an 80° metallic wedge for the entire X band. Maximum value of 13.1 dB is achieved at 8 GHz when the third iterated stage with $h = 1.6\text{ mm}$.

6.3 90° METALLIC WEDGE LOADED WITH DIELECTRIC BACKED SCF ARRAY

Measurement results for the 90° wedge are given in Figures 6.5, 6.6 and 6.7.

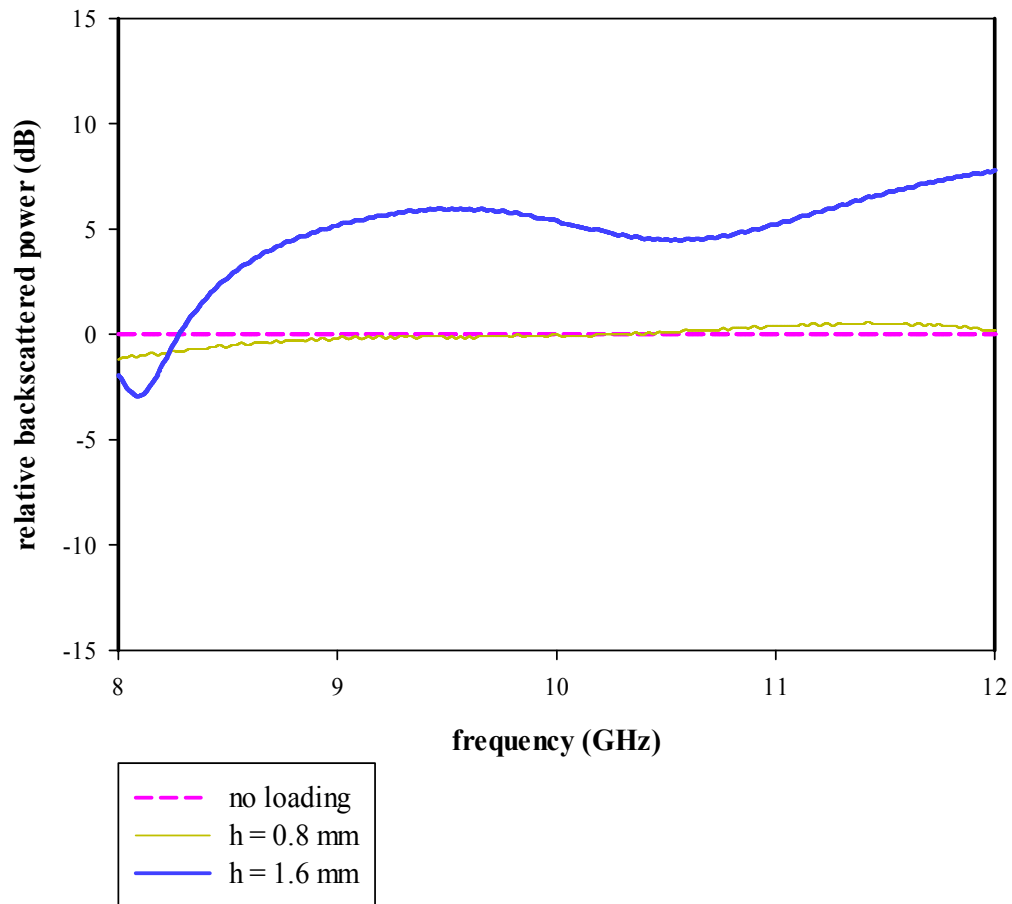


Fig 6.5 Measured variation of relative backscattered power with frequency for 90° wedge loaded with first iterated SCF array

For the first iterated stage, $h = 0.8$ mm gives little effect but enhancement is obtained for $h = 1.6$ mm in the entire X band.

Figure 6.6 shows the frequency response of relative backscattered power for 90° wedge loaded with second iterated stage of SCF array with different dielectric thickness (h). Relative backscattered power enhancement is achieved in the frequency range 8.98 GHz to 12 GHz with $h = 0.8$ mm and 8.75 to 12 GHz with $h = 1.6$ mm.

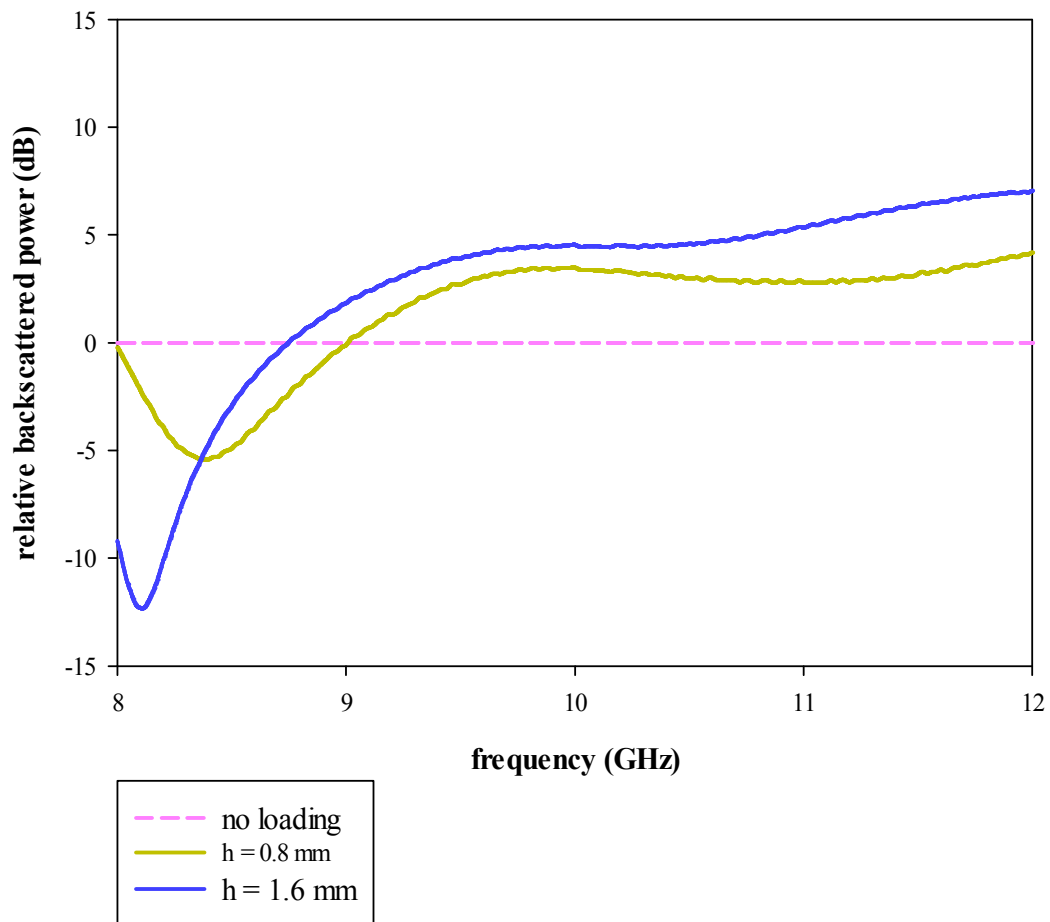


Fig 6.6 Measured variation of relative backscattered power with frequency for 90° wedge loaded with second iterated SCF array

A maximum enhancement of 7.15 dB in relative backscattered power is obtained for 12 GHz.

The third iterated stage of SCF array when loaded over the 90° wedge with different dielectric thickness gives frequency response of the relative backscattered power as shown in figure 6.7. Dielectric thickness of $h = 1.6$ mm gives an enhancement in relative backscattered power over the entire X band while $h = 0.8$ mm also gives an enhancement over the range 8.18 GHz -12 GHz.

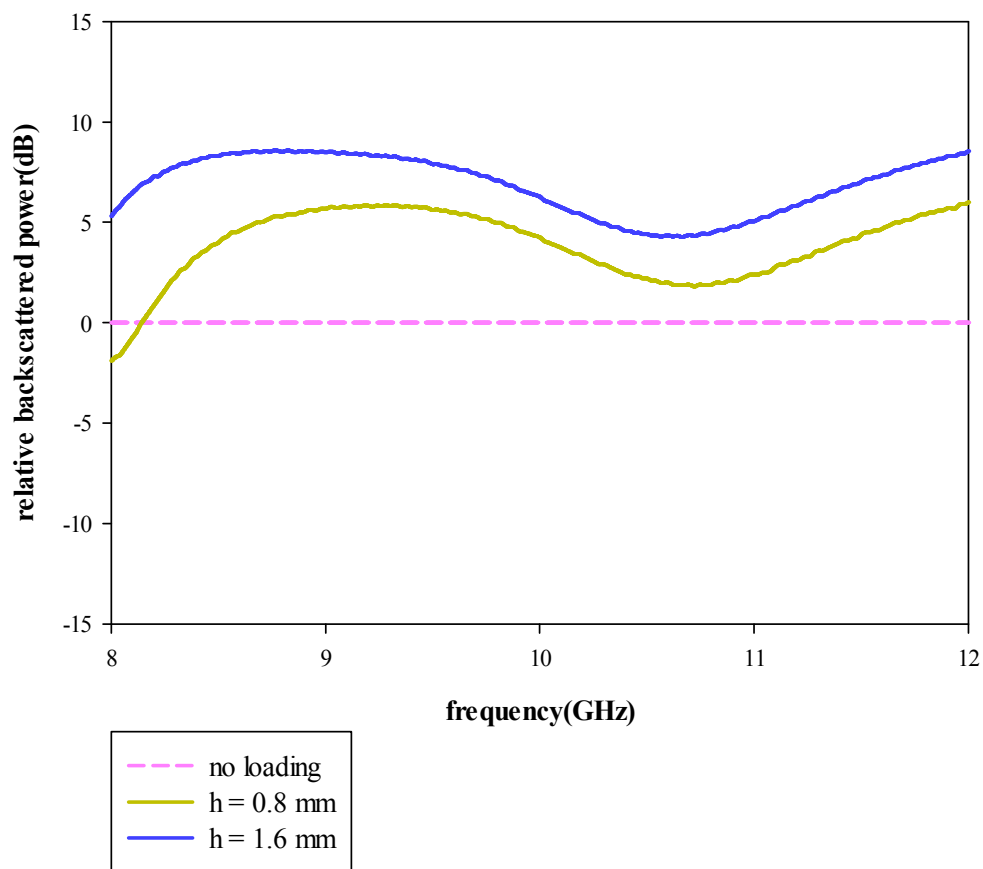


Fig 6.7 Measured variation of relative backscattered power with frequency for 90° wedge loaded with third iterated SCF array

A 90° wedge loaded with third iterated stage of SCF having $h = 1.6$ mm gives enhancement in backscattering for the full X band. The maximum enhancement of 8.56 dB at 8.92 GHz is also measured for this configuration.

6.4 100° METALLIC WEDGE LOADED WITH DIELECTRIC BACKED SCF ARRAY

Fractal arrays were loaded on 100° metallic wedge and the measured results for different iterations are shown in figure 6.7, 6.8 and 6.9. The SCF array with $h = 0.8$ mm is having no significant effect in the control of relative backscattered power from the 100° wedge. For $h = 1.6$ mm enhancement in relative backscattered

power is achieved for a bandwidth of 9.41 - 12 GHz. Maximum enhancement is obtained as 4.85 dB at 10.56 for dielectric thickness $h = 1.6$ mm.

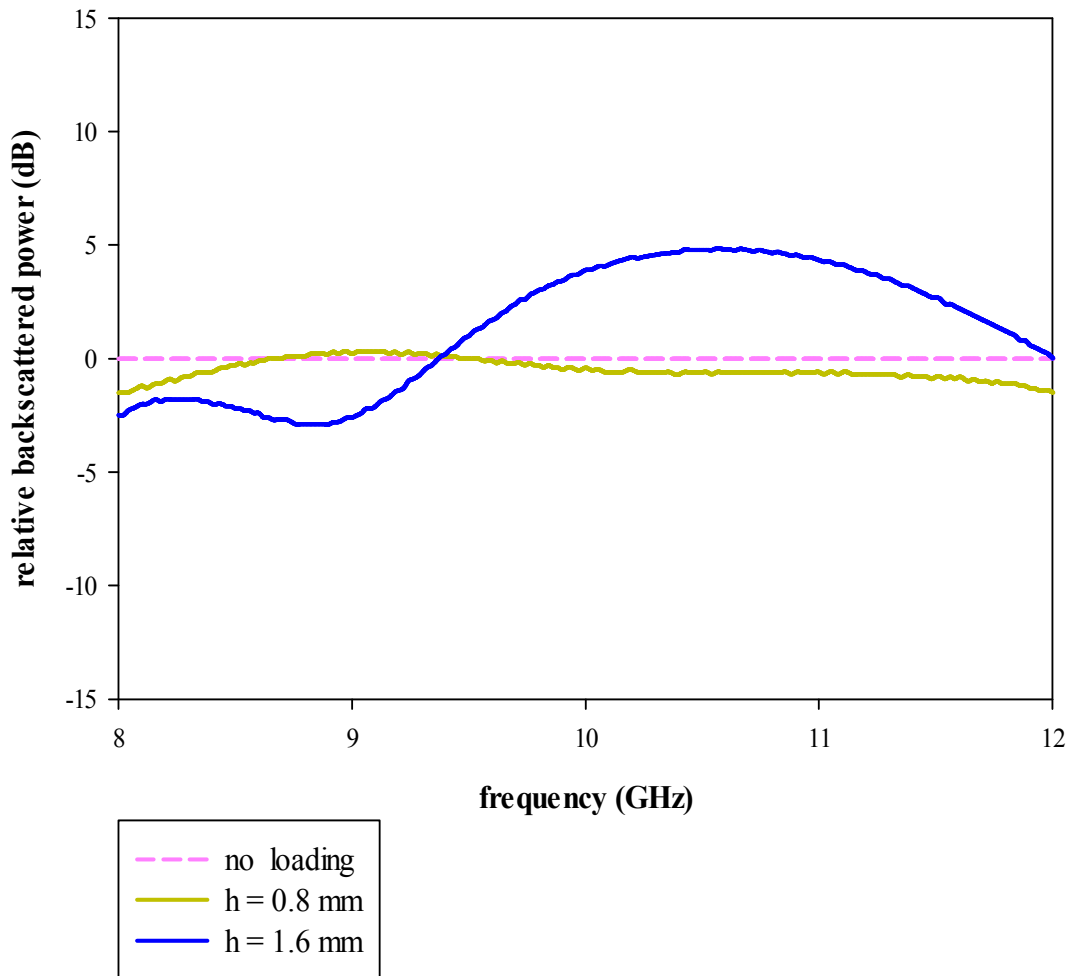


Fig 6.8 Measured variation of relative backscattered power with frequency for 100° wedge loaded with first iterated SCF array

Measured variation of relative backscattered power with frequency for 100° wedge with different dielectric thickness is shown in figure 6.9. Enhancement in backscattering is measured in the frequency range 9.10 – 12 GHz when $h = 0.8$ mm and 10.65 – 12 GHz when $h = 1.6$ mm respectively.

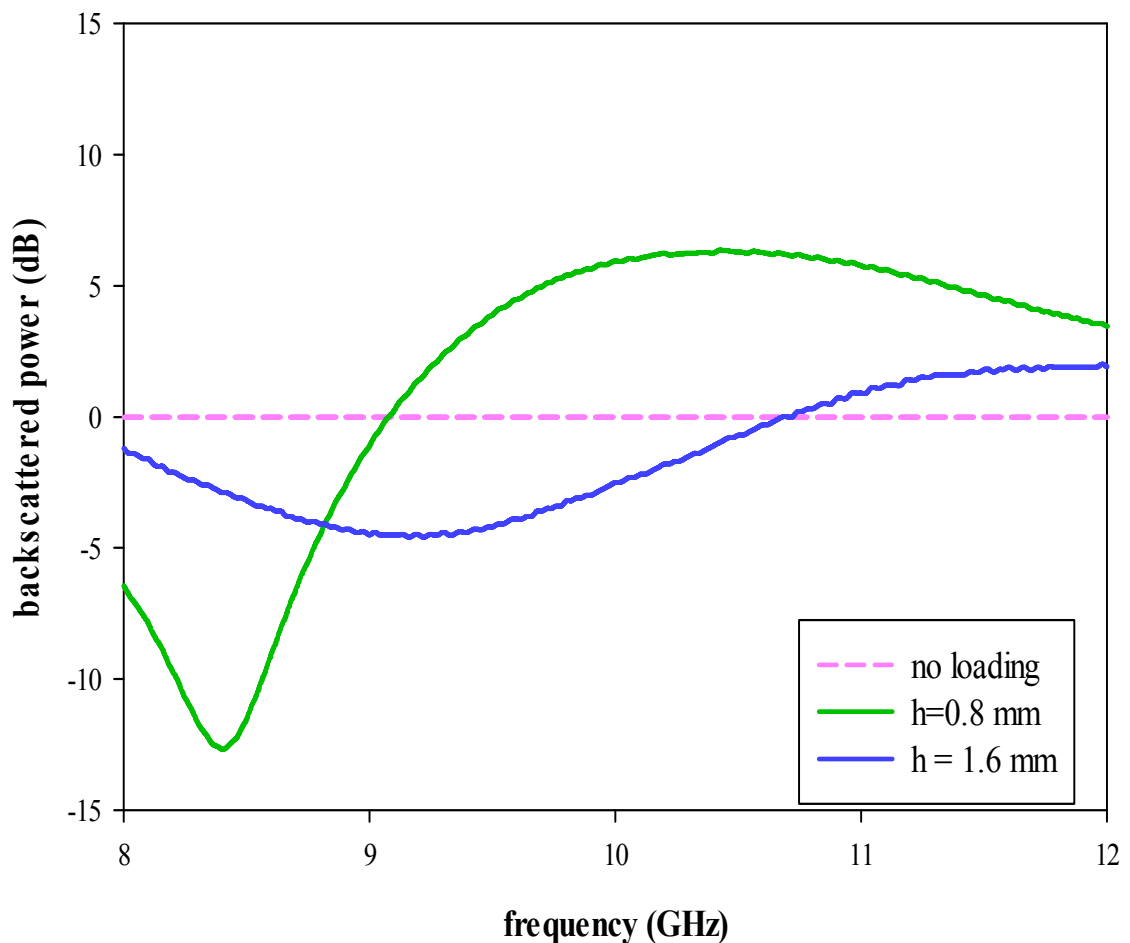


Fig 6.9 Measured variation of relative backscattered power with frequency for 100° wedge loaded with second iterated SCF array

Maximum enhancement in relative backscattered power is obtained as 6.34 dB at 10.42 GHz.

Figure 6.10 shows the frequency response of the relative backscattered power for 100° wedge with different dielectric thickness (h). From the figure it can be seen that enhancement in relative backscattering is achieved for both dielectric thickness of $h = 0.8$ mm and $h = 1.6$ mm for the entire X band.

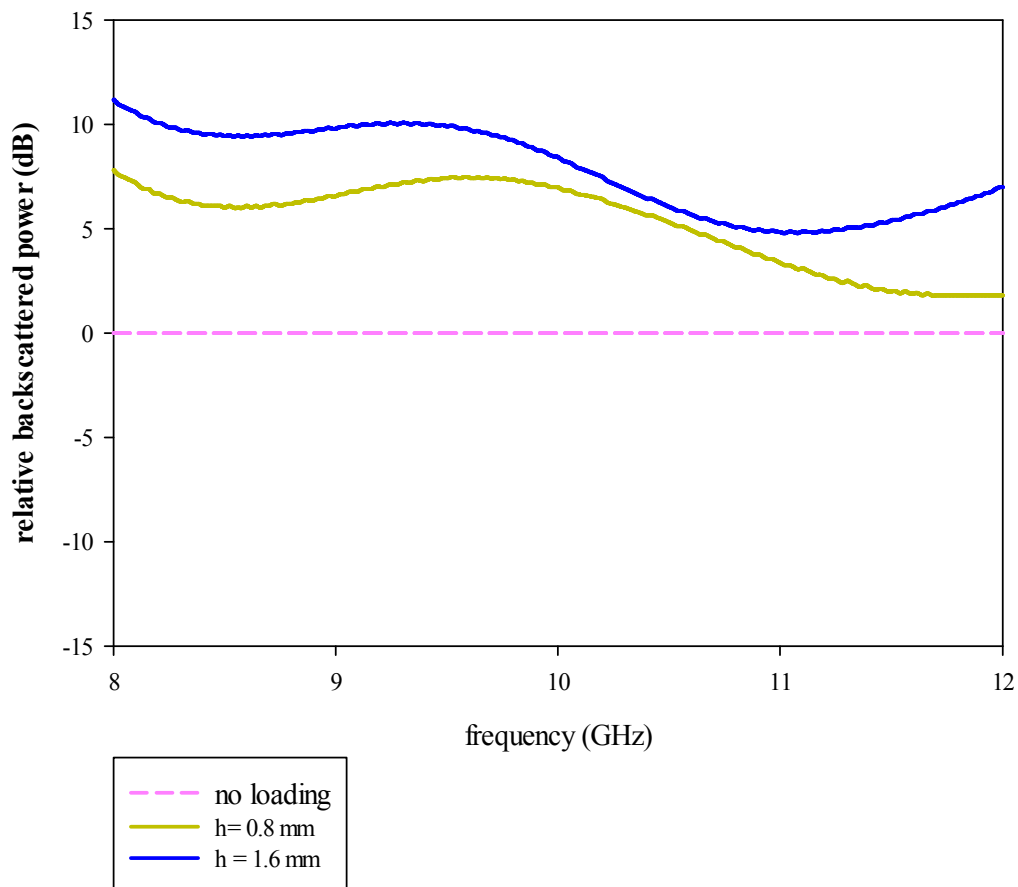


Fig 6.10 Measured variation of relative backscattered power with frequency for 100° wedge loaded with third iterated SCF array

Maximum enhancement of 11.2 dB is obtained at 8 GHz when $h=1.6$ mm.

Enhancement in relative backscattered power is achieved for the entire X band when loaded with the third iterated stage of the SCF array with dielectric thickness of $h = 0.8$ mm and $h = 1.6$ mm. Maximum enhancement is measured as 11.2 dB at 8 GHz, when the third iterated stage of SCF array with $h = 1.6$ mm is loaded over the 100° metallic wedge.

6.5 110° METALLIC WEDGE LOADED WITH DIELECTRIC BACKED SCF ARRAY

Figure 6.11 shows variation in relative backscattered power with frequency for 110° wedge loaded with first iterated SCF array for different dielectric thickness (h). For thickness $h = 0.8$ mm there is no significant variation in relative backscattered power. But for $h = 1.6$ mm enhancement is obtained for the frequency bands 8.66 – 9.86 GHz and 10.66- 12.0 GHz.

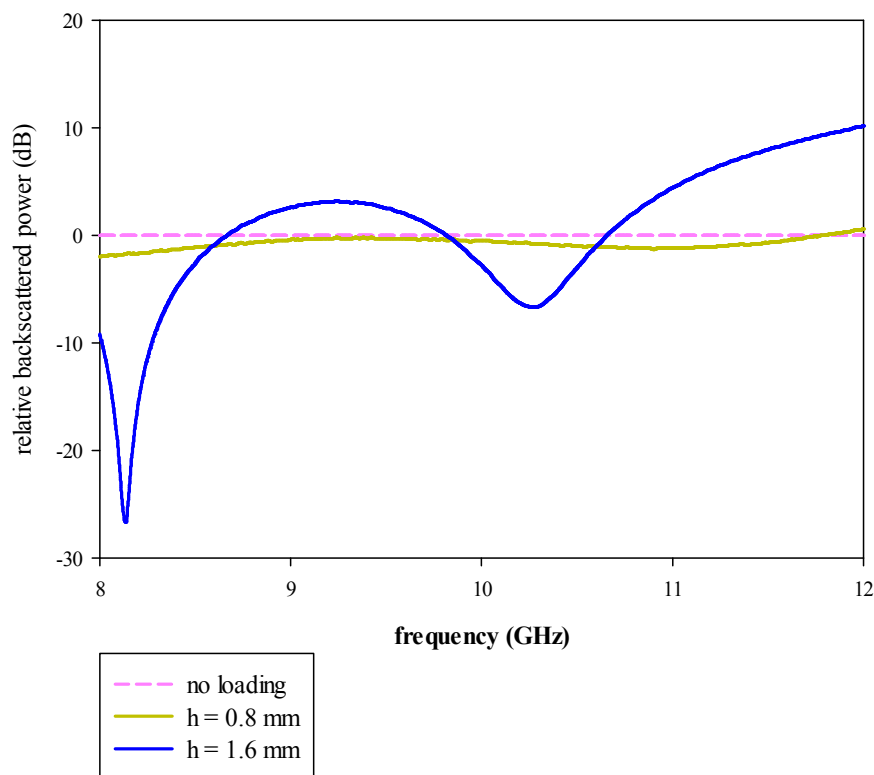


Fig 6.11 Measured variation of relative backscattered power with frequency for 110° wedge loaded with first iterated SCF array

Maximum enhancement is obtained as 10.19 dB at 12 GHz when the dielectric thickness $h=1.6$ mm.

Figure 6.12 shows measured variation of relative backscattered power with frequency for 110° wedge loaded with second iterated SCF array of different

dielectric thickness. Enhancement is obtained for the frequency band 9.71-12 GHz when the SCF array thickness $h = 0.8$ mm. Dielectric thickness of 1.6 mm gives no significant enhancement in relative backscattered power.

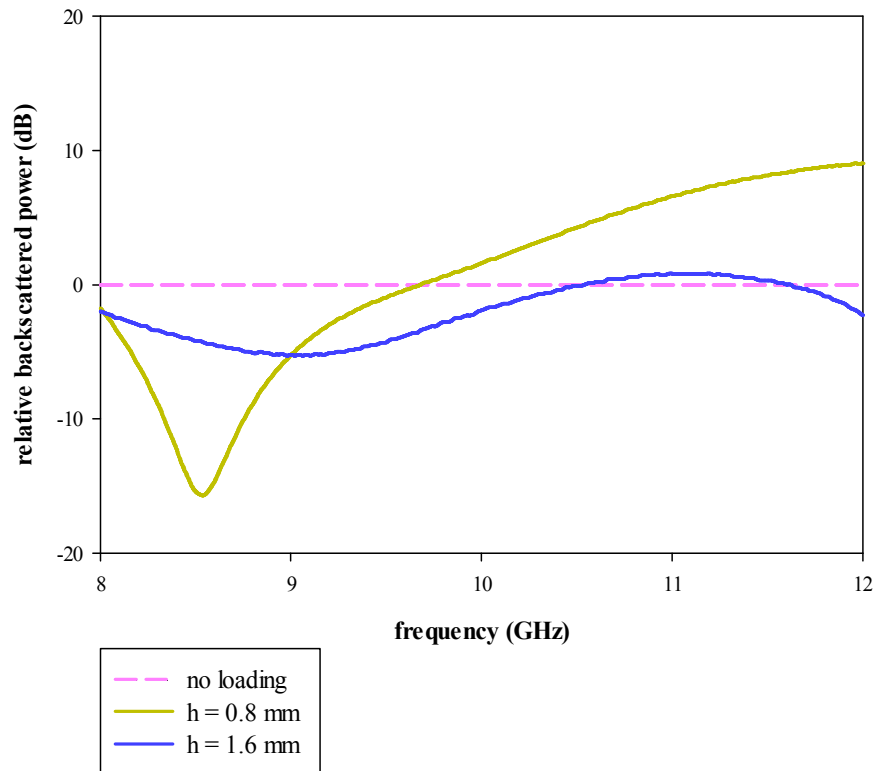


Fig 6.12 Measured variation of relative backscattered power with frequency for 110° wedge loaded with second iterated SCF array

Maximum enhancement of 9.04 dB is measured at 12 GHz when the SCF array dielectric thickness is 0.8 mm.

Measured variation of relative backscattered power with frequency for 110° wedge loaded with third iterated SCF array of different dielectric thickness (h) is shown in Figure 6.13. Enhancement in relative backscattered power is achieved for the entire X band when dielectric thickness $h = 1.6$ mm. Dielectric thickness of $h = 0.8$ mm also gives enhancement in relative backscattered power for the frequency band 8.28 – 12 GHz.

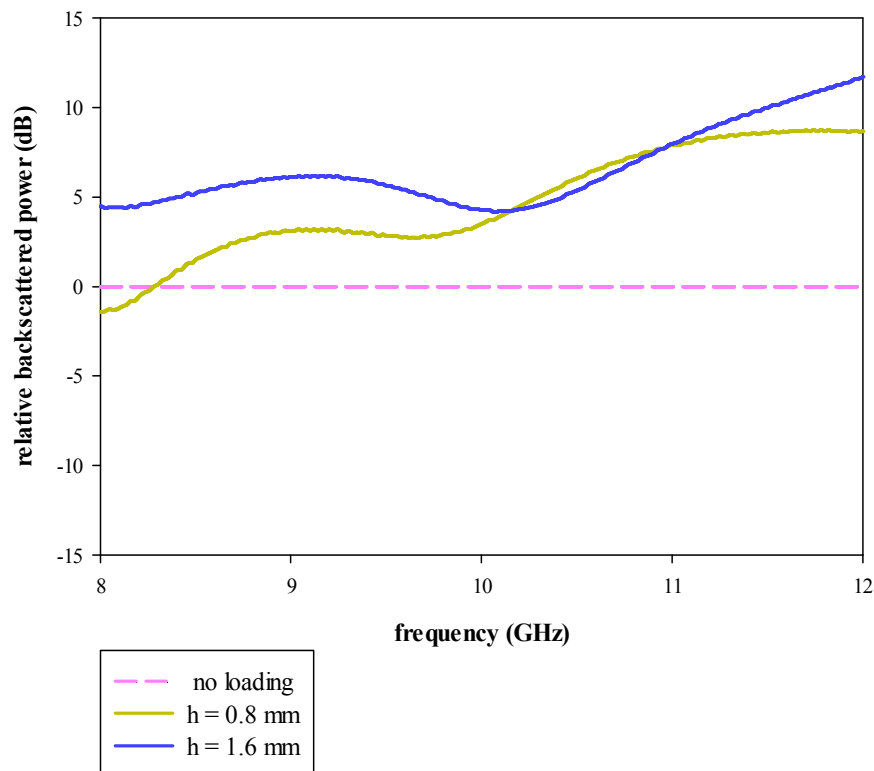


Fig 6.13 Measured variation of relative backscattered power with frequency for 110° wedge loaded with third iterated SCF array

Maximum relative backscattered power is obtained as 11.72 dB at 12 GHz when $h = 1.6$ mm.

For the 110° metallic wedge enhancement in relative backscattered power over the entire X band is achieved by loading the third iterated stage of the SCF array with a dielectric thickness $h = 1.6$ mm. Maximum enhancement in relative backscattered power is also obtained for this configuration as 11.72 dB at 12 GHz.

6.6 120° METALLIC WEDGE LOADED WITH DIELECTRIC BACKED SCF ARRAY

Figure 6.14 shows measured variation of relative backscattered power with frequency for 120° wedge loaded with first iterated stage of SCF array of different

dielectric thickness (h). When $h = 0.8$ there is no significant enhancement in relative backscattered power. A dielectric thickness of $h = 1.6$ mm gives an enhancement in relative backscattered power for the range 9.80 - 11.48 GHz.

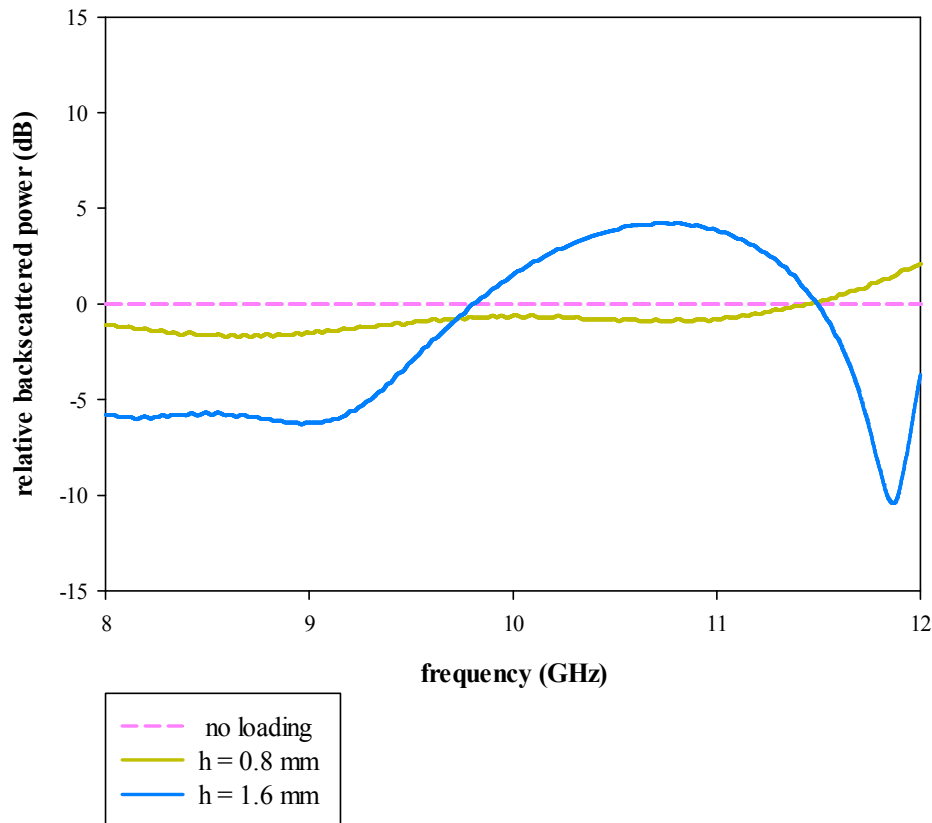


Fig 6.14 Measured variation of relative backscattered power with frequency for 120° wedge loaded with first iterated SCF array

A maximum enhancement of 4.25 dB is obtained for frequency 10.71 GHz when $h = 1.6$ mm.

The second iterated stage of the SCF array gives a variation in measured backscattered power when loaded over 120° wedge with substrates of different thickness (h) as shown in Figure 6.15.

Enhancement in relative backscattered power is achieved for the frequency range 9.81 -12 GHz when $h=0.8$ mm and 11.04 -12 GHz when $h= 1.6$ respectively.

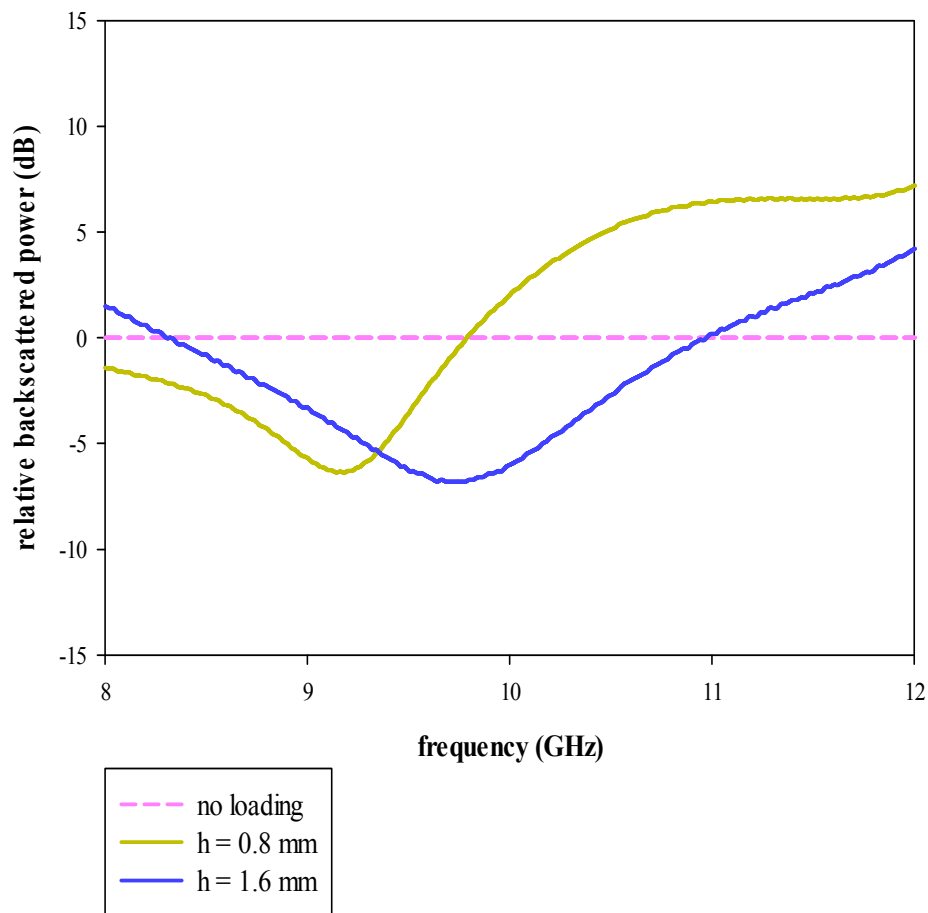


Fig 6.15 Measured variation of relative backscattered power with frequency for 120° wedge loaded with second iterated SCF array

Obtained maximum enhancement is measured as 7.28 dB at 12 GHz when $h=0.8$ mm.

Figure 6.16 shows measured variation of relative backscattered power with frequency for 120° wedge loaded with third iterated SCF array of different dielectric thickness (h). Enhancement in backscattering is achieved over the frequency range 9.24 – 12 GHz when $h=0.8$ mm and 8.98 to 12 GHz when $h = 1.6$ mm respectively.

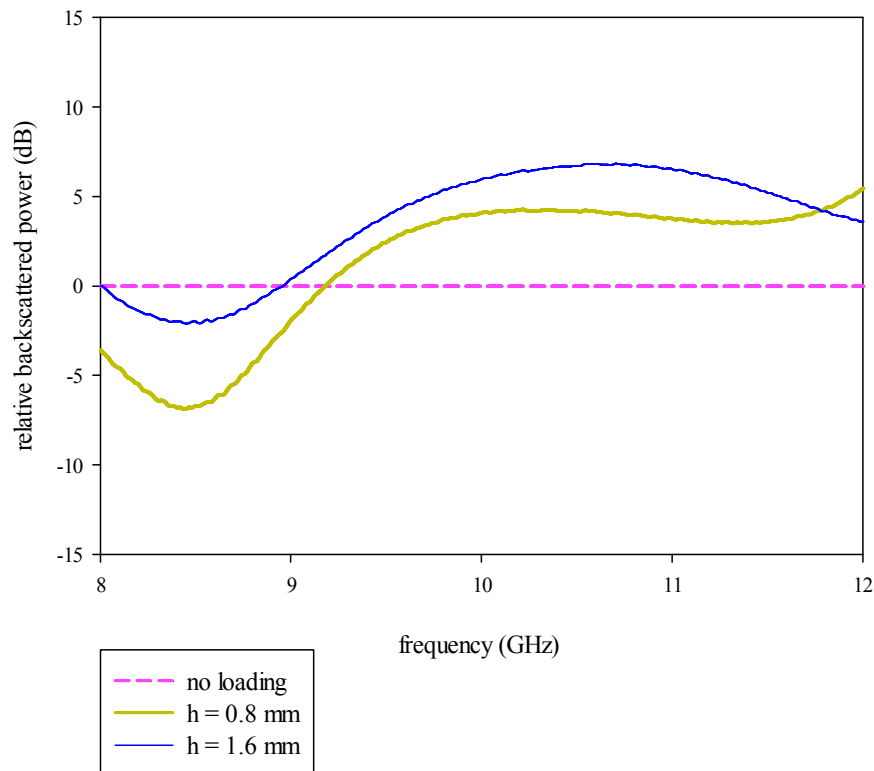


Fig 6.16 Measured variation of relative backscattered power with frequency for 120° wedge loaded with third iterated SCF array

Maximum enhancement in relative backscattered power of 5.45 dB is achieved at 12 GHz when SCF array is loaded with $h = 0.8$ mm thickness.

6.7 CONCLUSION

Studies on wedges of different wedge angles show that it is possible to enhance the backscattering by loading fractal arrays of proper thickness. Thus the RCS of the target can be increased to get better visibility if necessary.

7 CONCLUSIONS

This chapter presents the conclusions of the research works carried out. Scope for future work is also discussed.

TABLE OF CONTENTS

7.1 Flat plates

7.2 Dihedral Corner Reflectors

7.3 Metallic Wedge

7.4 Scope for future Work

A detailed study on the Scattering properties of metallic objects loaded with dielectric backed fractal structures are conducted in the present work .SCF arrays of various iterations and different dielectric thickness are used throughout the experimental study. Backscattering which determines monostatic scattering radar cross section of flat plates with 3D structures such as dihedral corners and metallic wedges of different angles are also investigated.

7.1 FLAT PLATES

Backscattering reduction of more than 10 dB is attained over the entire X band by loading the second iterated stage of the 4×4 SCF array with a dielectric thickness of 3.2 mm. A maximum reduction of 31.7 dB is obtained at 11.08 GHz for this structure. At 9.5 GHz a reduction of 28 dB is also attained. The reduction is more

than 20 dB for a significant portion of the band. Thus it is established that wideband RCS reduction is obtained using SCF array technique.

At a frequency of 11.08 GHz the received power is maximum at an angle of 25° and for frequency 9.5 GHz the received power is maximum at an angle of 10° . This means that the backscattering reduction is achieved by the scattering of incident power in other directions. The minimum value of backscattered power at normal incidence is obtained for $h=0.107\lambda$.

Blazing effect is observed using SCF arrays. Blazing can produce wide angle elimination of specular reflection from a flat metal plate. The elimination of specular reflection below -10 dB occurs over a wide angular range of 0° - 58° for the present structure. Maximum reduction in reflected power of 34.5 dB is observed at an angle of incidence of 26° . Here the specular reflection is reduced and backscattering is increased in this angular range.

Reduction of reflected power below -10 dB is achieved for a frequency band of 1.72 GHz for an angle of incidence 26° . This is observed for other angles also. For angle of incidence 39° the reduction of specular reflection below -10 dB is obtained over a frequency band of 1.9 GHz, with a maximum reduction of -27 dB at 9.8 GHz. Thus the 4×4 fractal structure is very effective in wide angle elimination of specular reflection over a wide frequency band.

By stacking different iterated stages of SCF arrays a 10 dB reduction in backscattering is obtained over 80 percent of the X band. The maximum backscattering reduction obtained is 32 dB at 11.08 GHz.

The effect of interleaving different iterated stages of the fractal arrays are also considered. Different types of interleaved structures were constructed and measured results show dielectric backed interleaved structure gives good backscattering reduction. For a dielectric thickness of 2.4 mm, the backscattered power reached a minimum value of -36 dB at 9.26 GHz. The -10 dB band width is also better when the horizontal interleaved structure is used.

7.2 DIHEDRAL CORNER REFLECTORS

Dihedral corner reflectors of different angles, which form part of any large size targets is investigated. Backscattering reduction of 80° corner and 90° corner are achieved over the entire X band by loading SCF arrays. Different thickness and different iterations are studied. It is also established that if the dielectric thickness is optimally chosen, enhancement or reduction in backscattering is obtained for different angles.

Enhancement in backscattering is observed for the 100° dihedral corner reflector. Reduction in backscattering is obtained from 10.41 GHz to 12 GHz when the 100° corner reflector is loaded with 2.4 mm FR4 substrate backed third iterated stage of the SCF array.

Enhancement in backscattering over the entire X band is observed by loading 110° corner with dielectric backed SCF array. Backscattering reduction is obtained for frequency bands 8.76 GHz to 9.08 GHz and 9.46 GHz to 11.42 GHz.

For the 120° corner reflector backscattering reduction is achieved for a large range of frequency in the X band when loaded with the first iterated stage of the SCF array. The second and third iterated stages of the SCF arrays when loaded over the 120° dihedral corner reflector give enhancement in backscattering.

7.3 METALLIC WEDGE

Wedges of different angles are also investigated. Backscattering is measured by loading different iterated stages of dielectric backed SCF arrays over metallic wedges with angles varying from 80° to 120° .

The second iterated stage of SCF array with $h = 0.8\text{mm}$ and third iterated stage of SCF array with $h = 1.6\text{ mm}$ give enhancement in relative backscattering from an 80° metallic wedge for the entire X band.

A 90° wedge loaded with third iterated stage of SCF having $h = 1.6$ mm gives enhancement in backscattering for the full X band.

Enhancement in backscattered power is achieved for the entire X band when 100° metallic wedge is loaded with the third iterated stage of the SCF array with dielectric thickness of $h = 0.8$ mm and $h = 1.6$ mm.

For the 110° wedge enhancement in relative backscattered power is achieved for the entire X band when dielectric thickness $h=1.6$ mm for the SCF array.

For the 120° metallic wedge enhancement is achieved for 75.75 percent of the X band by loading the third iterated stage of the SCF array with a dielectric thickness $h = 1.6$ mm.

7.4 SCOPE FOR FUTURE WORK

Scattering studies on actual target models consisting of Corners, Wedges and cylindrical sections are to be investigated so as to find a method to reduce or enhance the backscattering. The study reveals dielectric backed SCF array acts as a fractal grating and gives blazing effect. Transmission studies through these fractal gratings can also be a topic for future study. Interleaving can also be optimized so as to get better performance over a wider bandwidth.

Author's Resume

Education:

- Ongoing: PhD (Electronics), Cochin University of Science and Technology,
Cochin, Kerala.
- 1997 M Tech Electronics, Cochin University of Science and Technology.
- 1992 MSc Physics, Mahathma Gandhi University.
- 1989 BSc Physics, Mahathma Gandhi University.

Teaching Experience:

- 1997 – 2006 Lecturer, Department of Electronics, Cochin University of
Science and Technology, Cochin, Kerala.
- 2006 – 2019 Assistant Professor, Viswajyothi College of Engineering and
Technology, Muvattupuzha, Ernakulam, Kerala.

Areas of Interest:

- Radar Cross section.
- Fractal Electrodynamics.
- Antennae.

Personal Details:

- Date of birth 31-05-1969
- Contact Cyriac M Odackal
- Address Odackal (H), Pala (PO), Kerala, 686575
- Email id cyriacpala@yahoo.co.uk

LIST OF PUBLICATIONS

JOURNALS:

Cyriac M. Odackal, Thomaskutty Mathew, A. O. Lindo and C. K. Aanandan “Wide Angle Elimination of Specular Reflection Using Metallo-dielectric Structure Based on Sierpinski Carpet Array” Journal of Emerging Technologies and Innovative Research, pp 501-505, Volume 5, Issue 9, September 2018.

Cyriac M. Odackal, A. O. Lindo, Thomaskutty Mathew, and C. K. Aanandan “ Backscattering Reduction of Flat Metallic Surface using Stacked Sierpinski Carpet Fractal Arrays” Journal of Emerging Technologies and Innovative Research, pp 80-85, Volume 6, Issue 1, January 2019.

Ullas G. Kalappura, Paulbert Thomas, **Cyriac M. Odackal** and K T Mathew “Modified Cavity Perturbation Method for Microwave Characterization of Conducting Polymers” Int.Jou.Advanced Materials Science, vol.4 No.1 pp.7-20,(2013).

Ullas G Kalappura, Paulbert Thomas, **Cyriac M. Odackal** and K.T. Mathew “Preparation and Dielectric Charactersterization of Arrowroot-Chitosan film for Microwave Phantom Applications", Microwave Review, Vol. 18 No. 2, pp.17-20 (2013).

CONFERENCES:

Cyriac M. Odackal, A. O. Lindo, C. K. Aanandan, and Thomaskutty Mathew “Backscattering Reduction of Dihedral Corner Reflector with Metallo-dielectric Structure Based on Sierpinski Carpet Array” Progress In Electromagnetics Research Symposium (PIERS), Singapore, November 2017.

Cyriac M Odackal, Thomaskutty Mathew, Lindo A O, Tony D, Neeraj K Pushkaran, C K Aanandan “Backscattering Reduction Using Stacked Dielectric Backed Fractal Arrays” International Symposium of Antennas and Propagation Kochi December 2018.